Space Programs Summary No. 37-28, Volume VI

for the period May 1, 1964 to June 30, 1964

Space Exploration Programs and Space Sciences

JET PROPULSION LABORATORY
CALIFORNIA INSTITUTE OF TECHNOLOGY
PASADENA, CALIFORNIA

July 31, 1964

Space Programs Summary No. 37-28, Volume VI

for the period May 1, 1964 to June 30, 1964

Space Exploration Programs and Space Sciences

JET PROPULSION LABORATORY
CALIFORNIA INSTITUTE OF TECHNOLOGY
PASADENA, CALIFORNIA

July 31, 1964

Preface

The *Space Programs Summary* is a six volume, bimonthly publication designed to report on JPL space exploration programs, and related supporting research and advanced development projects. The subtitles of all volumes of the *Space Programs Summary* are:

Vol. I. The Lunar Program (Confidential)

Vol. II. The Planetary–Interplanetary Program (Confidential)

Vol. III. The Deep Space Network (Unclassified)

Vol. IV. Supporting Research and Advanced Development (Unclassified)

Vol. V. Supporting Research and Advanced Development (Confidential)

Vol. VI. Space Exploration Programs and Space Sciences (Unclassified)

The *Space Programs Summary,* Volume VI consists of an unclassified digest of appropriate material from Volumes I, II, and III and a reprint of the space science instrumentation studies of Volumes I and II. This instrumentation work is conducted by the JPL Space Sciences Division and also by individuals of various colleges, universities, and other organizations. All such projects are supported by the Laboratory and are concerned with the development of instruments for use in the NASA space flight programs.

W. H. Pickering

W. H. Pickering, *Director*
Jet Propulsion Laboratory

Space Programs Summary No. 37-28, Volume VI

Prepared under Contract No. NAS 7-100, National Aeronautics & Space Administration

Contents

LUNAR PROGRAM

I. *Ranger* Project 1
   A. Introduction 1
   B. Spacecraft Systems Testing 2
   C. Environmental Testing 4
   D. *Ranger 6* Trajectory Analysis 5

II. *Surveyor* Project 14
   A. Introduction 14
   B. Spacecraft System Development 14

THE PLANETARY–INTERPLANETARY PROGRAM

III. *Mariner* Project 17
   A. Introduction 17
   B. Spacecraft Systems Testing 18
   C. Design and Development 21

THE DEEP SPACE NETWORK

IV. Introduction 31

V. The Deep Space Instrumentation Facility 33
   A. Tracking Stations Engineering and Operations 33
   B. Communications Research and Development 38
   C. Advanced Antenna System Hydrostatic Thrust Bearing 41
   Reference 42

SPACE SCIENCES

VI. Space Instruments Development 43
   A. *Mariner* TV Subsystem Science and Engineering Calibration . . 43
   B. The *Mariner* Vidicon as a Ruggedized Space Component . . . 48
   Reference 51

VII. Applied Science 52
   A. Utilization of *Surveyor* TV Imagery for Photogrammetry and Construction of Photomosaics 52

LUNAR PROGRAM

I. *Ranger* Project

A. Introduction

The *Ranger* Project was established to develop a space flight technology for transporting engineering and scientific instruments to the Moon and planets. Nine *Ranger* launchings, using *Atlas D–Agena B* vehicles, are now planned; six of these flights have been made.

Rangers 1 and 2 (Block I) were not lunar-oriented, but were engineering evaluation flights to test the basic systems to be employed in later lunar and planetary missions. Several scientific experiments were carried on a noninterference basis. Indications are that both spacecraft performed satisfactorily within the constraints of the obtained satellite orbit. *Rangers 3, 4, and 5* (Block II) carried a gamma-ray instrument, a TV camera, and a rough-landing seismometer capsule; all three of these flights experienced failures.

The objective of the *Ranger* Block III (*Rangers 6* through 9) flights is to obtain TV pictures of the lunar surface which will be of benefit to both the scientific program and the U.S. manned lunar flight program. The *Ranger 6* spacecraft, which was launched from Cape Kennedy, Florida, on January 30, 1964, and impacted the Moon on target on February 2, 1964, did not accomplish the primary flight objective due to a failure of the TV subsystem to transmit pictures. An extensive failure analysis was conducted. A document was prepared which covered the findings of the analysis as well as the recommendations for the *Ranger 7* through 9 configuration.

Reassembly of the *Ranger 7* TV subsystem from all new and reworked units was completed, and the subsystem was returned to JPL from RCA. Extensive testing of the TV subsystem as a subsystem and as part of the *Ranger 7* spacecraft was carried out at JPL, after which the *Ranger 7* spacecraft was shipped to Cape Kennedy on June 17, 1964. Testing of the proof test model continued at JPL.

Ranger Block IV, planned as a series of three flights, and *Ranger* Block V, planned as a six-flight series, were cancelled due to budgetary reasons by the Office of Space Sciences, NASA, in July and December, 1963, respectively.

B. Spacecraft Systems Testing

1. Ranger 7

All *Ranger 7* attitude-control modules were replaced with the spare units. It had been determined that the operating time on the gyros would approach 1000 hr at launch, which would be more than that allowed by safety factors. Also, the vibration levels of two flight-acceptance vibration test cycles were considered excessive.

A preliminary mission verification test and a 66-hr high-temperature mission test were successfully performed. A 66-hr low-temperature mission test was also accomplished. During this test, one potentially serious problem occurred. At approximately the time that the Real Time Command 0's were being sent to the spacecraft prior to the terminal phase, an unexplained transfer to the data encoder auxiliary clock was observed. Normally, this would occur only if the central computer and sequencer 400-cps or 25-pps outputs were lost or severely degraded in amplitude. Investigation showed that this problem occurred because the strip recorder was generating an electrical transient. The problem was corrected.

An electrical test was performed on the spacecraft bus in the 25-ft Space Simulator. The TV subsystem was mated to the spacecraft bus. An operational verification test (Fig. 1) showed that two TV cameras experienced a form of RF interference while radiating from the high-gain antenna. However, this interference was consistent with previous results of a test in an uncontrolled RF environment.

The spacecraft was disconnected from ground control, and the chamber door was sealed. Direct-access cables were removed from the spacecraft to simulate as near a flight condition as possible. All tests were satisfactorily conducted. The TV subsystem was commanded into the warmup mode, and TV operation was normal throughout the maneuver sequence. The RF interference reported at ambient environment was also noted for this test phase.

The explosive-safe-area TV high-power test was performed with the spacecraft mounted on a fixture with special RF monitor leads in the midcourse-motor squib locations. Measurements of the absorbed energy at the squib locations with the TV subsystem operating in the full-power mode showed results similar to those obtained with the proof-test-model spacecraft in the same test configuration. An evaluation of the test results indicated that it was safe to operate the TV subsystem in full power with live pyrotechnics in the midcourse location. The spacecraft was then suspended from overhead cables, and the antenna was run from a nested position to about 150 deg with the TV subsystem in the full-power mode to ensure that the RF interference noted during the Space Simulator testing would not be a problem under free-space radiation conditions. Evaluation of the pictures which were recorded showed normal spacecraft operation throughout the expected range of high-gain antenna deployment.

A backup functions test was performed; all spacecraft operations were normal. The attitude-control jet vane angles were recalibrated. An attitude-control valve leak rate test showed that one valve was leaking in excess of 150 cm^3/hr.

The spacecraft was removed from the test stand and prepared for shipment. *Ranger 7* was shipped to Cape Kennedy on June 17, 1964.

2. Proof Test Model

After torsional tests were performed, the *Ranger* proof test model was returned to the *x-y* shaker for the post-modal vibration survey. The results of this survey were normal, with no indication of problems resulting from the vibration tests.

A system test was then conducted. All subsystems operated normally during the test, except a -*x* jet vane. This problem was corrected by installing the *Ranger 9* flight jet vane assembly.

A special TV 16-hr vacuum verification test was performed. It was noted that degassing the ion gage inside the spacecraft hexagonal structure caused excessive noise at the data encoder and on the central recorder record.

Three mission verification tests were performed. During the second test, a momentary dropout was noted on the P-channel, and a 5-sec disturbance occurred in which the high-current regulator output dropped below 21 v and the power also dropped. Both of the disturbances appeared to be in the P-channel only.

A spacecraft bus attitude-control gas system leak check was completed. This check, performed at 1500 psi, indicated a leak rate of 85 cm^3/hr. The bus and all modules were inspected. No significant problems were detected as a result of the environmental tests. The antenna actuator assembly was replaced with the type-approval unit. A problem with the original actuator, detected during the

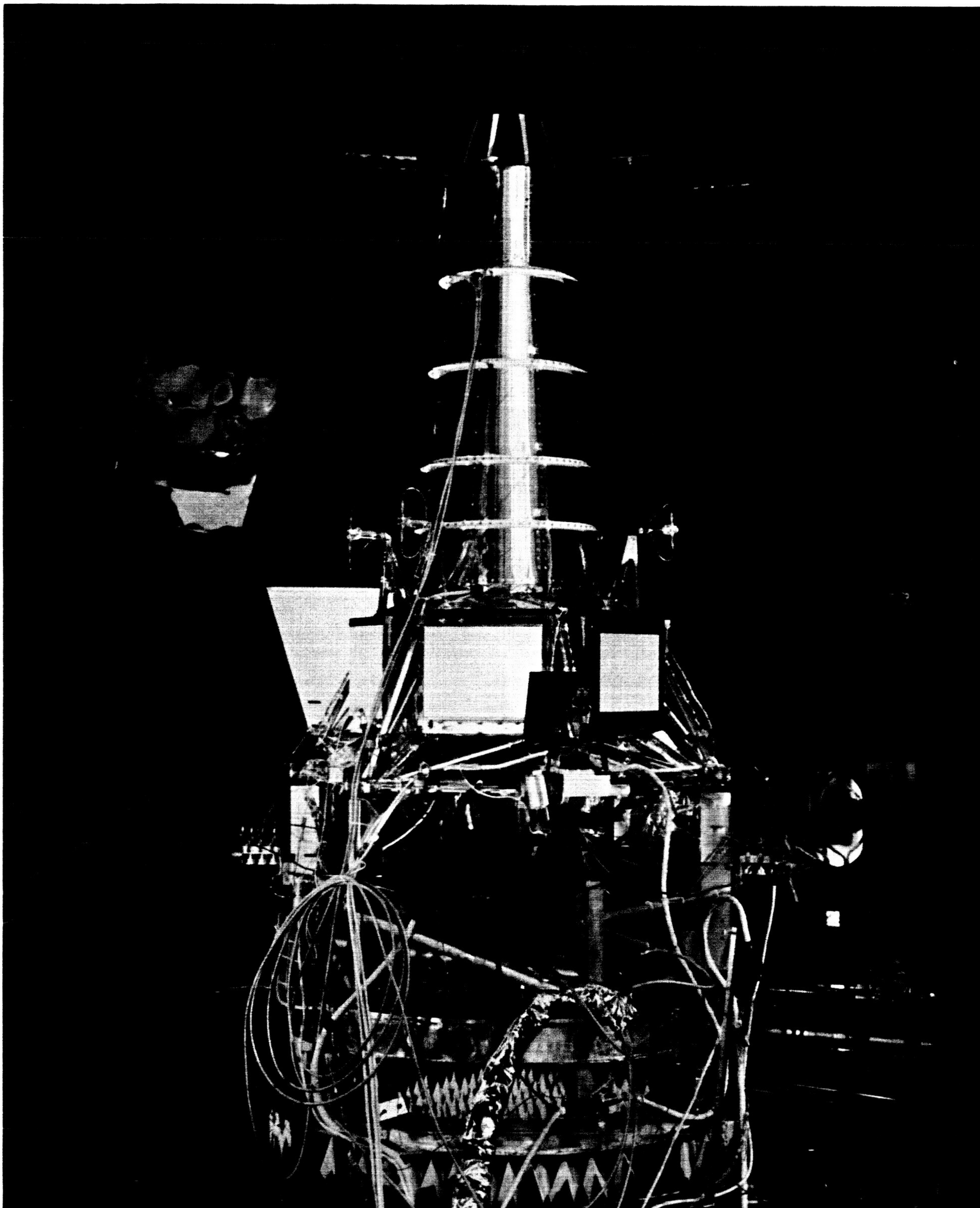

Fig. 1. *Ranger 7* configuration for operational verification test

mission tests, appears to be a motor bearing problem; the cause is still being investigated. Indications are that the antenna actuator and the jet vane actuator problems are a result of the higher-than-expected *g*-levels which occurred during the vibration tests.

Seven special TV tests were performed in the 7-ft vacuum chamber in an attempt to isolate the dropout problems observed during the mission tests. The TV subsystem was instrumented with 38 channels of DC instrumentation so that the problem could be isolated if it recurred. The special tests were run in the chamber at various temperatures and combinations of full power. During the vacuum runs, no disturbances of the type which occurred during the mission tests were noted. However, prior to the vacuum runs, a disturbance was noted during the instrumentation setup. Preliminary indications are that the most suspect area is the P-channel transmitter power supply.

A test was performed on the TV subsystem to obtain additional information on the modulator frequency change as a function of high-current regulator voltage. The results of this test are still being evaluated. The TV subsystem was then inspected. The P-channel transmitter power supply was removed and replaced with a life-test-vehicle unit. The former unit was returned to RCA in order to obtain more information about the disturbance problem.

A qualification-test-model high-current regulator was installed in the TV P-channel in order to obtain some operating history on a high-current regulator unit which is similar to the *Ranger 7* flight unit. Checkout of the TV subsystem indicated normal operation. The backup functions system test was performed. The spacecraft was radiated with the electromagnetic interference sources, except for the *Agena* telemetry source, which was inoperative. The operational test on the RF link was then performed with electromagnetic interference radiation; no significant spacecraft problems were encountered.

C. Environmental Testing

1. PTM Vibration-Vacuum Testing

The *Ranger* proof test model (PTM) was subjected to a combined environment of vibration and launch pressure-change simulation in the JPL 25-ft Space Simulator. The test was made to verify the operational integrity of the *Ranger* PTM in an environment which simultaneously simulated the launch rate of pressure change and subjected the vehicle to axial vibration; it marked the first time at JPL that a large system was vibration-tested under changing pressure conditions approaching those experienced during launch.

For the test, a Ling A-249-2 30,000-lb(f) shaker was installed on the shaker pad (Fig. 2). The mechanical design of the shaker installation was such that an insignificant amount of energy was transmitted to the chamber from the vibration system. The spacecraft was instrumented with 42 accelerometers, and the shaker with six accelerometers. All testing was done in the longitudinal (z) axis. The test consisted of three phases: random noise vibration, high-frequency sinusoidal, and low-frequency sinusoidal.

At a specified time during each test, the simulator was subjected to a rapid evacuation by a parallel arrange-

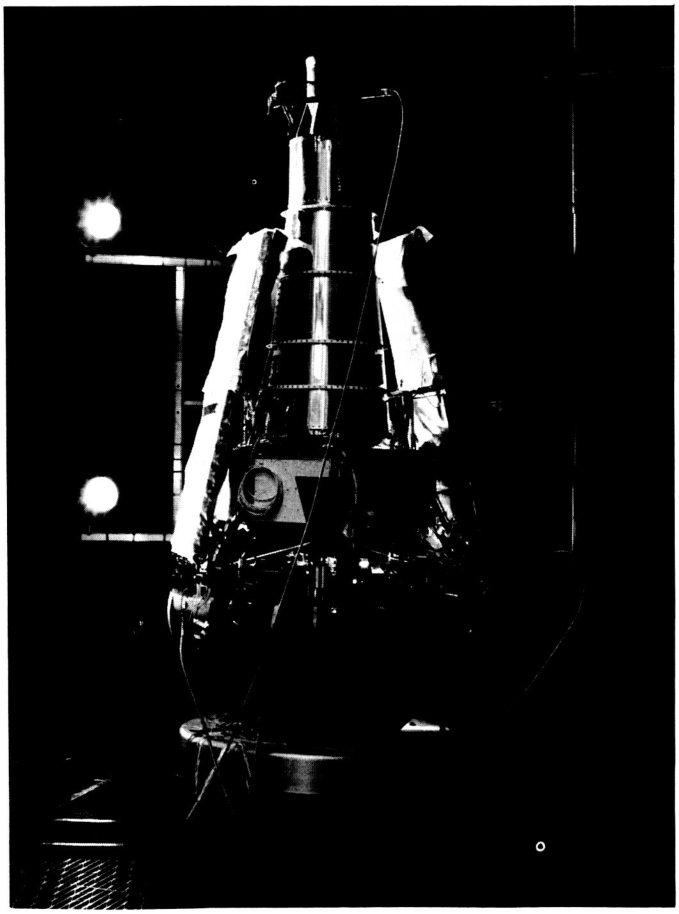

Fig. 2. PTM configuration for vibration-vacuum tests

ment of the compressors for the JPL 20- and 21-in. Wind Tunnels. The wind-tunnel line was previously evacuated up to the chamber interface valve, and at the specified time the interface valve was opened. The simulator reacted to the opening of this valve within 3 ±1 sec.

The chamber was not evacuated below 10 torr in order to minimize shaker outgassing. The significant feature of the chamber pressures obtained in these tests (13, 15.2, and 14.5 torr/sec) is that the flight value is approximately 13.5 torr/sec. The maximum pressure change in these runs was timed to occur during specified vibrational modes, e.g., the resonance range of the structure on the low-frequency sinusoidal sweep. The correlated timing was necessary in order that the spacecraft be subjected to extreme conditions (more critical than flight) to aid in verifying the spacecraft acceptability.

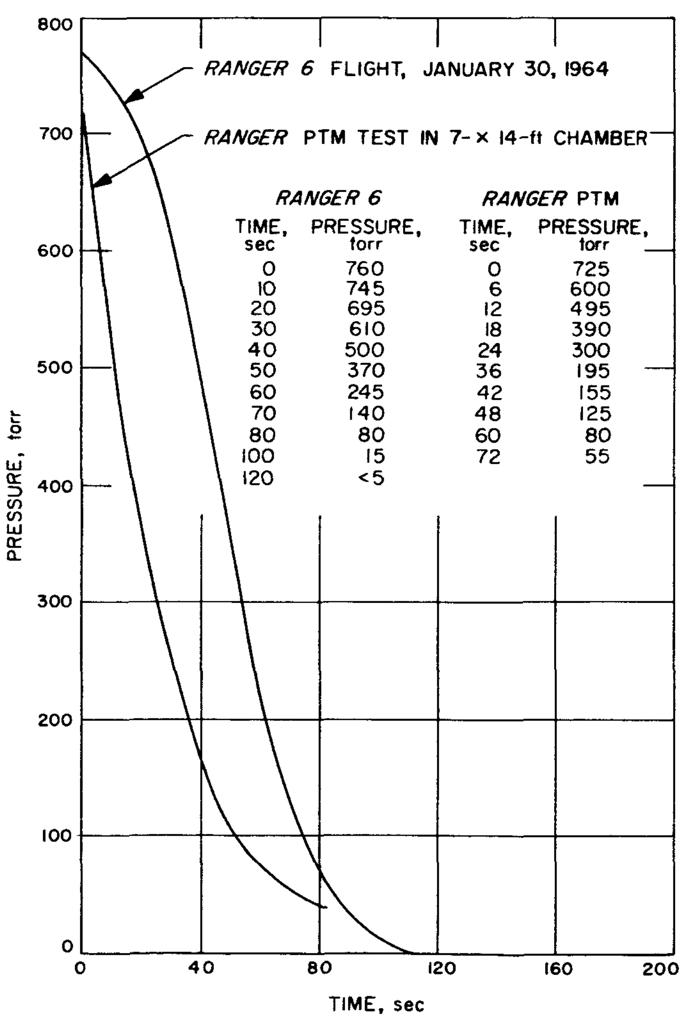

Fig. 3. Launch pressure profiles

2. *Thermal-Vacuum Testing*

Thermal-vacuum tests of complete spacecraft assemblies have usually been conducted by first evacuating the environmental test chamber to a pressure of 10^{-4} torr or lower and then cooling the cold walls of the chamber, at which time the testing of the spacecraft electrical systems is carried out. Since some spacecraft systems are actually energized at some time prior to booster firing, it is desirable to simulate early portions of the spacecraft flight as closely as possible. To accomplish this, the 7- × 14-ft chamber was connected to the wind-tunnel compressors in the same manner as that used to evacuate the 25-ft Space Simulator. With this large pumping capacity, changes in pressure from local atmospheric conditions to about 1/10 of atmospheric pressure are accomplished in the test chamber at rates approximating the actual launch pressure changes in this range of altitudes. Fig. 3 compares the launch pressure profile of the *Ranger 6* flight with a profile of a test recently conducted on the *Ranger* PTM in the 7- × 14-ft chamber.

D. *Ranger 6* Trajectory Analysis

1. *Launch Phase*

The *Ranger 6* spacecraft was launched at 15:49:09.09 GMT on January 30, 1964, from the Atlantic Missile Range (now the Air Force Eastern Test Range) using the *Atlas D–Agena B* boost vehicle. After liftoff, the booster rolled to a launch azimuth of 95.0 deg (east of north) and performed a programmed pitch maneuver until booster cutoff. During the sustainer and vernier stages, adjustments in vehicle attitude and engine cutoff times were commanded as required by the ground guidance computer to adjust the altitude and velocity at *Atlas* vernier engine cutoff. After *Atlas–Agena* separation, there was a short coast period prior to the first ignition of the *Agena* engine. At a preset value of sensed velocity increase, the *Agena* engine was cut off. At this time the *Agena* and spacecraft combination was coasting in a nearly circular parking orbit. After a prescribed coast time in the parking orbit, the second ignition of the *Agena* engine was initiated. The parking orbit coast time, as determined by the ground guidance computer, was transmitted to the *Agena* during the *Atlas* vernier stage. The ascent trajectory profile is shown in Fig. 4; a sequence of events from launch to acquisition of the Earth by the spacecraft is shown in Fig. 5.

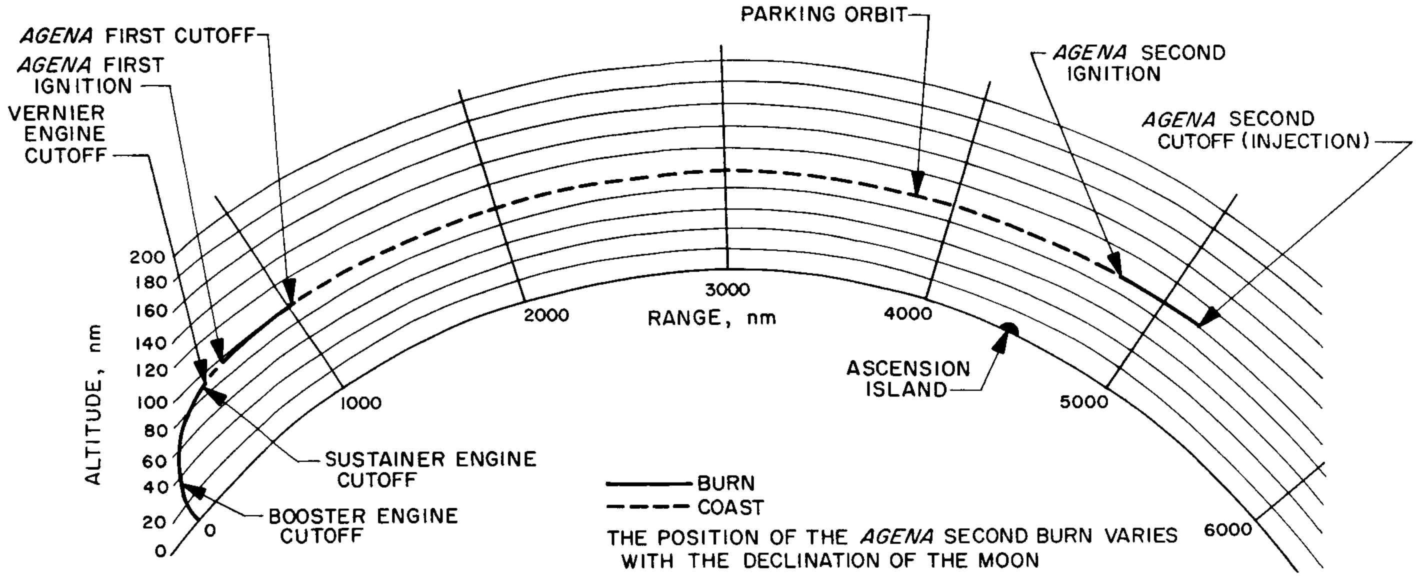

Fig. 4. Ascent trajectory profile

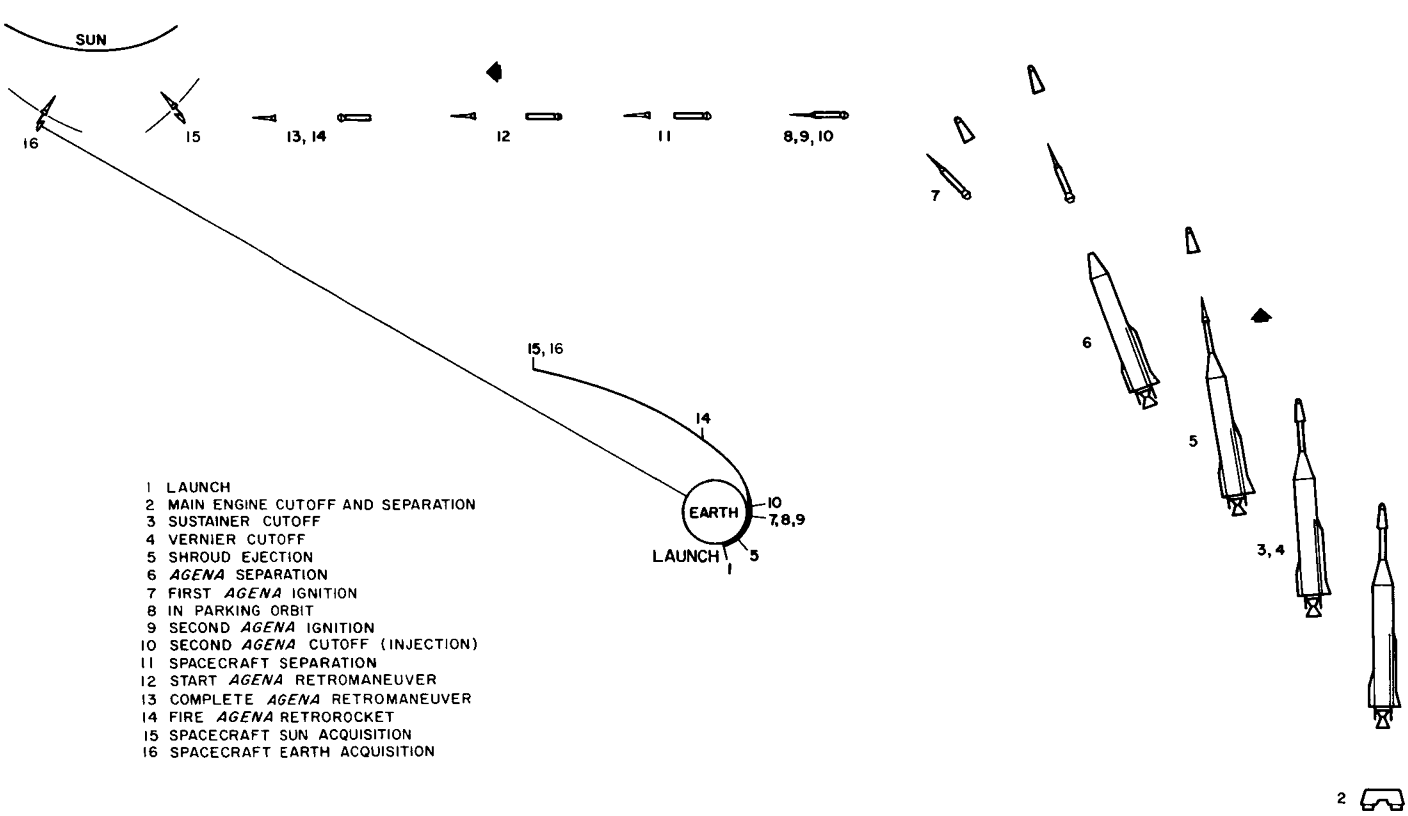

Fig. 5. Sequence of events to Earth acquisition

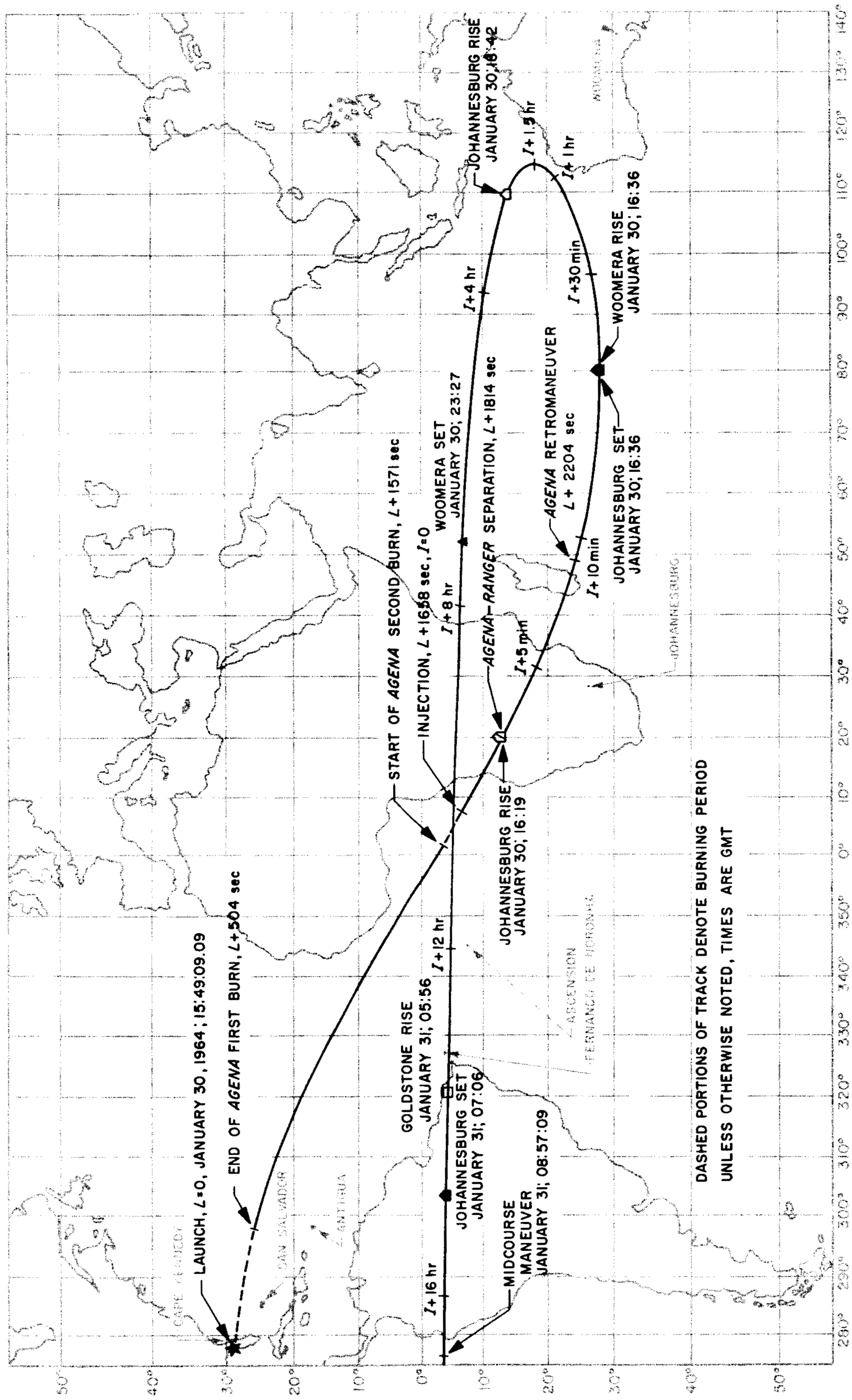

Fig. 6. Earth track *Ranger 6* trajectory

2. Cruise Phase

Injection into lunar orbit (termination of the boost phase) occurred at 16:16:47 GMT, at which time the *Agena* and spacecraft were traveling at a speed of 10.968 km/sec (inertial). The geocentric latitude and longitude were −7.19 and 8.05 deg, respectively, with injection taking place over the western coast of South Africa. The *Agena* and spacecraft separated 2.6 min after injection occurred. The *Agena* then performed a programmed 180-deg yaw maneuver and ignited its retrorocket. The retrorocket impulse was designed to eliminate interference with the spacecraft operation and reduce the chance of the *Agena* impacting the Moon. Tracking data indicated that the *Agena* did miss the Moon's surface by approximately 3630 km on the northern trailing edge.

Within 1 hr after injection, the spacecraft was receding from the Earth in almost a radial direction with decreasing speed. This reduced the geocentric angular rate of the spacecraft (in inertial coordinates) until, at 1.5 hr after injection, the angular rate of the Earth exceeded that of the spacecraft. This caused the Earth track of the spacecraft to reverse its direction from increasing to decreasing Earth longitude (Fig. 6). Plots of the geocentric distance and speed of the probe as well as the Earth-probe-Sun (EPS), Sun-probe-Moon (SPM), and Earth-probe-Moon (EPM) angles versus time from launch are presented in Figs. 7 through 9.

Tracking data gathered and reduced during the first 6 hr after injection indicated that the spacecraft would miss the Moon on the leading edge, with a closest approach altitude of 809 km at a selenographic latitude and longitude of −9 and 191 deg, respectively. The lunar transit time from injection was then 64.64 hr. The *Ranger 6* transfer trajectory is illustrated in Fig. 10.

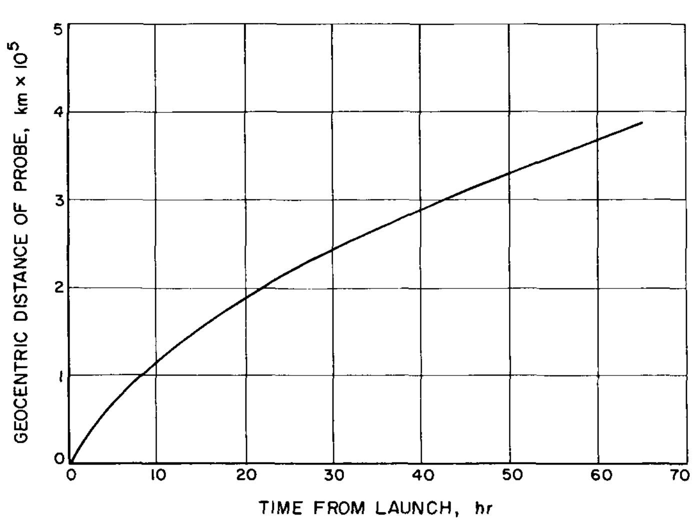

Fig. 7. Geocentric distance of probe vs time from launch

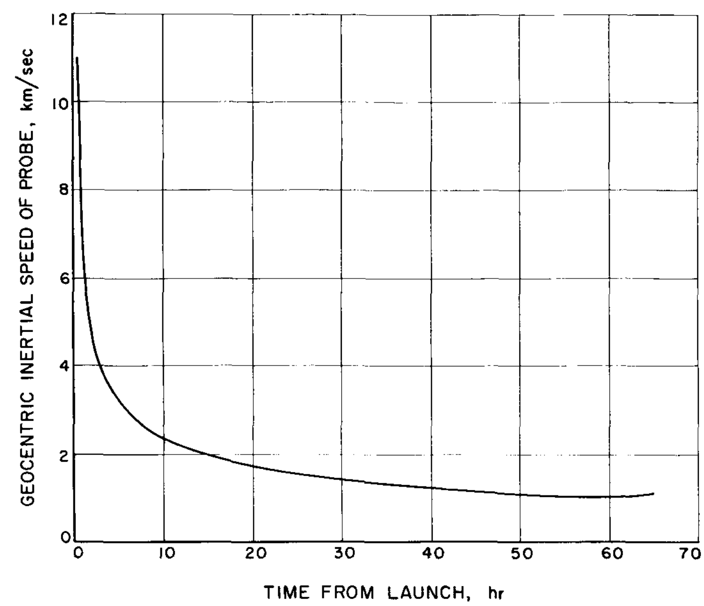

Fig. 8. Geocentric inertial speed of probe vs time from launch

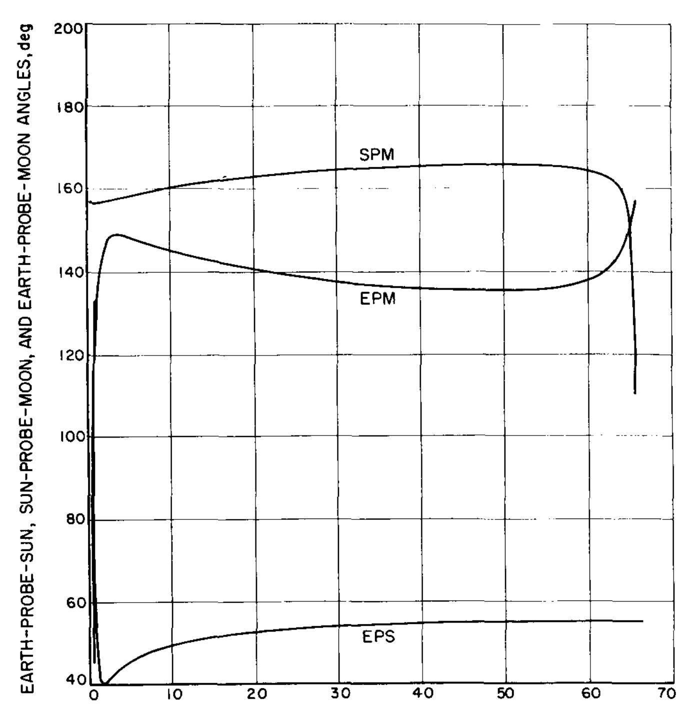

Fig. 9. Earth-probe-Sun, Sun-probe-Moon, and Earth-probe-Moon angles vs time from launch

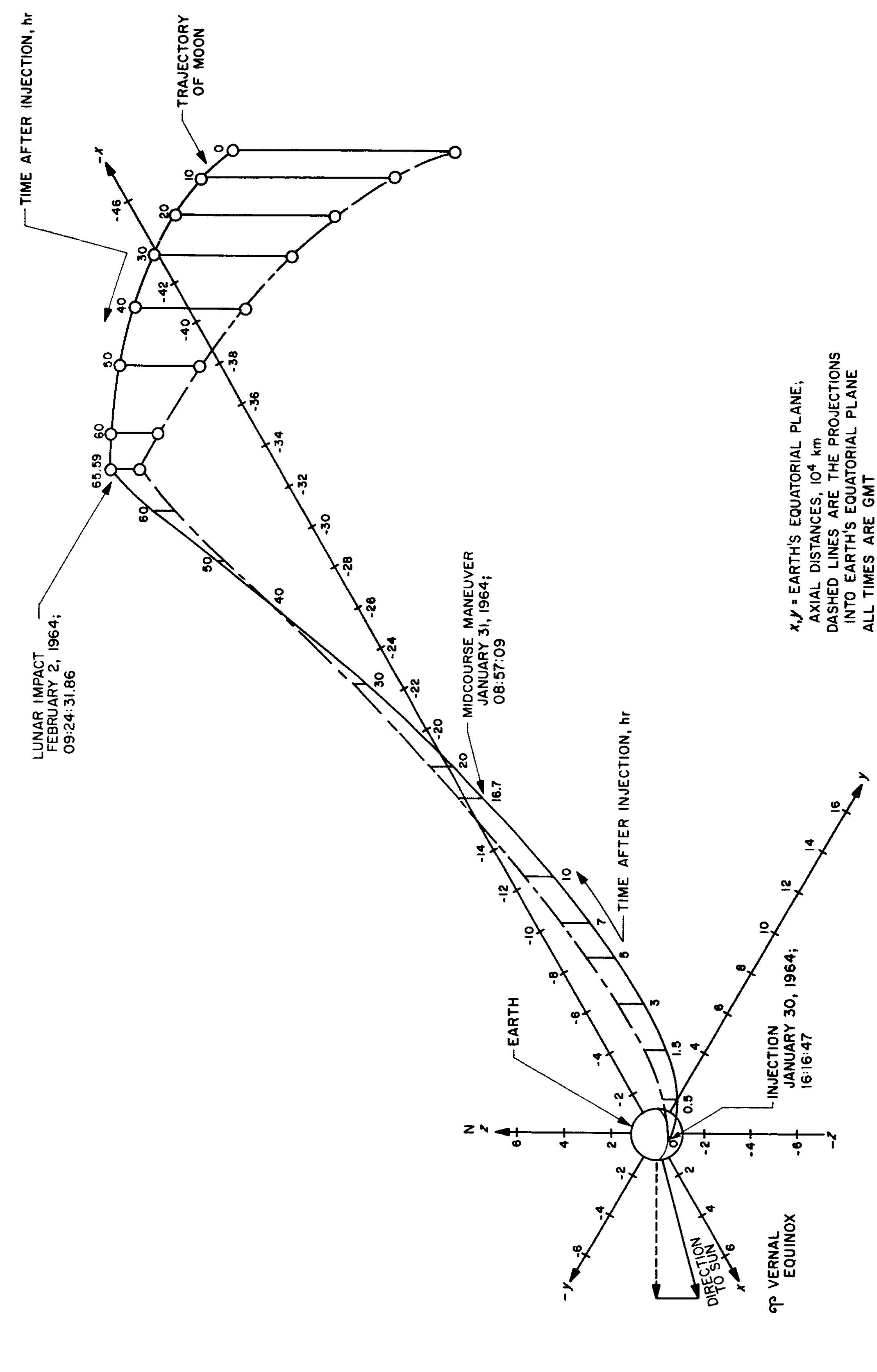

Fig. 10. ***Ranger 6 transfer trajectory***

3. *Midcourse Maneuver Phase*

The midcourse maneuver was calculated to adjust the trajectory to impact at a selenographic latitude of 8.5 deg and a selenographic longitude of 21.0 deg, with a flight time from injection to impact of 65.129 hr. The adjustment of impact time was made to utilize the TV camera backup turn-on clock as designed. The commanded speed change was 41.27 m/sec. To properly align the thrust direction of the midcourse motor for the maneuver, a −11.96-deg roll turn and −70.98-deg pitch turn were commanded. The midcourse motor was ignited at 08:57:09 GMT on January 31, 1964, at which time the spacecraft was at a geocentric distance of 170,000 km, traveling with an inertial speed of 1.891 km/sec relative to Earth. At the end of the 67-sec burn duration of the midcourse motor, the geocentric distance had increased to 170,125 km and the inertial speed relative to Earth was reduced to 1.852 km/sec. Analog data received at the Goldstone Tracking Station and relayed to the JPL Space Flight Operations Facility gave every indication that the midcourse maneuver was executed exactly as commanded. This was further verified by the observed doppler data, which were essentially the same as those predicted for the maneuver. Injection and encounter conditions for the premidcourse orbit used to determine the midcourse maneuver are given in Table 1.

Table 1. Orbit used for determination of the *Ranger 6* midcourse maneuver

Injection conditions[a]	
Epoch	January 30, 1964; 16:16:41.0 GMT
Earth-fixed sphericals	
R	6567.0215 km
ϕ	−6.8722887 deg
θ	7.4732279 deg
V	10.551346 km/sec
γ	1.2443904 deg
σ	118.93418 deg
Inertial Cartesians	
x	6103.6462 km
y	2292.1199 km
z	−785.78784 km
$\dot{x}$	−3.7715114 km/sec
$\dot{y}$	8.9531506 km/sec
$\dot{z}$	−5.0943372 km/sec
Encounter conditions and miss parameters	
Closest approach	February 2, 1964; 08:54:31 GMT
Selenocentric altitude	813 km
Selenocentric latitude	−9.6 deg
Selenocentric longitude	191.1 deg
Time of flight from injection	64.63 hr[b]
$\mathbf{B}$	4813 km[c]
$\mathbf{B \cdot T}$[d]	−4518 km
$\mathbf{B \cdot R}$[d]	1660 km

[a] See Table 2 for definition of terms.
[b] 1σ uncertainty of 66 sec.
[c] 1σ uncertainty of 79.5 km.
[d] $\mathbf{B \cdot T}$ and $\mathbf{B \cdot R}$ are referenced to the true lunar equator (Fig. 11). (For *Ranger 6* work, the true lunar equator is used as the reference plane. If $\mathbf{N}$ is a unit vector in the lunar north direction, then $\mathbf{T} = \mathbf{S}_I \times \mathbf{N}$ and $\mathbf{R} = \mathbf{S}_I \times \mathbf{T}$.)

Table 2. Definition of terms

Parameter	Definition (Earth as central body)
x, y, z	Vernal equinox Cartesian coordinates in a geocentric equatorial system. The origin is the center of the central body. The principal direction (x) is the vernal equinox direction of date, and the principal plane (x, y) is the Earth equatorial plane of date. z is along the direction of the Earth's spin axis of date, km.
$\dot{x}, \dot{y}, \dot{z}$	First time derivatives of x, y, and z, respectively; i.e., Cartesian components of the probe space-fixed velocity vector, km/sec.
R	Probe radius distance, km
ϕ	Probe geocentric latitude, deg
θ	Probe east longitude, deg
V	Probe Earth-fixed velocity, km/sec
γ	Path angle of the probe Earth-fixed velocity vector with respect to the local horizontal, deg
σ	Azimuth angle of the probe Earth-fixed velocity vector measured east of true north, deg

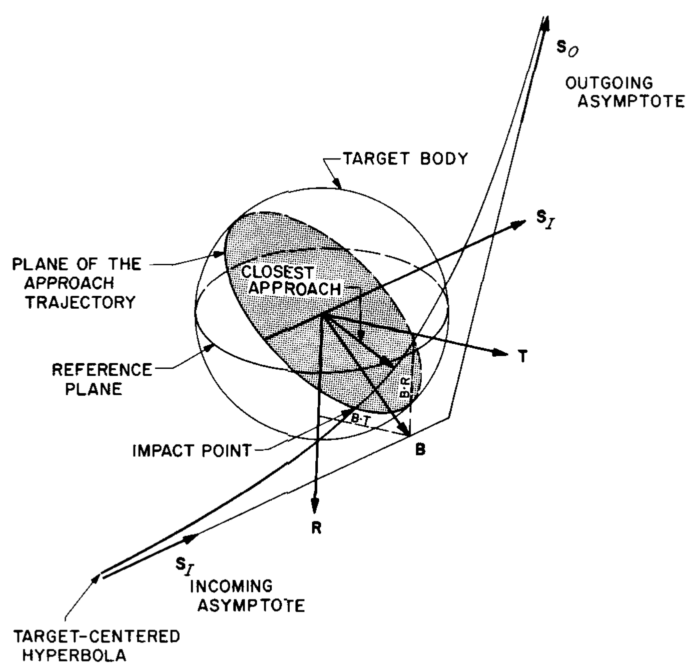

Fig. 11. Definition of the miss parameter B

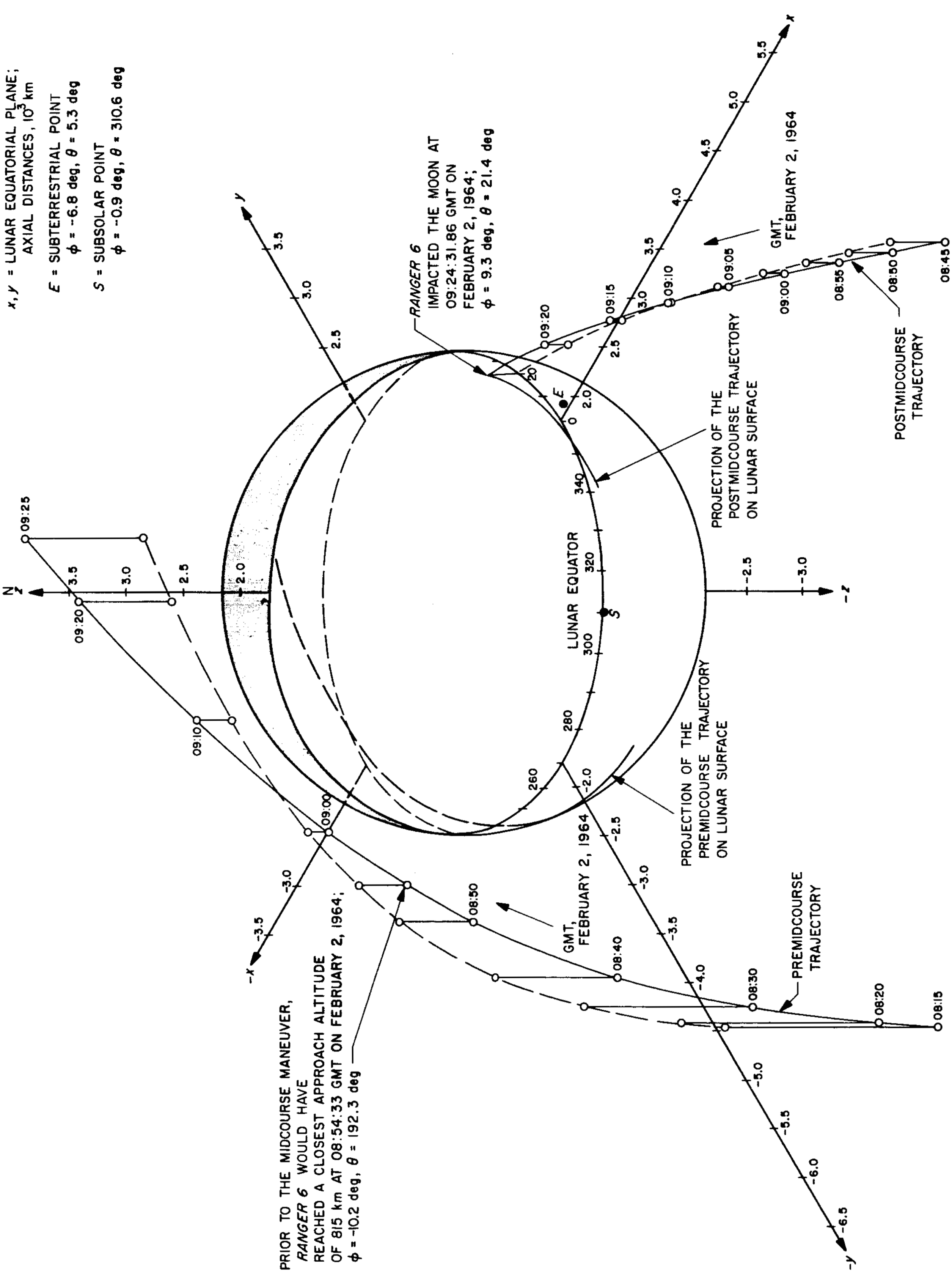

Fig. 12. *Ranger 6* premidcourse and postmidcourse encounter trajectories

4. Postmidcourse Maneuver Cruise Phase

Following the midcourse maneuver, the spacecraft reacquired the Sun and Earth, thus returning to the cruise mode on its way to lunar impact. At about 59 hr from injection, the spacecraft experienced a minimum inertial velocity of 1.029 km/sec relative to the Earth. This gave evidence that the spacecraft was being accelerated towards the Moon by lunar gravity.

5. Encounter Phase

Postmidcourse tracking data to within 1 hr after impact were reduced during flight and resolved the encounter conditions to a high degree of confidence. Lunar impact was indicated to occur at a selenocentric latitude and longitude of 9.39 and 21.51 deg, respectively. Impact time, as determined by accurate recordings of telemetry signal termination, was at 09:24:31.86 GMT on February 2, 1964. The encounter conditions and the corresponding postmidcourse conditions are tabulated in Table 3.

The spacecraft descended upon the Moon in a somewhat grazing trajectory with an angle at impact of 47 deg from the vertical. The traces of the final portions of the premidcourse and postmidcourse trajectories are illustrated in Fig. 12. Figs. 13 through 17 present trajectory parameters plotted versus GMT prior to impact of the *Ranger 6* spacecraft on the Moon.

Table 3. Last postmidcourse orbit of *Ranger 6*

Postmidcourse conditions[a]	
Epoch	January 31, 1964; 08:58:21 GMT
Earth-fixed sphericals	
R	170130.42 km
ϕ	−3.5973897 deg
θ	276.78513 deg
V	12.154424 km/sec
γ	8.5337484 deg
σ	271.02087 deg
Inertial Cartesians	
x	−169769.50 km
y	−2954.4363 km
z	−10674.843 km
$\dot{x}$	−1.8068983 km/sec
$\dot{y}$	−0.39521089 km/sec
$\dot{z}$	0.10056300 km/sec
Impact parameters	
Impact epoch	February 2, 1964; 09:24:32.18 GMT
Selenocentric latitude	9.39 deg
Selenocentric longitude	21.51 deg
Time of flight from injection	65.59 hr[b]
$\mathbf{B}$	2859 km[c]
$\mathbf{B \cdot T}$[d]	2754 km
$\mathbf{B \cdot R}$[d]	−768 km

[a] See Table 2 for definition of terms.
[b] 1σ uncertainty of 1.6 sec.
[c] 1σ uncertainty of 21.3 km.
[d] $\mathbf{B \cdot T}$ and $\mathbf{B \cdot R}$ are referenced to the true lunar equator (Fig. 11). (For *Ranger 6* work, the true lunar equator is used as the reference plane. If $\mathbf{N}$ is a unit vector in the lunar north direction, then $\mathbf{T} = \mathbf{S}_I \times \mathbf{N}$ and $\mathbf{R} = \mathbf{S}_I \times \mathbf{T}$.)

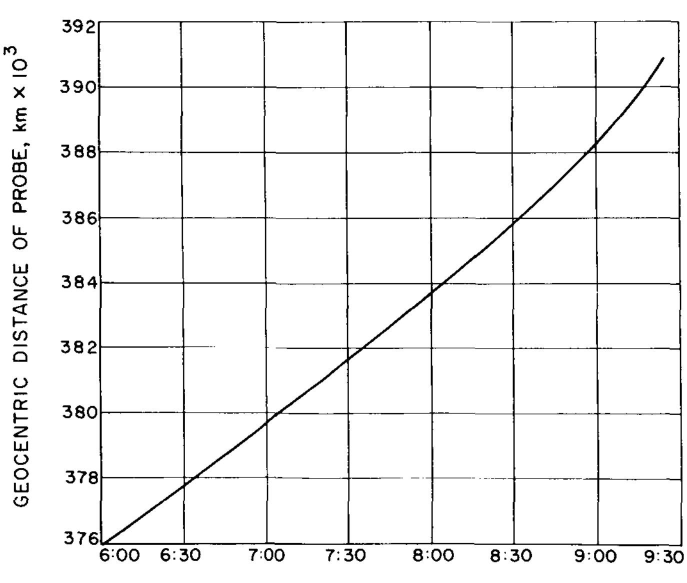

Fig. 13. Geocentric distance of probe vs GMT at lunar encounter

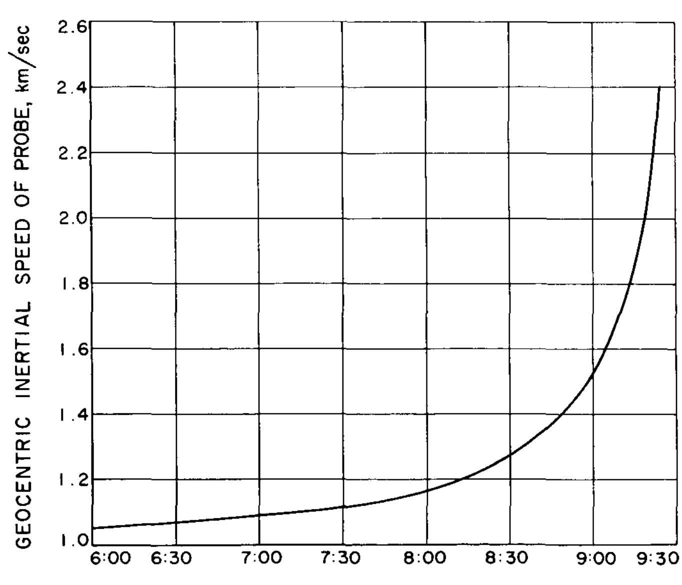

Fig. 14. Geocentric inertial speed of probe vs GMT at lunar encounter

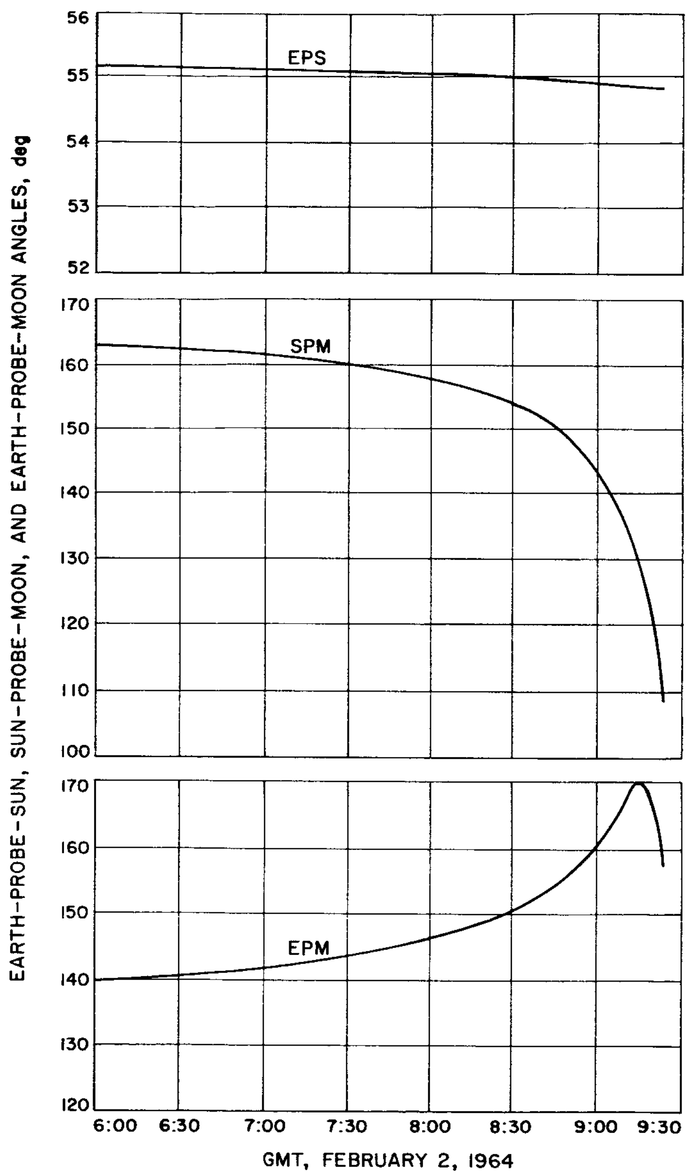

Fig. 15. Earth-probe-Sun, Sun-probe-Moon, and Earth-probe-Moon angles vs GMT at lunar encounter

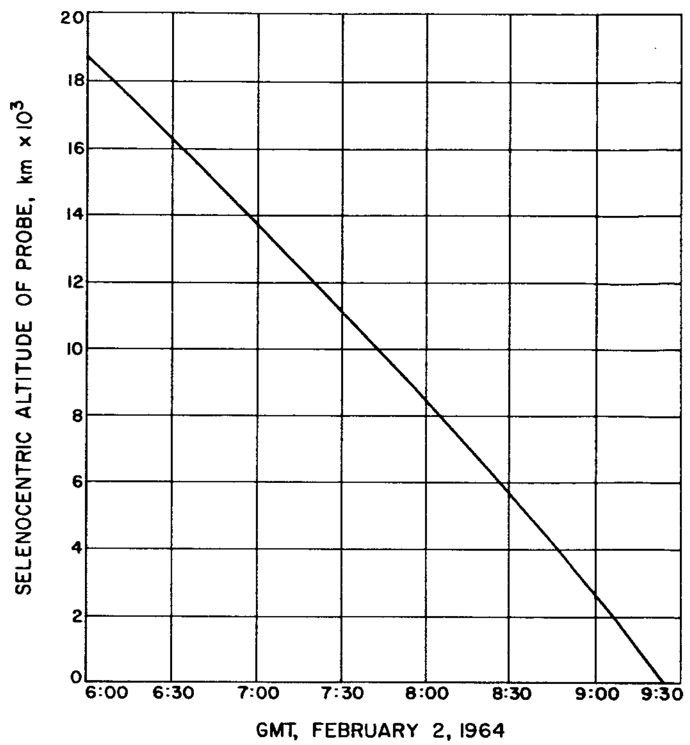

Fig. 16. Selenocentric altitude of probe vs GMT at lunar encounter

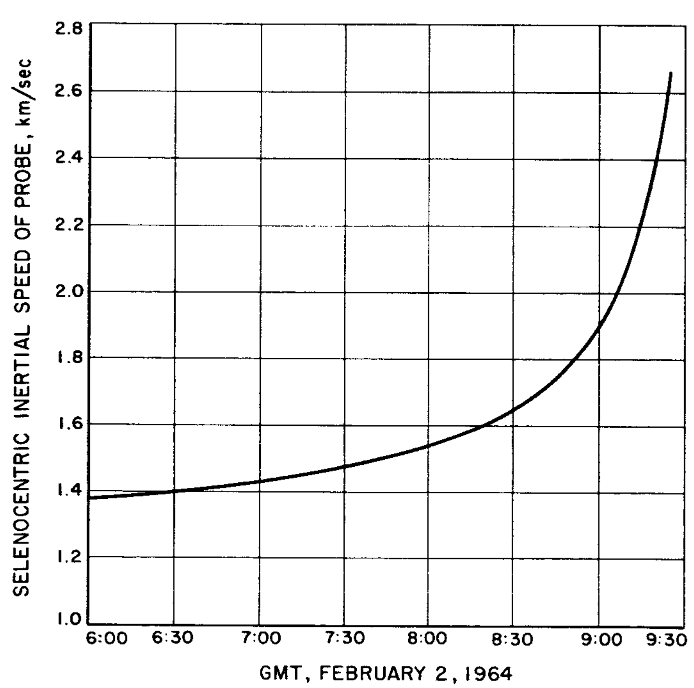

Fig. 17. Selenocentric inertial speed of probe vs GMT at lunar encounter

II. *Surveyor* Project

A. Introduction

The *Surveyor* Project will take the next step in developing lunar technology by attempting soft landings on the Moon, beginning in 1965 with a group of test missions whose objective is to demonstrate successful soft landing by post-landing spacecraft operation. An engineering payload including elements of redundancy, diagnostic telemetry, touchdown instrumentation, and survey TV will be used.

The general objective after 1965 is to conduct lunar exploration to extend our knowledge of the nature of the Moon and to discover and verify the suitability of sites for *Apollo* spacecraft landings. The flights planned for 1966 will carry a scientific payload selected from the following experiments: two-camera TV, micrometeorite ejecta, single-axis seismometer, alpha-particle scattering, soil properties (surface sampler), and touchdown dynamics.

In 1965 and 1966, the 2150-lb (separated weight) spacecraft will be injected into the lunar trajectory by direct ascent, using single-burn *Atlas–Centaur* vehicles. The midcourse correction capability will be 50 m/sec in 1965 and 30 m/sec in 1966.

Hughes Aircraft Company is under contract to develop and manufacture the first seven spacecraft.

B. Spacecraft System Development

The following material relating to the *Surveyor* spacecraft system development was prepared by the Hughes Aircraft Company. The principal model designations and vehicles discussed are defined in Table 1.

Table 1. Model and vehicle designations

Designation	Description
SC-1–4	Flight spacecraft with engineering payload
SC-5–7	Flight spacecraft with scientific payload
A-21	Model designation for spacecraft with engineering payload (SC-1–4)
A-21A	Model designation for spacecraft with scientific payload (SC-5–7)
T-21	Model A-21 prototype system test spacecraft
T-21A	Model A-21A prototype system test spacecraft
T-2	Simplified spacecraft for evaluation of terminal descent propulsion and flight control
S-2	Test spaceframe for vibration, shock, and static structural tests
S-6, -7	Test spaceframe for vernier propulsion system tests
S-8	Test spacecraft for flight control buzz tests

System engineering. The A-21 spacecraft configuration has received structural improvements as a result of dynamic testing of the S-2 vehicle; definition of configuration details for the A-21A spacecraft is continuing. A 3-wk project review was conducted by JPL. The SD-1 and SD-2 spacecraft dynamic models for use in *Centaur* tests were flight acceptance tested and delivered to General Dynamics, Astronautics Division.

Scientific payload. In connection with the revised scientific payload, command and data channel requirements have been determined and details of integrating the instruments and their auxiliaries into the spacecraft are being determined. Preliminary payload test plans have been prepared, and test equipment is being received and checked out.

System analysis. The analyses reported include (1) a determination of impact speeds for direct ascents in 1965 and 1966, (2) an evaluation of spacecraft shadowing by the Moon for night landing, (3) derivation of mission operating time for the Space Technology Laboratories (STL) vernier engines, (4) formulation of relationships between injection conditions and launch parameters for direct ascent, (5) derivation of a method for computing maximum midcourse correction capability for particular missions, (6) a determination of vernier propellant requirements by a Monte Carlo simulation, (7) a study of television mirror stepping accuracy as it affects lunar surface coverage, (8) a TV color filter analysis, (9) an evaluation of allowable phase jitter in the spacecraft transmitter, and (10) a review of Earthshine effects on the secondary Sun sensor.

Flight control. Study of incorporating the MIRA 150A vernier engine indicates that the flight control system will require modifications in both the midcourse maneuver and terminal descent programs. Type approval testing of the secondary Sun sensor was completed.

Electronics. Out-of-tolerance performance of transmitter and receiver oscillator modules under vibration was corrected by development of a crystal isolation mount. The accuracy of omnidirectional antenna pattern measurements is being investigated in view of newly discovered effects of range reflections. Provisions for decoding commands for safety dumping of the nitrogen and helium supplies prior to launch have been incorporated in the engineering mechanisms auxiliary; a modified unit has been successfully tested. Circuit changes to prevent extraneous command pulses on power removal from the central command decoder have been breadboard tested and are being incorporated in the type approval model. A prototype altitude marking radar with thermal control improvement is nearly ready for test.

Electrical power supply. The first flight-type solar panel has successfully completed flight acceptance testing. Prototype main batteries with a new cell design have completed type approval dynamic tests. The auxiliary battery completed the type approval program successfully. Redesign of the boost regulator and battery charge regulator substantially increased efficiency.

Thermal control. Thermal control techniques applicable to the MIRA 150A venier engine are under study. A lunar horizon simulator was defined for thermal-vacuum testing the T-21 and flight spacecraft. The transit thermal management program, now complete, can analyze the 66-hr period with 5 min of computer time. An initial operational and thermal evaluation of the Hughes S-4 solar simulator was made, and a test with MT-1 Sector I will be made in July to compare results with the S-4 to those from the JPL facilities.

Engineering mechanics. Two shock absorbers tested to destruction failed at loads safely higher than the design condition; another unit successfully withstood four cycles of vibration at type approval levels. Plans for retesting the upgraded S-2 dynamic test vehicle (S-2A) have been completed. Structural tests of curved tube sections for possible use with the antenna/solar panel positioner were made.

Propulsion. Preparations are continuing for conducting the last two planned developmental firings of the retro-engine at Arnold Engineering Development Center (AEDC) in July. The ten retro-engines for quality assurance testing have been loaded and prefiring conditioning has started. The Space Technology Laboratories MIRA 150A has been designated by JPL as the vernier engine, and procurement and development to accommodate this new engine are underway. Vernier system loading and unloading tests using the S-7 vehicle are proceeding at the Air Force Missile Development Center (AFMDC). A 7 Al-4 Mo titanium helium tank under development performed satisfactorily in a burst test. A 7178-T6 aluminum propellant tank with tungsten inert-gas welds has completed development and will be used to support the spacecraft test program.

Spacecraft vehicle and mechanisms for basic bus. A 4-wk upgrade of the T-21 spacecraft was completed in May, and preparations are being made for a July upgrade to precede vibration, shock, and thermal-vacuum testing. Design and fabrication of the T-21A structure is continuing. The S-2 vehicle was updated, and the S-8 buzz test vehicle is being built. New structure was designed to support the MIRA 150A vernier engines. Preparations are being made to employ the T-1 vehicle in retro-engine separation tests. Redesign of the antenna/solar panel positioner to meet higher design loads has been completed. Improved stepping repeatability has been achieved in the TV mirror drive motors through development of a new detenting mechanism. Three sets of equipment comprising the separation sensing and arming device have been flight acceptance tested.

Reliability, quality assurance, and system test. As a result of reliability and quality assurance investigations, a design improvement in the subcarrier oscillator was made and improved inspection and test procedures formulated. A quality assurance plan for Hughes operations at Goldstone has been issued.

In the attempts to conduct the first balloon drop test of the T-2 descent test vehicle at AFMDC, the vehicle was accidentally released and the recovery provisions disabled so that T-2 was destroyed; a thorough investigation indicated that the squib firings which caused the accident probably were initiated by static electrical discharge. The spare vehicle, T-2S, has been built up and verification tests of the improved release and recovery system are imminent. The T-2H helicopter tests over varying terrain with the QA-1 radar altimeter and doppler velocity sensor are approaching completion. Following upgrade of the T-21 spacecraft, system tests resumed with certain subsystem functional testing, to be followed by mission sequence and RFI tests. Design of the scientific instrument STEA is nearly completed.

Mission operations. Spacecraft initial acquisition tests using the Hughes S-band ground transponder were conducted at Goldstone, including use of the transponder in helicopter flights simulating the mission trajectory.

Lunar roving vehicle study (LRV). A study of the feasibility of integrating LRVs of two different designs (Bendix and General Motors) into the *Surveyor* spacecraft was completed. Detailed weight, center of gravity, and configuration analyses were conducted for 12 spacecraft configurations. It was concluded that either LRV can be fitted into the spacecraft.

THE PLANETARY-INTERPLANETARY PROGRAM

III. *Mariner* Project

A. Introduction

The early objective of the Planetary-Interplanetary Program is the initial probing of the planets Mars and Venus by unmanned spacecraft. The initial probing of Venus was successfully accomplished by *Mariner 2*. The next step toward this objective is the initial probing of Mars by a *Mariner C* spacecraft planned for the 1964–1965 opportunity.

The primary objective of the *Mariner C* mission (*Mariner* Mars 1964 Project) is to conduct close-up (flyby) scientific observations of the planet Mars during the 1964–1965 opportunity and to transmit the results of these observations back to Earth. The planetary observations should, to the greatest practicable extent, provide maximum information about Mars. A TV system and a reasonable complement of field and particle experiments will be carried.

A secondary objective is to provide experience and knowledge about the performance of the basic engineering equipment of an attitude-stabilized flyby spacecraft during a long duration flight in space farther away from the Sun than the Earth. An additional secondary objective is to perform certain field and/or particle measurements in interplanetary space during the trip and in the vicinity of Mars.

It is planned to conduct two launchings of *Mariner C* missions from two separate pads. All activities will be planned to exploit the limited launch period to the maximum extent. To accomplish this, spacecraft and launch vehicles will be processed in parallel, so that following the launch of the first space vehicle the second vehicle may be launched without delay, no earlier than two days after the first.

Both *Mariner C-2* and *C-3* spacecraft have completed system test series which were very successful. Problems were uncovered, isolated, and corrected.

The ultraviolet photometer was removed from the spacecraft. Investigation revealed that this experiment had caused an arcing which obliterated all the TV data in a previous system test. It was not considered possible to complete a redesign of the experiment to correct this problem and unequivocally qualify the design in time to meet the launch date.

An occultation experiment was approved for the mission. The only effects of including this experiment were a change of aiming point (at Mars) and a minor change in spacecraft hardware, consisting of repositioning the limits and stowed position of the scan platform. The data obtained from this experiment should provide invaluable information regarding the scale height and pressure in the atmosphere of Mars.

B. Spacecraft Systems Testing

1. *Mariner C-2 and C-3*

Subsystem tests, ground integrity tests, and interfacing tests for *Mariner C-2* were completed. The first system test was very successful; only minor problems were encountered. Attitude-control leak tests showed that some torquing had to be performed after detection of a large leak; the leak rate after this corrective action was satisfactory.

Mariner C-3 subsystem tests, system interface tests, and partial ground checks are being performed as the hardware is delivered and installed. A system test was satisfactorily completed.

Mariner C-2 and *C-3* spacecraft were mated to the three flight shroud-adapter systems (Figs. 1 and 2). The following tests were performed: (1) spacecraft/shroud system verification, (2) mating combinations of shroud systems and spacecraft, (3) electrical continuity checks on adapter inflight connector cables, (4) RF compatibility checks between shroud and spacecraft systems, (5) mating procedures verification, and (6) spacecraft dummy runs.

During these tests, mechanical operations were quite successful. The problems which did occur concerned:

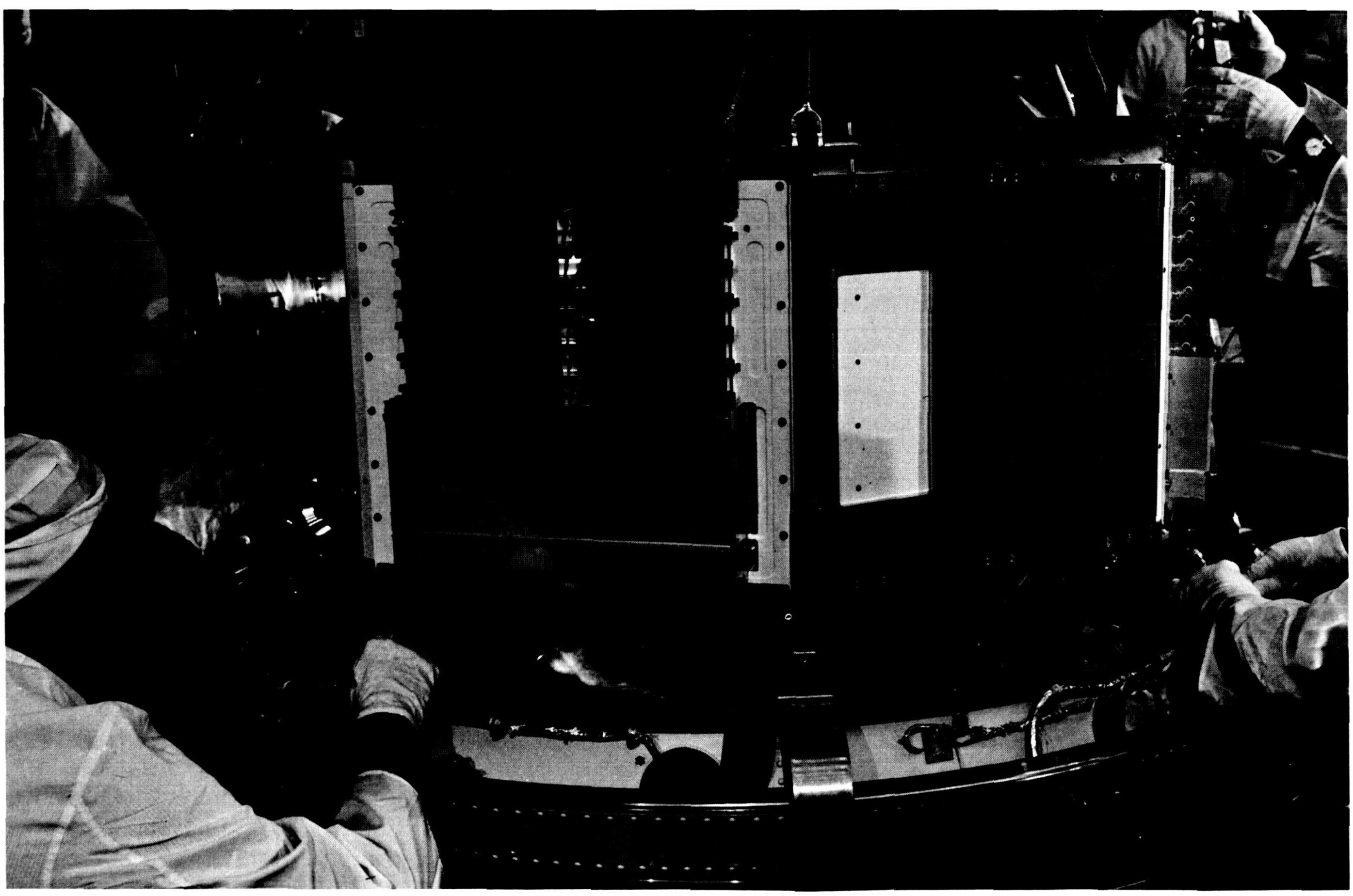

Fig. 1. Spacecraft being mated to the adapter

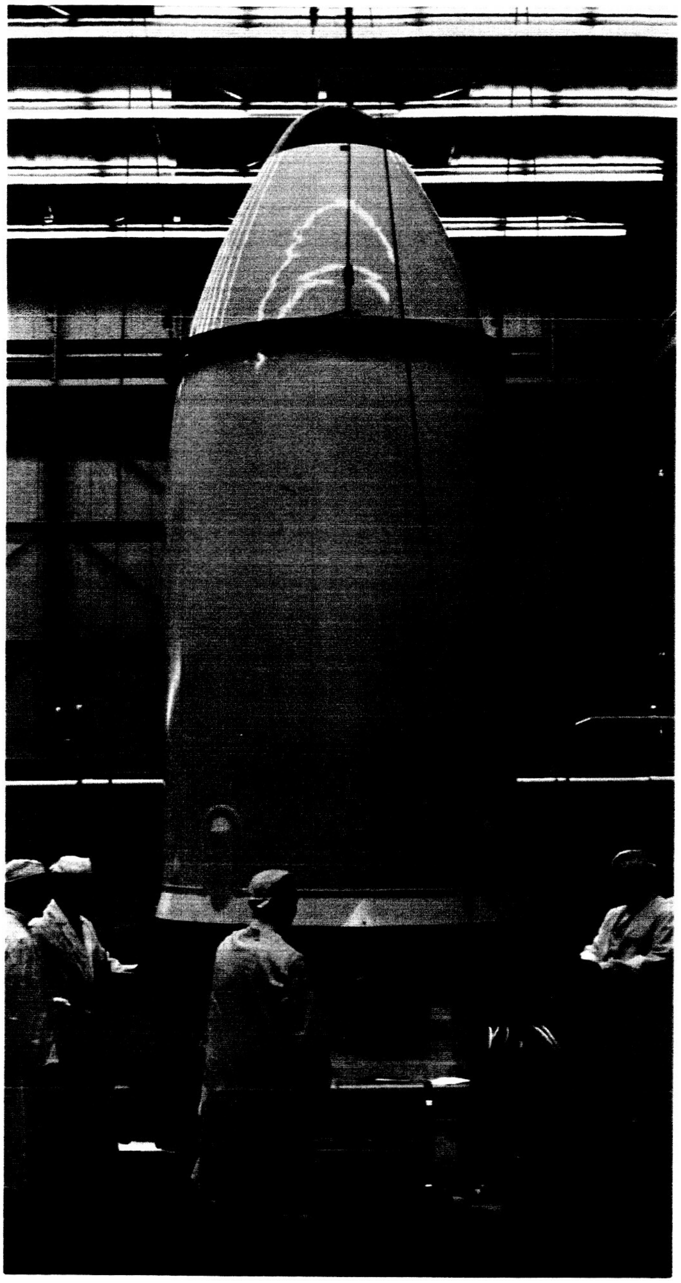

Fig. 2. Encapsulated shroud-spacecraft system being removed from trailer

(1) certain time-consuming mating procedures, and (2) certain pieces of flight ground equipment that were not available.

2. Mariner C-1 (Proof Test Model)

A system verification test and a thermal verification test were performed. The tests were satisfactory, with the preliminary results indicating no problems. Design of the temperature control shields installed on the spacecraft was changed primarily to reduce weight.

A pre-countdown test was made to check out the compatibility of the launch complex equipment with the spacecraft and the evolution of the procedures that will be used for the launch pad activities. All systems functioned normally. Throughout the test the spacecraft was radiated electromagnetically. Preliminary results showed that the spacecraft is unaffected by off- and on-board sources in the launch configuration with the shroud on. 100 w of S-band power were radiated from the spacecraft omni-antenna; the results indicated that there is no danger of the squibs being activated by this relatively high-powered RF environment.

Two countdowns were performed. The first countdown was a short one in which the spacecraft was conditioned into the launch mode and evaluation was limited essentially to the observation of the telemetry signals; the second countdown exercised the spacecraft extensively by using all of the umbilical and RF command links. All systems performed as designed.

The pyrotechnic shock test was conducted. The test consisted of activating the pyrotechnic explosive device that releases the shroud V-band and the spacecraft V-band, as well as the spacecraft pyrotechnics that release the solar panels and scan platform. The results indicated that the spacecraft can survive these environments without difficulty; although, when the shroud V-band is released, pellet-like fragments from the explosive bolts are discharged and it is not known at this time whether they can penetrate the shroud and damage the spacecraft.

The simulated midcourse interaction test was performed (Fig. 3). Objectives of the test were to verify that the autopilot subsystem was capable of maintaining and controlling the spacecraft attitude during burning of the postinjection propulsion system motor and to verify that the dynamic properties of the spacecraft structure did not have a harmful effect on the autopilot performance. The test was concluded successfully.

The following tests were conducted in order to verify the design and operational compatibility between the spacecraft and the Space Flight Operations System:

Real-time system tests. A series of these tests was conducted during the *Mariner* proof test model (PTM) and flight spacecraft system tests on a noninterference basis with the Spacecraft Assembly Facility. The spacecraft transmitted telemetry data in real time to the Deep Space

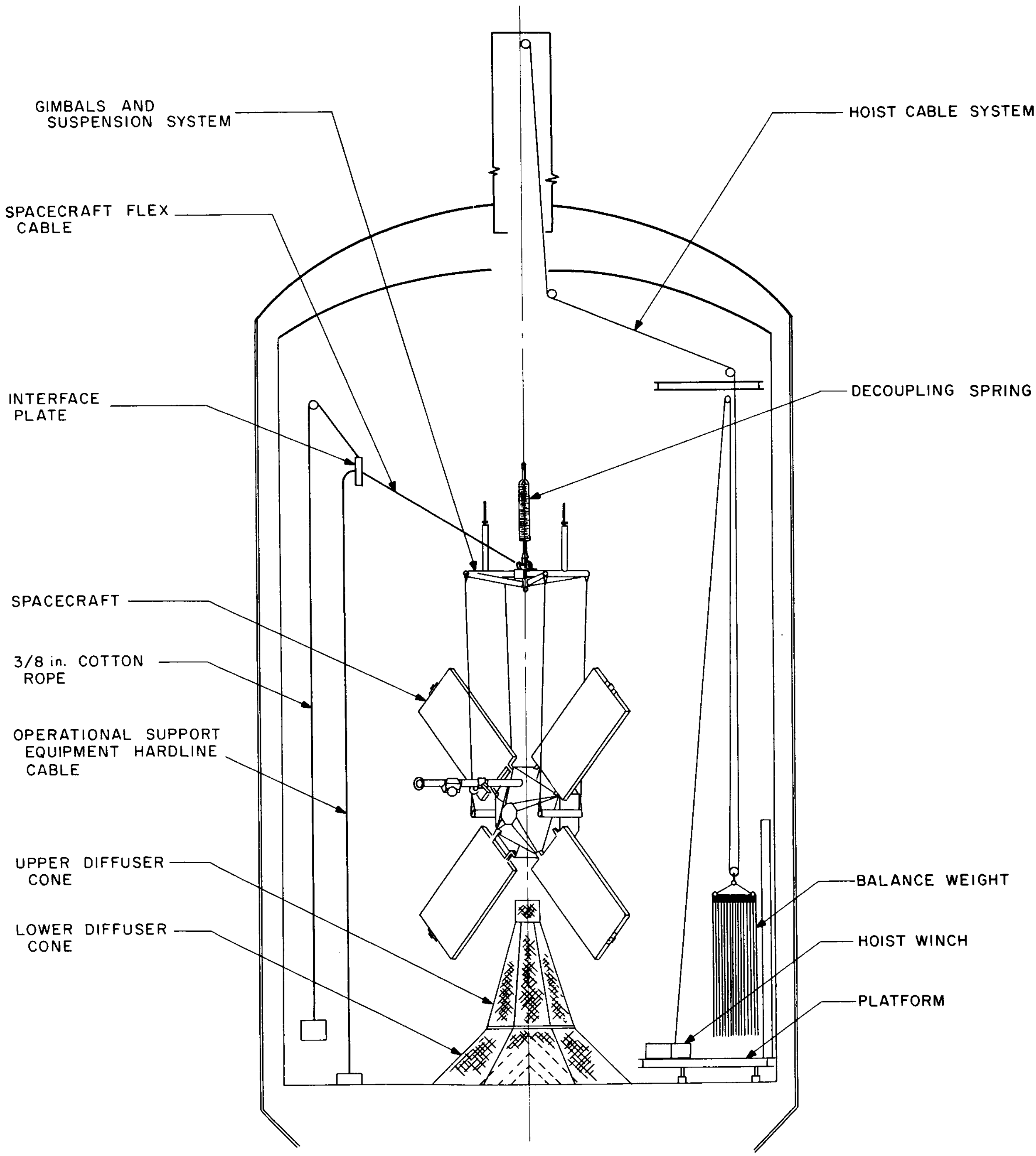

Fig. 3. Simulated midcourse interaction test in the 25-ft Space Simulator

Instrumentation Facility (DSIF) ground data handling system. The teletype encoder output then transmitted to the Space Flight Operations Facility (SFOF) data processing system in real time through the SFOF communications system. The SFOF received, processed, and displayed the data being received for examination by the analysis groups. Anomalies and problem areas were investigated and are being corrected.

Real-time closed loop test. The spacecraft PTM was operated through discrete portions of the flight in corresponding periods of time. These periods covered the spacecraft events from launch minus 30 min through planet postencounter. The data processing system in the SFOF received, processed, and displayed the telemetry data in real time. This data was then analyzed by the analysis groups. All spacecraft commands were used to verify their validity and the spacecraft reactions.

DSIF-SFOF compatibility test. This test was employed to verify the compatibility of the DSIF Pioneer site with the SFOF. *Mariner C* telemetry was inputted to the DSIF S-band receiver and then through the *Mariner C* demodulator and teletype encoder. The resultant data was forwarded to the SFOF, where it was compared with the original data. Anomalies and problem areas were investigated and corrected.

3. Spacecraft Separation Tests

Tests separating a mass, inertial, and geometrical mockup of the spacecraft from the adapter are being performed. The initial series of separation tests indicated the following results: (1) the spacecraft will separate from the *Agena* with a tipoff rate of less than the permitted 3 deg/sec; (2) the lanyard system originally designed to retain the separated V-band to the *Agena* does not prevent the band from hitting the spacecraft after separation; and (3) the system for measuring separation tipoff rates does not perform its assigned function.

A combination spring-lanyard system was developed for retaining the V-band to the *Agena* after separation. This design prevents the band from hitting the spacecraft after separation. An additional series of tests will be required to develop a separation-tipoff-rate measurement system that meets the requirements.

4. STM Testing

Followup vibration tests of the structural test model (STM) were conducted. The primary objectives were:

(1) Qualification as flight-type the hardware not on the STM during previous testing.

(2) Determination of better dynamic response information, particularly relative to the planet scan platform and the Canopus tracker.

(3) Better determination of the effects of propellant tank pressure on the dynamic response characteristics of the STM in the modes most affected by motion of the postinjection propulsion system.

Minor failures to flight-type hardware observed during the tests are being corrected. "Direct-write" plots of all low-frequency data have been examined, and further analysis will be made of the most significant data. Response information pertaining to the scan platform and the star tracker is being analyzed.

The tests showed that the higher propellant tank pressures produce an increase in the dynamic responses of the postinjection propulsion system support frame and the spacecraft structure. This increase was anticipated on the basis of previous test results. Loads produced were well within the structural capability of the postinjection propulsion system and the spacecraft structure.

C. Design and Development

1. Solar Panels

Analysis and verification tests of solar panel deployment indicated that it is safe structurally to eliminate the solar panel retarder and allow the panels to deploy unretarded. Implementation of the free-fall system required removal of the retarder, reversion back to two deploy springs per panel, modification of the thermal shield to cover the holes, and redesign of the cruise damper so that the unretarded rotational energy could be absorbed without damage to either the spacecraft or the solar panel.

Final tests were conducted to study the dynamic behavior of the solar panel-skid rail system when exposed to a simulated shroud impact due to a nonstandard shroud ejection. Results indicated that the skid rails provide conservatively adequate protection for the solar panel system during impact.

2. Low-Gain Antenna

The low-gain antenna is designed to provide a broad coverage, low-gain radiation pattern for use during the early portion of the *Mariner C* flight when the high-gain antenna is not pointed in the proper direction for communication. The antenna radiation pattern is approximately a cardioid of revolution with the maximum centered on the spacecraft $-z$-axis. Maximum gain is more than 6.0 db and more than 5.0 db for each of two frequency ranges.

The basic configuration of the low-gain antenna is a 4-in.-D round waveguide, 88 in. long. The base of the waveguide is mounted on the spacecraft bus, with the tube axis parallel to the spacecraft $-z$-axis, thus placing the radiating end 88 in. above the bus and solar panels. A tapered-helix mode launcher is used to launch a right-hand, circularly polarized mode (Fig. 4). A constant circumference taper from the round waveguide into an open-end cross propagates the waveguide mode (Fig. 5). Increased pattern control is realized by addition of a ground plane. Excessive back-directed, left-hand circularly polarized radiation is reduced by 16 parasitically excited monopoles behind the ground plane.

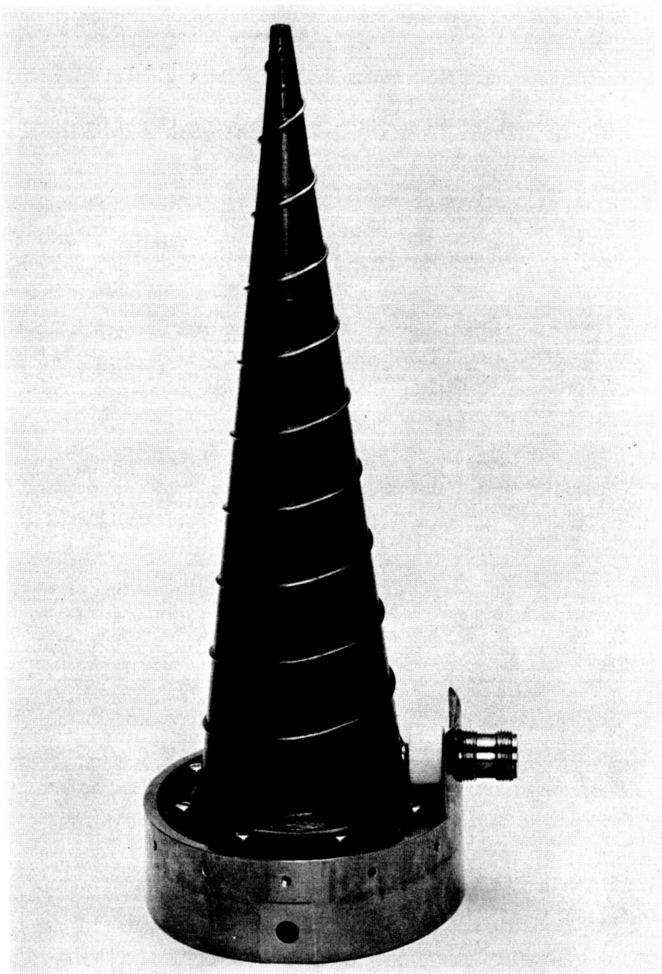

Fig. 4. Low-gain antenna waveguide mode launcher

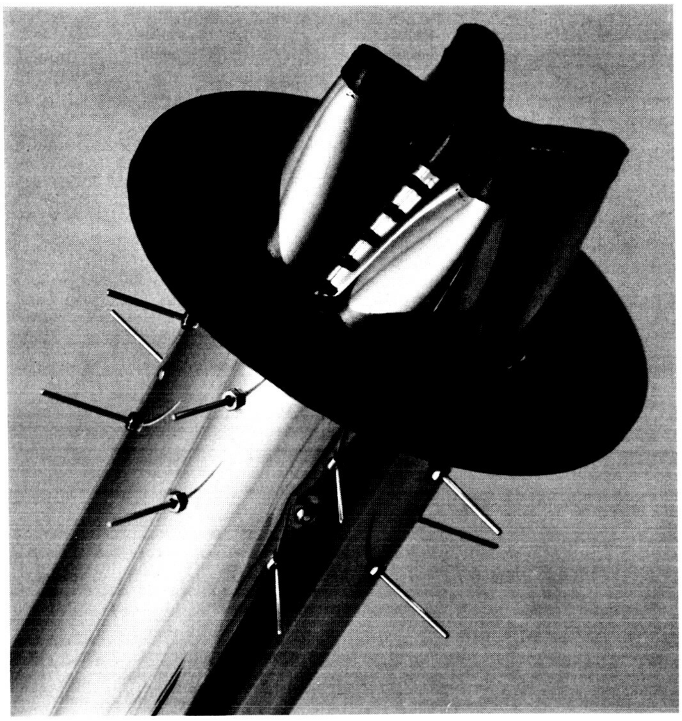

Fig. 5. Low-gain antenna radiator

3. High-Gain Antenna

A high-gain antenna (Fig. 6) is used on the *Mariner C* spacecraft in order to provide the required communication performance at planetary ranges for both telemetry and commands. During the last 160 days of the spacecraft mission (which includes the first 20 days after planetary encounter) when the high-gain antenna is required, the Earth's look angle relative to the spacecraft varies by only 19 deg in cone angle and by no more than 7 deg in clock angle. This, coupled with a peak gain requirement of only 23 db, allows the use of a paraboloidal sector mounted to the spacecraft in a fixed position. The use of a fixed high-gain antenna improves the reliability of the communication system by eliminating the requirement for an antenna pointing actuation system.

The high-gain antenna has a paraboloidal 46-in. by 21.2-in. elliptical sector. A dual cup turnstile feed (Fig. 7) is used to illuminate the sector properly. The use of a dual cup ground plane, with the turnstile, establishes a

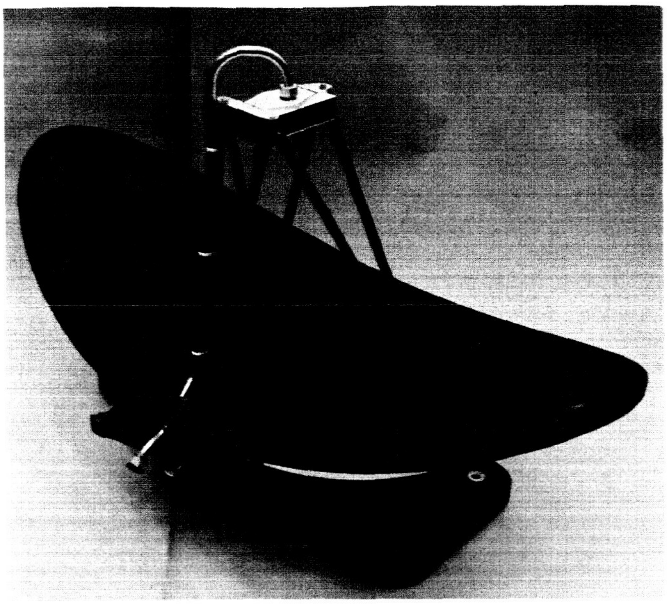

Fig. 6. High-gain antenna assembly

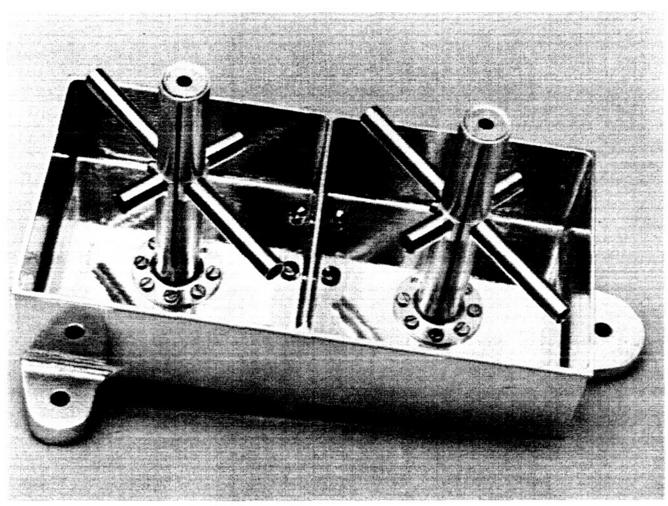

Fig. 7. High-gain antenna feed assembly

constant ellipticity over the required region to be illuminated, which in turn produces constant ellipticity over the sector's main beam. The cup design also reduces the feed rear-directed radiation to better than 25 db below the primary feed radiation peak.

4. Temperature Control

The absorptivity standard has been redesigned to increase the number of accurate determinations of sample temperature and to provide data immediately following launch.

The platinum resistance thermometers and Klixon switches in the standard have been replaced by digital thermometers. The digital thermometer sensors employ mercury thermometer switching units (Fig. 8). The sensors fit the same envelope as the previous design and similarly require no power.

The absorptivity-standard data is now in the form of a constant resistance signal which periodically changes in magnitude to signify the time at which a known temperature is reached. Because the temperature varies slowly, the hourly data readout interval does not limit accuracy.

5. Solar Vane Actuation System for Attitude Control

Attitude control is required for most lunar and planetary spacecraft to maximize solar panel electrical output by orienting them perpendicular to the Sun's rays and to maintain communications through highly directional antennas. Spacecraft attitude control has generally been accomplished by means of a cold-gas system. This system uses cold-gas storage tanks and associated plumbing, solenoid valves, nozzles, and reference-position indicators, such as Sun sensors, Earth detectors, or star trackers. The position indicators detect deviations from the desired spacecraft attitude and feed this information into logic circuitry which activates the appropriate solenoid valves. This allows cold gas to escape through a given set of nozzles, imparting a reaction to the spacecraft to correct its position. This process continues for the duration of the flight with jet firings occurring at 1-min to 1-hr intervals depending on inertia, size of jets, and amount of solar pressure unbalance.

As the length of flight increases, however, larger volumes of gas have to be carried. This increased volume, and the larger storage tanks required, increases the system weight. The use of a passive attitude-control system may reduce, if not eliminate, the weight associated with a cold-gas system. In addition, such a passive system may increase reliability by simply reducing the number of components involved.

Although there are many methods of passive attitude control, a system utilizing solar pressure would seem

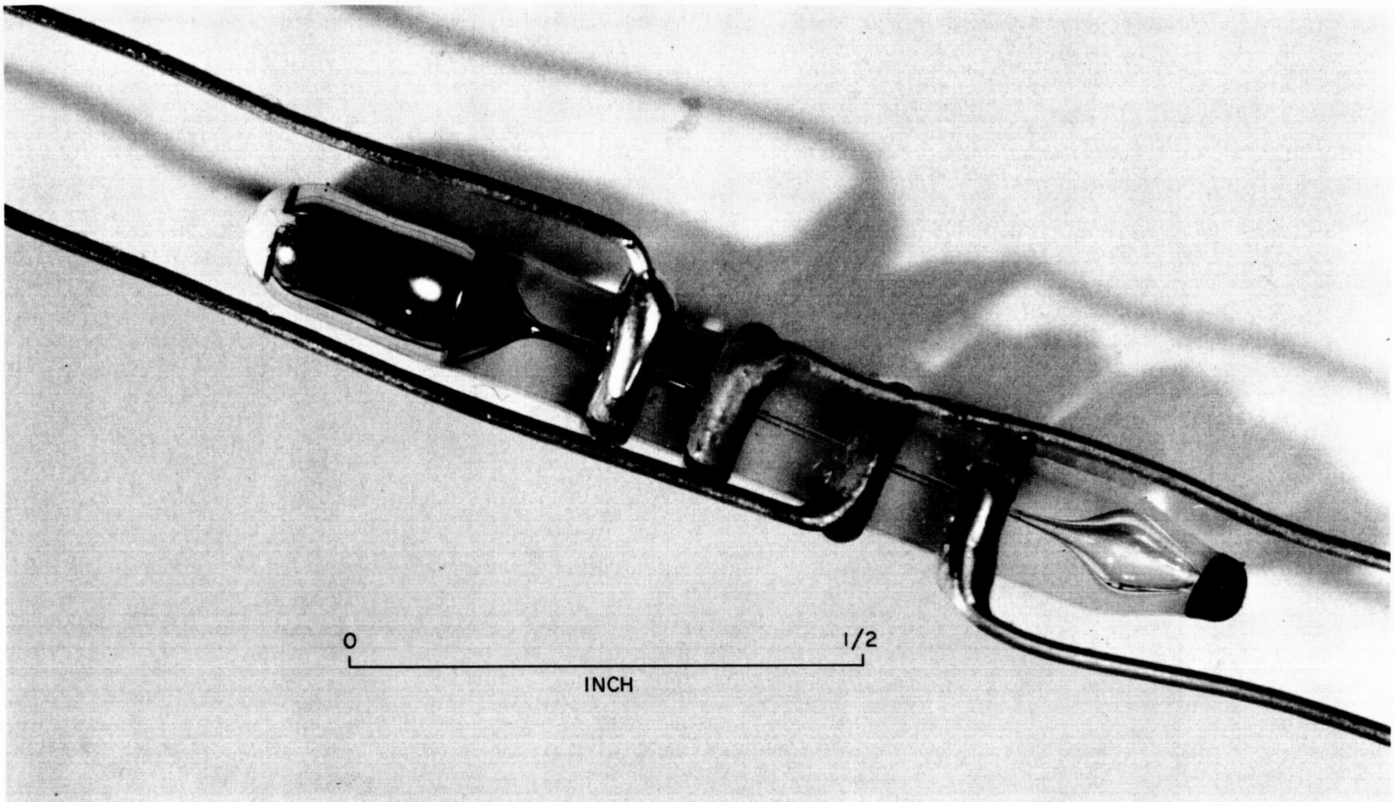

Fig. 8. Digital thermometer sensor

to be the most promising, since solar pressure is readily available. As an example, a spacecraft with its center of solar pressure aft of the center of mass is passively stable. In a system using this type of solar pressure control, however, there are two major problems:

(1) The system has no inherent damping and would continue to oscillate, depending upon initial rate and position.

(2) The neutral position of the passive system does not usually lie at the desired spacecraft position; any prelaunch adjustments would be futile due to the extremely small forces involved.

Thus, the objective is to design a system using passive solar pressure, provide damping, and be adjustable in flight to align neutral positions to desired spacecraft positions. The system now to be discussed solves these problems with state-of-the-art hardware.

The system proposed uses both an active and passive system to provide redundancy for attitude control and to obtain data points on the performance of a passive system on an actual spacecraft. A cold nitrogen gas-jet

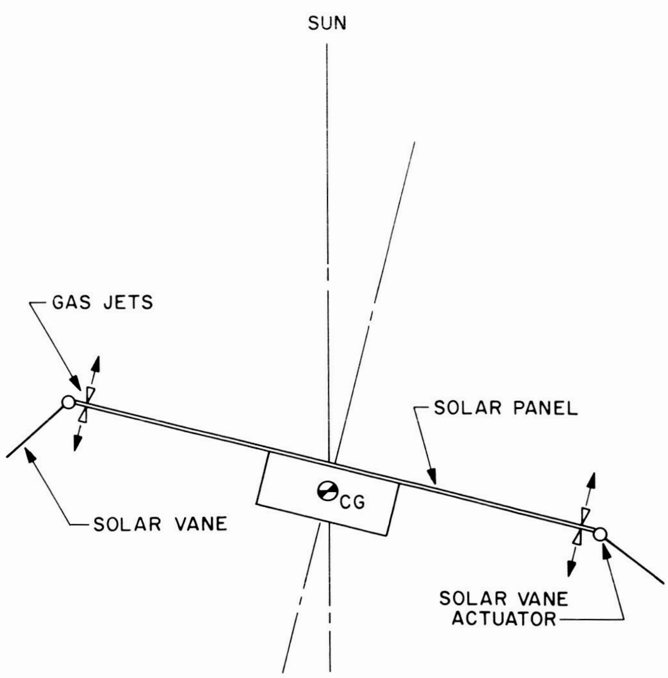

Fig. 9. Typical spacecraft configuration for solar vane actuation system

system serves as the active system, while the passive system consists of four solar pressure vanes and their actuators. The jets, vanes, and actuators are mounted at the end of the solar panel (Fig. 9) to maximize the torque output around the spacecraft center of mass. The control logic for the motor-gearhead portion of the vane actuator is arranged so that each time a gas jet is actuated, the vane is moved to add solar torque in the direction of the jet firing. Thus, any unbalance in the spacecraft will result in jet firings which in turn move the vanes. This procedure is continued until the active attitude-control system aligns the null position with the desired spacecraft position as determined by the reference position indicators. Once the null position is established, the thermal-mechanical portion of the vane actuator introduces damping into the system.

One of the purposes of designing a new system was to replace a more complex system. Although the system described in this report is more complex, since it has *both* the active and passive attitude-control subsystems, the successful performance by the passive attitude-control subsystem will lead to future systems whereby it is the only means of attitude control. This will lead to reduced weight and increased reliability by reducing the number of moving parts. For a spacecraft of different size or mass, the desired properties of such a vane actuator would be different, but the techniques used here would be directly applicable.

6. Central Computer and Sequencer

The central computer and sequencer (CC&S) consists of approximately 2500 components assembled into 8 subassemblies $1 \times 1 \times 6$ in. and 1 subassembly $1.375 \times 2.5 \times 6$ in. (Figs. 10 and 11). The CC&S is responsible for spacecraft time-sequenced events (excluding the science experiment sequence). In performing this function, the CC&S must keep track of the spacecraft time after launch, and execute commands at predetermined times during the *Mariner C* mission.

The CC&S (Fig. 12) performs the following functions:

(1) Provides a 38.4-kc sync frequency used as a spacecraft time reference.

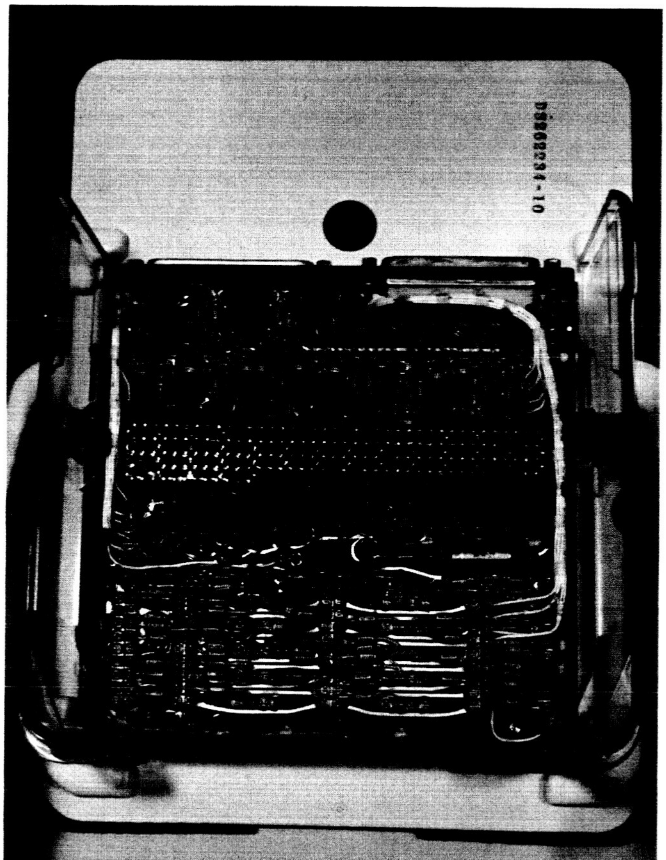

Fig. 10. Typical CC&S subassembly

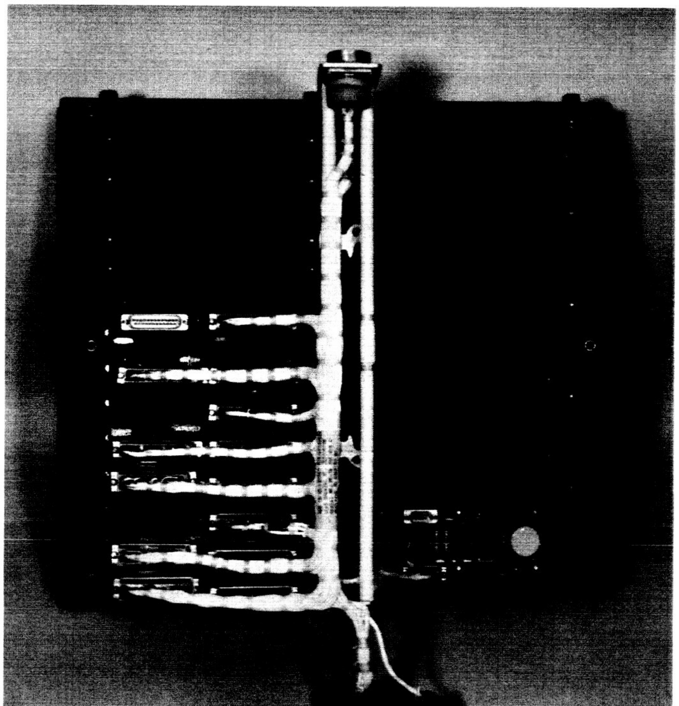

Fig. 11. Assembled CC&S with interconnect harness

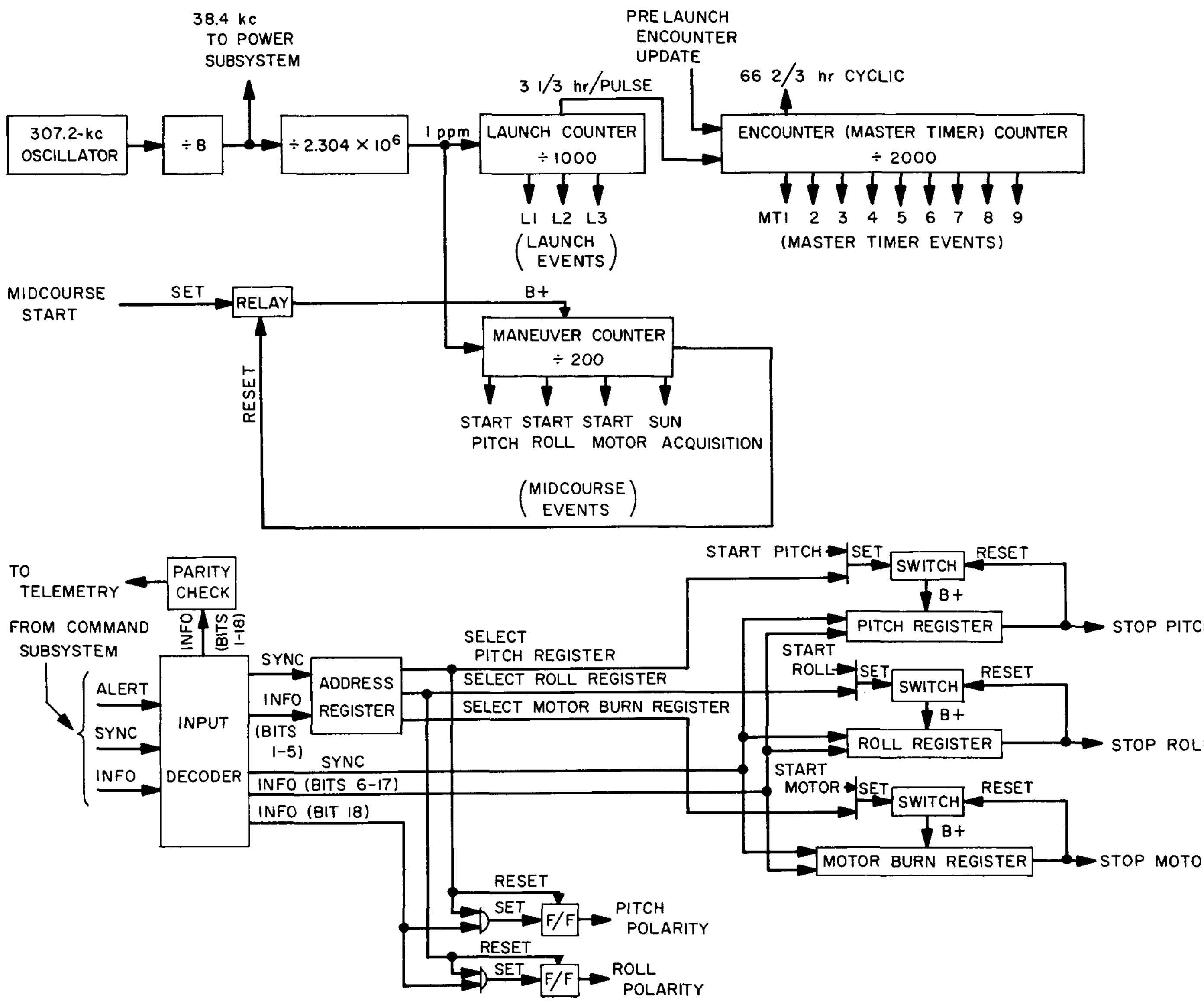

Fig. 12. CC&S block diagram

(2) Provides commands, shortly after launch, to extend solar panels and turn on attitude-control power (L1, L2, L3).

(3) Provides decoding and duration storage capability for the three midcourse maneuver parameters—pitch, roll, and velocity correction.

(4) Provides sequenced commands to the attitude-control system for spacecraft positioning, and start and stop commands to the pyrotechnics for motor burn during the midcourse maneuver.

(5) Provides on-pad adjustment capability of the planetary encounter start and stop commands normally sent to the science subsystem in the vicinity of the planet.

(6) Provides commands at predetermined times prior to and after encounter start to change the Canopus cone angle, data rate, and transponder operation modes (master timer sequence).

(7) Provides a continuous 66⅔-hr periodic command to the radio subsystem for backup switching of redundant elements.

The 38.4-kc sync signal is a square wave obtained by frequency division from the central 307.2-kc oscillator in the CC&S. This oscillator is crystal-controlled with a frequency stability of ±0.01% over the temperature range of −10 to +85°C. This 38.4-kc signal is used by the power subsystem as a stable frequency sync for the spacecraft primary 2.4-kc AC power.

Further division of the crystal-oscillator-derived frequency yields frequencies of 1 pps, 1 ppm, and 1 pulse every 3⅓ hr. The 1-pps signal is used as the time reference during countdown of the pitch and roll midcourse maneuver turns. The 1-ppm signal serves as the basic count frequency for the launch events, L1 and L2. The 1-ppm signal is also used as the count input to the midcourse counter during the midcourse maneuver to provide pitch, roll, and velocity correction start commands at 60, 82, and 104 min, respectively, after the start of the midcourse maneuver. The 3⅓-hr pulses are used as the basic input to the pulse counter associated with the master timer and encounter commands.

In addition to the basic 3⅓-hr input, the encounter pulse counter can be advanced by update pulses from the CC&S–operational-support-equipment blockhouse panel prior to launch. These update pulses are necessary to adjust the time after launch L at which the *encounter start* command is given. With this blockhouse signal, the *encounter start* command can be adjusted to occur at any 3⅓-hr increment between $L + 3⅓$ hr and $L + 277$ days. The *encounter stop* command is actuated a fixed 13⅓ hr after *encounter start*.

Since all commands are referenced to launch, or a short time before, the CC&S must be inhibited until the proper time is reached in the countdown. The *Mariner C* CC&S is normally inhibited before spacecraft power is turned on, and is released at $L - 3$ min. The *inhibit* is located at the 1-pps point in the counter chain and thus blocks all signals whose frequency or repetition rate is beyond 1 pps.

In addition to the blockhouse *inhibit* and *update* functions, there is also a *clear* command to enable the CC&S counters to be cleared to zero before the *inhibit* is released. The *relay hold* function, which is initiated prior to spacecraft power-on, commands all relays to the reset position and holds them there until spacecraft-*Agena* separation. This prevents any command relay from being actuated erroneously on the launch pad or from the mechanical stress of the launch sequence.

The CC&S also receives and stores the midcourse correction parameters that are associated with the pitch, roll, and motor burn durations. These parameters are received by radio command and stored in their respective storage shift registers prior to the start of the midcourse maneuver, which is initiated also by radio command. During the midcourse maneuver, these stored parameters are used to compute the length of time of each turn and the motor burn; from these computations are generated the respective *start* and *stop* commands which are relayed to the attitude-control and pyrotechnic subsystems.

All CC&S commands, with the exception of the 38.4-kc sync and the event blip output, are relay contact closures which either apply or remove user power from the signal lines between the CC&S and the other spacecraft systems. Each command relay, upon actuation, generates an event blip which is sent to the telemetry subsystem for subsequent transmission to the ground (Earth). The 38.4-kc sync signal and the event blip output are transformer-coupled to the user.

7. Data Encoder

The functions of the *Mariner C* data encoder are: (1) accept spacecraft measurement data in the form of analog voltages and digital information; (2) convert the data into 7-bit nonreturn to zero (NRZ) words in serial form; (3) modulate a subcarrier with the binary data; and (4) add synchronization information, which forms a signal to be presented to the radio transmitter.

The data encoder operates at two data rates (8⅓ and 33⅓ bits/sec) and four data modes. Fig. 13 is a functional block diagram of the system.

Two system rates are derived from the 2400-cps main power frequency. This basic signal is divided down by binary dividers to furnish frequencies termed $4f_s$ and $2f_s$, which are the data and sync subcarriers, respectively. Two sets of $4f_s$ and $2f_s$ are selected to provide two system rates. The $2f_s$ frequency is used to clock the pseudonoise (PN) sync-code generator, which generates bit-sync and word-sync timing pulses for the data encoder.

Ninety analog and digital engineering plus ten subcommutation and frame synchronization channels are accommodated on the completely solid-state commutator.

All high-level analog signals are normalized to a 0- to 3-v range. All low-level analog inputs are normalized to a 0- to 100-mv range and then amplified by 30. Digital inputs are handled in the transfer and seven-stage storage registers, and are clocked to the data selector by the programmer.

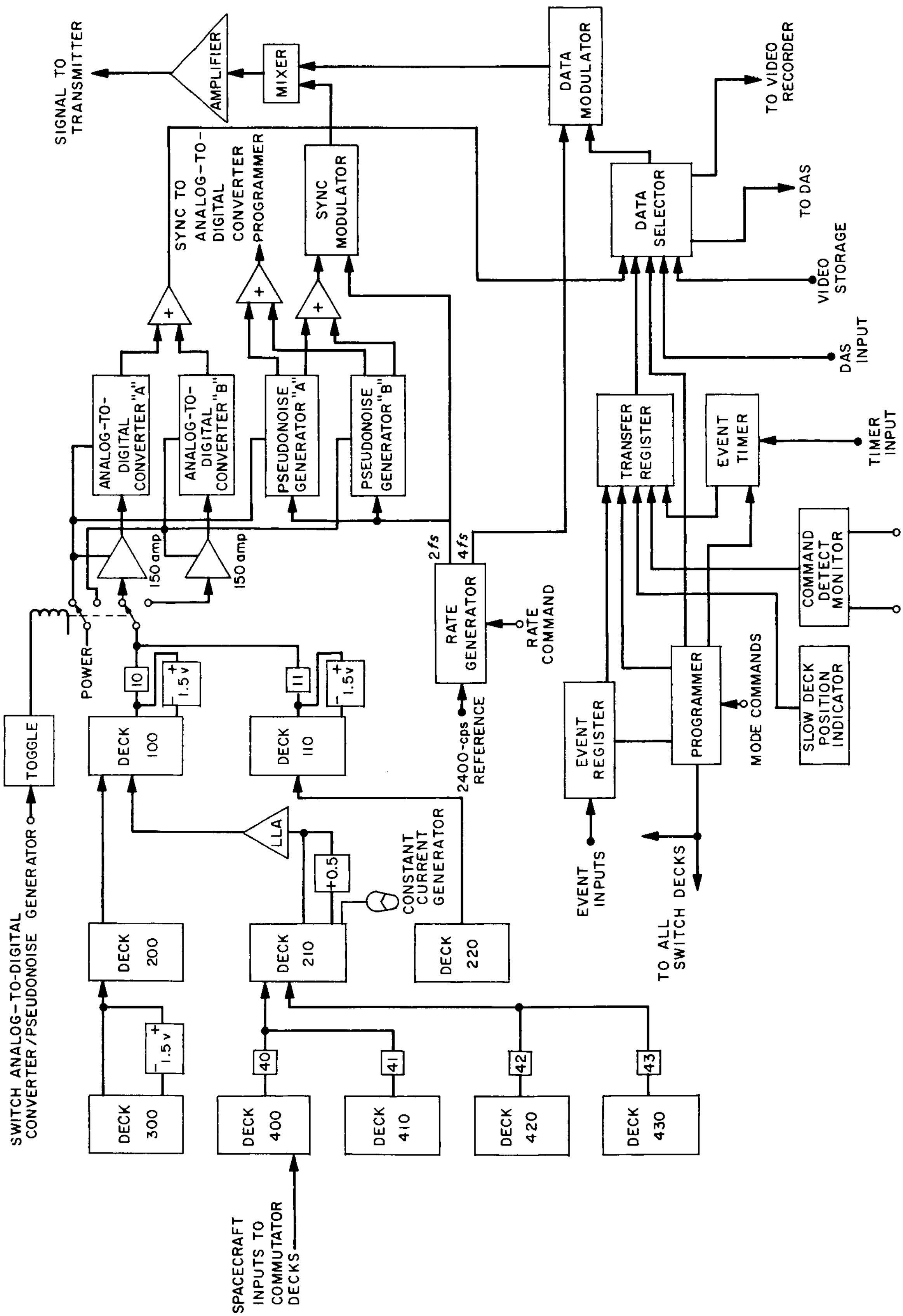

Fig. 13. Data encoder functional block diagram

Event inputs, consisting of switch closures, are sensed and stored in four event registers. The programmer reads out these registers into the data selector.

The programmer utilizes complementary flip-flop sequencers, synchronized in pairs or groups of three, to provide circuit redundancy without additional circuitry. The programmer outputs consist of time-multiplexed gates which drive the commutator switches, transfer register, and other signal-handling circuits.

Analog input signals, from the commutator, are routed to a high-impedance, unity-gain isolation amplifier. The analog signals are then converted to 7-bit digital words by a successive-approximation technique in the analog-digital converter. Four parallel digital data inputs are processed into serial 7-bit binary words and inserted at the appropriate time in the data format. The four sources of data are the analog-to-digital converter, transfer-register, science data automation system, and video storage. The data format is programmed by the mode controls through the commutator programmer. These circuits provide gating signals to the data selector circuit to indicate which data source is to be accepted into the data train. Appropriate gating in the data selector applies the proper output to the steering inputs of a 1-bit buffer synchronizer flip-flop, which assures precise synchronization of each source of data with the data encoder bit sync.

To increase the inherent reliability of the data encoder, a standby analog-to-digital converter and pseudonoise generator is used in the system. In the event of a failure of one of the two circuits, power can be switched by real-time command to the standby circuit.

In the biphase modulator, the 7-bit NRZ data is used to biphase modulate the $4f_s$ data subcarrier. The sync-channel of the modulator combines the pseudonoise code and $2f_s$ clock in *exclusive or* addition. The data channel is mixed with the sync channel at the proper voltage ratio. This mixed signal is then routed through output isolation amplifiers to the spacecraft transmitter and the ground support equipment.

THE DEEP SPACE NETWORK

IV. Introduction

The Deep Space Network (DSN) is a precision communication system which is designed to communicate with, and permit control of, spacecraft designed for deep space exploration. The DSN consists of the Deep Space Instrumentation Facility (DSIF), the Space Flight Operations Facility (SFOF), and the DSN Ground Communication System.

The DSIF utilizes large antennas, low-noise phase-lock receiving systems, and high-power transmitters located at stations positioned approximately 120 deg around the Earth to track, command, and receive data from deep space probes. The overseas stations are generally operated by personnel provided by cooperating agencies in the respective countries, while stations within the United States are operated by United States personnel. The names and locations of these DSIF stations are:

Name	Location
Goldstone Pioneer site Echo site Venus site (R&D) Mars site (under construction)	Goldstone, California
Woomera	Island Lagoon, Australia
Canberra (under construction)	Canberra, Australia
Johannesburg	Johannesburg, South Africa
Madrid (under construction)	Madrid, Spain
Spacecraft Monitoring	Cape Kennedy, Florida

The SFOF is located in a three-story building at the Jet Propulsion Laboratory in Pasadena, California, and utilizes operations control consoles, status and operations displays, computers, data processing equipment for analysis of spacecraft performance and space science experiments, and communication facilities to control space flight operations. This control is accomplished by generating trajectories and orbits, and command and control data, from tracking and telemetry data received from the DSIF in near real time. The SFOF also reduces the telemetry, tracking, command, and station performance data recorded by the DSIF into engineering and scientific information for analysis and use by the scientific experimenters and spacecraft engineers.

The DSN Ground Communication System consists of voice circuits, and normal and high data-rate teletype circuits provided by the NASA World-Wide Communications Network between each overseas station and the SFOF, teletype and voice circuits between the SFOF and the Goldstone stations and Cape Kennedy, and a microwave link between the SFOF and Goldstone, provided by the DSN.

The DSN has facilities for simultaneously controlling a newly launched spacecraft and a second one already in flight and, within a few months, will be able to control simultaneously either two newly launched spacecraft plus two in flight, or the operations of four spacecraft in flight at the same time. The DSIF is equipped with 85-ft antennas having gains of 53 db at 2300 Mc and a system temperature of 55°K, making it possible to receive significant data rates at distances as far as the planet Mars when the spacecraft utilizes directional antennas. To improve the data rate and distance capability of the DSIF, a 210-ft antenna is under construction at the Goldstone Mars site, and two additional antennas of this size are scheduled for installation at overseas stations. The SFOF has two 7094, two 7040, two 1401, and one SC 4020 computers; four disc files; various input/output units; printers, plotters, and computer interrogation consoles; and teletype, telephone, interphone, public address, and closed circuit television communications systems.

It is the policy of the DSN to continuously conduct research and development of new components and systems and to engineer them into the DSN to maintain a state-of-the-art capability.

The DSN is a NASA Facility, managed by the Jet Propulsion Laboratory through a contract between NASA and the California Institute of Technology. The Office of Tracking and Data Acquisition is the cognizant NASA office.

Section V that follows is a digest of the information that appears in *SPS 37-28*, Vol. III.

V. The Deep Space Instrumentation Facility

A. Tracking Stations Engineering and Operations

1. Flight Project Engineering

a. Surveyor. The command and data console (CDC) at the Pioneer site was checked out and temporary cables were laid to the Deep Space Instrumentation Facility (DSIF). CDC/DSIF compatibility tests were performed. A prototype version of the *Surveyor*/CDC system tester, which will be used to simulate the spacecraft, was installed adjacent to the CDC.

A series of tests was made with the full Goldstone duplicate standard S-band configuration, which includes two receiver and two angle channels, to obtain experimental data on: (1) the best procedure for first acquisition of *Surveyor* by the DSIF, and (2) the typical times involved in carrying out this procedure.

For these tests, the *Surveyor* S-band test transponder was installed in a helicopter together with a suitable power supply and antenna. A flight path was developed for the helicopter which simulated the first pass of *Surveyor* at Johannesburg. This was varied slightly during the tests in order to simulate a variation in time and azimuth of first visibility.

The helicopter flight path was adjusted to give an effective angular tracking rate of about 0.06 deg/sec, which is the maximum rate expected for *Surveyor*. The transponder transmitter power output and the Goldstone duplicate standard transmitter power output were adjusted to present signal power levels at both receivers that were typical of levels expected in an actual mission.

On each run, the helicopter pilot gave an estimated "10 sec to go" call before he appeared above the local horizon; this was used as the starting point for the acquisition procedure. The times taken to accomplish each event of the acquisition procedure were recorded.

The longest time between events occurred in switching from auto-track on the S-band acquisition aid (SAA) to auto-track on the S-band Cassegrain monopulse feedhorn and bridge system. This operation depends on the tracking performance in the SAA mode and requires that the angle error be sufficiently small to be within the S-curve of the SAA mode before the transfer can be made.

Of the 16 runs made by the aircraft, acquisition was not completed during 3 of the runs. In all remaining runs, the procedure was completed and two-way lock established in less than 3 min. During 10 of the runs, it was possible to lock the ground transmitter onto the transponder receiver with the servo in auto-track on the SAA antenna.

b. Mariner C. Compatibility tests were conducted to evaluate the performance of the *Mariner C* telecommunication system operating with the DSIF S-band ground system. The *Mariner C* type-approval-model radio system was used. The tests were conducted over a signal path link between the Pioneer site and the Goldstone Spacecraft Test Facility.

During these tests, the performance of pertinent ground equipment such as the read–write–verify, the teletype encoder, the receiver and transmitter, the ranging subsystem, and the telemetry demodulator and decommutator was evaluated; calculated system parameters, such as threshold signal strengths and carrier modulation losses, were verified. The majority of the tests indicated nominal performance. Data reduction and evaluation are being performed.

2. S-Band RF System

The S-band RF system is comprised of receiver, transmitter, and antenna microwave subsystems, operating in conjunction with the acquisition aid subsystem in the DSIF tracking and communications system Goldstone duplicate standard 1964 model. The S-band system provides a dual-channel reception capability and can be operated in various configurations of antennas, low-noise amplifiers, and receivers for acquisition and tracking and/or listening modes. System design is such that state-of-the-art improvement can be incorporated quickly, easily, and economically.

Installation of the first RF system at the Pioneer site was completed during March 1964. Testing and performance evaluation, including compatibility tests with *Mariner* and *Surveyor* equipment, are in process.

3. Station Control and Monitor Console

A program is underway to provide a station control and monitor console at the DSIF stations to display information for the station manager that will provide him with an over-all evaluation of the station S-band system performance. This information should provide an indication of nonstandard situations which would be detrimental to the performance of the station and acquisition of data.

Phase II of this program has been initiated. This phase will involve the utilization of the on-site digital instrumentation system to monitor specific station and spacecraft parameters, to analyze these data, and to provide a continual assessment of station status and performance.

4. L-Band Calibration

A calibrated transmitter signal source, for use as a power level standard, has been sent to the overseas DSIF stations for calibration and evaluation of the various L-band RF systems. Through the use of this calibrated signal source, the Johannesburg Station detected and corrected a discrepancy in its receiver calibration. This error was caused by an improperly shielded test transponder, which is normally used for the receiver calibration. In an effort to reduce system errors and to maintain accuracy of the receiver calibrations, the calibrated transmitter will be periodically shipped to the various overseas stations and used for signal level reference.

5. Determination of Geocentric Locations of DSIF Stations

A new determination has been made of the geocentric locations of the DSIF stations positioned around the Earth. A re-evaluation of the accuracy of existing locations was prompted by NASA's adoption of a unique ellipsoid for the figure of the Earth, the "Kaula" or "165" spheroid, also known as the "NASA Earth Model" spheroid. Changes in geocentric positions were determined from the Kaula adjustments, and also from new survey data.

6. Computer Program for Stereographic Projection Generator and Plotter

The use of stereographic station projections (Fig. 1) has proved to be a valuable aid in visualizing tracking problems and analyzing space trajectory/antenna relationships. However, the production of originals for these projections for the DSIF stations has always been a laborious and time-consuming task. Previously, parameters were computed and given to a draftsman, who in turn plotted the curves manually. With establishment of new DSIF antenna sites and the necessity for revision of the older plots, some means of simplifying and expediting the production of stereographic station projections was needed.

A Fortran computer program was written in order to output (on magnetic tape) x–y coordinates for the hour-angle and declination-angle intersections superimposed on the corresponding coordinates of the azimuth-elevation system for an arbitrary station location. The second half of the program reads the computed data from magnetic tape and automatically plots these intersections (Fig. 2). An added feature is the capability of superimposing stereographic representations of probe trajectories on the plot. The computer complex used for this program is located at the Goldstone Station, Echo site.

7. Agena Aspect-Angle Program

The function of this computing routine is to define the relationship of a DSIF station's line-of-sight vector to the control axes of an attitude-controlled *Agena* vehicle. Since the vehicle's transmitting antenna system is fixed relative to the control axes, this routine will determine the orientation of the line-of-sight in the antenna pattern, and thus the expected signal strength.

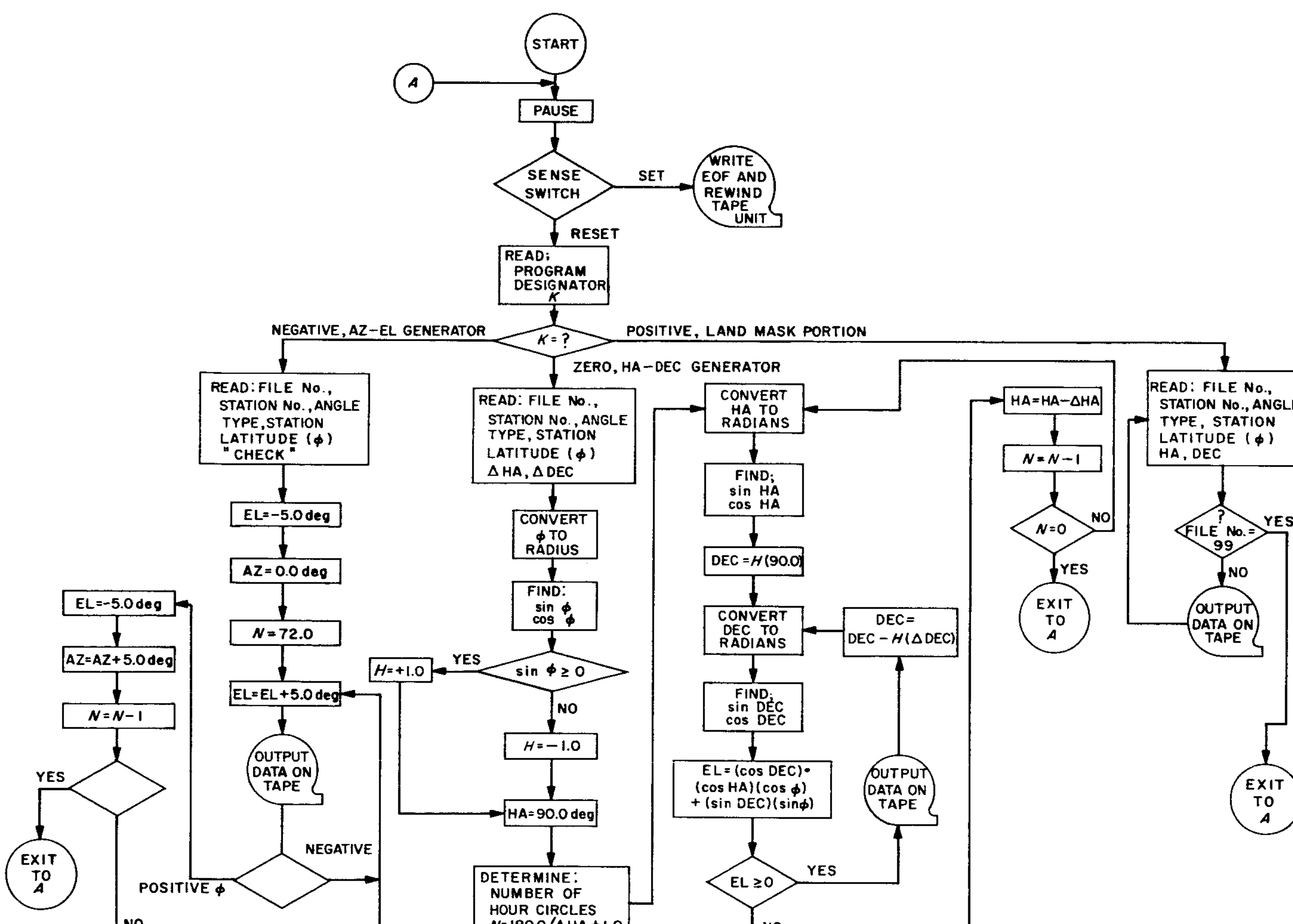

Fig. 1. Stereographic projection generator

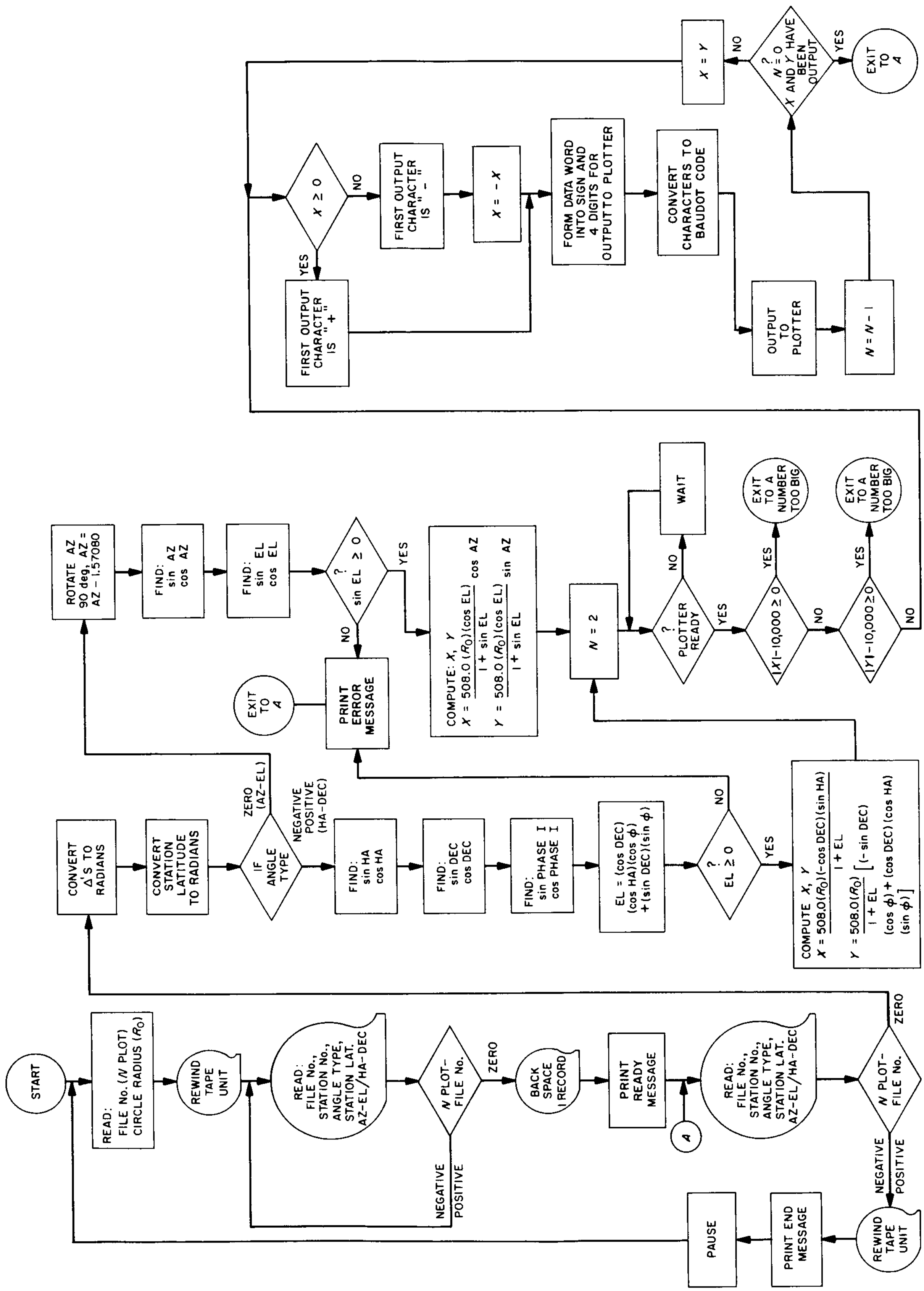

Fig. 2. Stereographic plotter

The governing assumptions are: (1) that the yaw axis is parallel to the local vertical, and (2) that there is zero yaw angle-of-attack.

Two aspect angles are defined: (1) PHA—the angle between the roll axis and the negative line-of-sight, and (2) PSA—the angle that the projection of the line-of-sight vector on the roll plane makes with the yaw axis, positive in the direction toward the positive pitch axis.

The routine has been programmed in Fortran II and is composed of 47 Fortran statements, including numerical checking commands.

8. Spacecraft Test Facility

The Phase I version of the Goldstone Spacecraft Test Facility was completed. The facility consists of a 12- by 18-ft shielded enclosure with a 12-ft ceiling height, erected near one end of a reinforced 60- by 30-ft concrete pad (Fig. 3).

A 4-ft-diameter antenna is mounted on a 20-ft tower adjacent to the enclosure and connected to it by a 40-ft length of ½-in.-diameter Spiroline. The Pioneer collimation tower carries two back-to-back S-band antennas, one directed toward the Pioneer DSIF antenna and the other toward the test facility.

The facility was designed to simulate interplanetary space loss of 260 to 270 db between a spacecraft transmitter and the DSIF antenna, when used in conjunction with a 50-db pad and up to 60 db of variable attenuation inside the enclosure.

Tests were conducted to verify the performance of the facility. Signal sources at various power levels were connected through suitable attenuators to the Spiroline terminal inside the enclosure. The attenuation was increased in 10-db steps until the DSIF receiver threshold was reached and the system dropped out of lock. The following data were recorded: (1) transmitter power, (2) power input to the Spiroline termination, (3) automatic gain control voltage recorded at the Pioneer receiver, and (4) power received at the maser input.

Test results verified the feasibility of this approach to the problem of simulating lunar or planetary space loss. Further testing under more rigidly controlled conditions is required to establish the exact path loss and its variation with time.

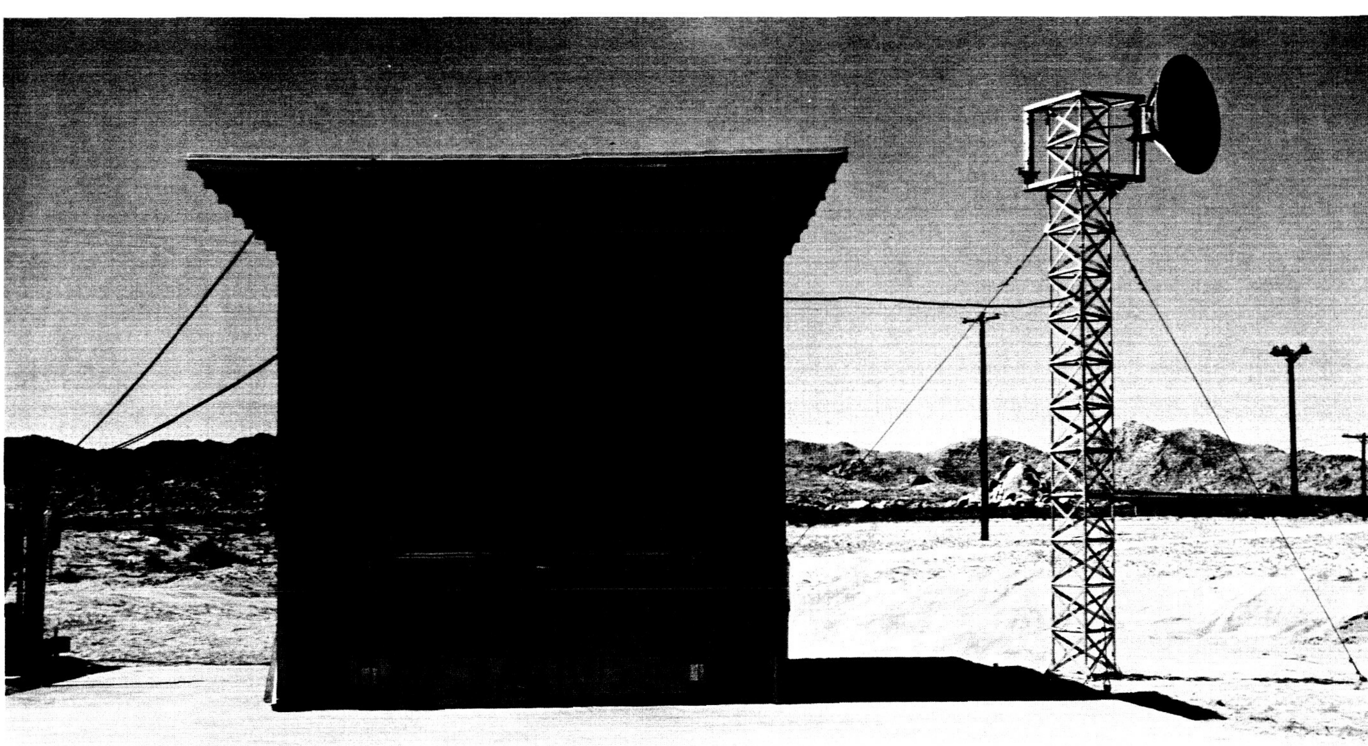

Fig. 3. Spacecraft Test Facility

B. Communications Research and Development

1. S-Band Acquisition Aid

A carefully calibrated helicopter track with full recording was performed at the Goldstone Pioneer site. Because previous servo switchover tests had demonstrated successful rapid switchover, this test was run with tracking entirely on the S-band acquisition aid (SAA) in an attempt to quantitatively evaluate the tracking accuracy of the SAA system. Particular attention was paid to the boresight alignment of the system.

Results showed a difference between the pre-track calibrations and the flight data for the boresight alignment of the SAA and the S-band Cassegrain monopulse (SCM) feedhorn and bridge system. This difference was presumably due to a combination of small misalignments between the SAA and SCM optical systems, drift in the receiver and servo systems, and structural distortions in the antenna during track. It is considered a minor effect.

The tracking performance of the SAA system as a function of elevation angle is shown in Fig. 4. In plotting this figure, tracking data was sampled at 2-sec intervals, and the angular coordinate with the largest error at each time was chosen for the plot. Parallax between the SAA and SCM, which varied from 0.01 to 0.07 deg during the track, was also corrected.

For elevation angles less than 9 deg, servo switchover from SAA to SCM appears hopeless. From 9 to 12 deg, switchover is possible by activation of the switchover

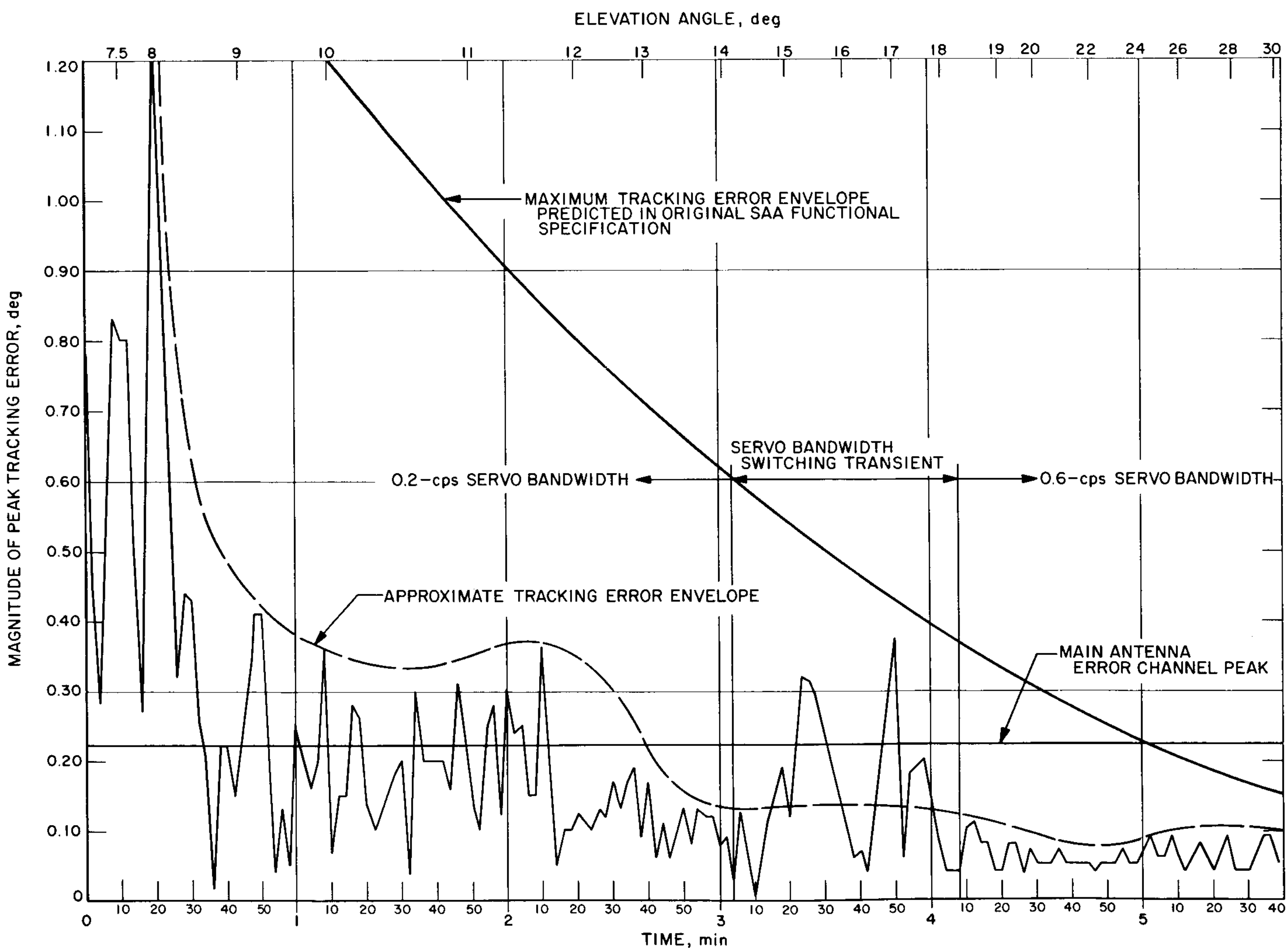

Fig. 4. S-band acquisition aid tracking performance

control at a time when both declination and hour-angle errors are less than 0.2 deg. For elevation angles greater than 12 deg, switchover can be successfully effected at any time.

Data on the relative signal level between SCM and SAA imply that two-way acquisition could be successfully achieved (above 9-deg elevation) with the transmitter on SCM rather than SAA. Such procedure would eliminate transmitter switchover with its attendant interlock and time-delay problem. This mode of two-way acquisition has, however, not yet been evaluated in detail.

From the results of these tests, it is felt that the S-band acquisition system has been successfully demonstrated.

2. Radio Calibration Technique

An X-band laboratory demonstration model of a simultaneous lobing radiometer receiver channel has been constructed. A noise tube is used to simulate the signal from a radio source. The IF and DC components of the demonstration model were operated at the Goldstone Echo site, using the 85-ft antenna and the L-band receiver system. It was possible with an effective system temperature of approximately 500°K to automatically track a radio star which produced an antenna temperature in the reference channel of 5°K; a source which produced a 59°K antenna temperature provided good automatic tracking. Data were taken to evaluate the tracking accuracy.

The experiment demonstrated the feasibility of autotracking noise sources to aid in the calibration of the DSIF antennas. A prototype S-band system is currently being built and bench tested.

3. Venus Voice-Bounce Experiment

In order to evaluate relatively broad-band deep space communications, a preliminary Venus voice-bounce experiment was performed using the radar transmitter at the Goldstone Venus site in either a frequency-modulated or single-sideband-modulated mode. The speech was compressed by a factor of 32 times because of limited bandwidth due to low signal-to-noise ratio. Intelligible recordings of voice messages were obtained.

4. Precision Long-Range Tracking S-Band Radar System

Deep-space radar has previously been used in many ways to measure interplanetary ranges, and many of these have not only drastically reduced the uncertainty in such ranges, but have indicated the true value of certain astronomical constants. A much improved method for precision planetary range tracking has recently been implemented at the Venus site—a method capable of distinguishing the sub-Earth point of the planet Venus to about 2 or 3 km.

The precision planetary tracking radar uses much the same physical equipment as the range-gated lunar radar (Ref. 1). However, the 85-ft antenna is used for both transmission and reception (the lunar experiment used a 6-ft antenna to receive), different methods are used to isolate the transmitter and receiver, a different set of variable digit-period coders is required, and the Mod III stored program controller operates under a different set of instructions. Detection, modulation, transmission, and reception are identical to the lunar radar. The significant improvement in this system over previous planetary schemes is one of extreme flexibility, high accuracy, and high precision. Flexibility is achieved by use of the Mod III stored program controller as the over-all system monitor, signal processor, and data handling unit. High accuracy and precision are obtained by the methods of modulation, detection, and signal processing used.

Using the 100-kw transmitter, maser receiver, and 85-ft Venus site antenna as part of the precision planetary tracking radar, the planet Venus was tracked with great success. The radar provided measurements of range to the planetary mean-tracking-point with peak variations less than 15 to 20 μsec of round-trip delay (2.25 to 3 km in range). The mean-tracking-point can thus be determined over a 1-hr period to better than 4-μsec accuracy. Calibration of the internal system delay was previously measured to be only about 0.55 μsec. Fig. 5 shows typical plots of this tracking data as a function of time. It must be remembered that part of the time is allotted for transmission, and tracking only occurs on the receive portion. The first parts of Figs. 5(a) and (b) show the loop pulling in from a deliberately induced error. Fig. 6 shows plots of S-curves, along with calibration numbers, and Fig. 7 indicates the day-to-day trend of the front-face range offset. Calibrations of the S-curve are estimated to about $\pm$20-μsec accuracy, for the most part; this represents the essential accuracy of the system for the day-to-day analysis.

As shown in Fig. 7, during the days that these data were taken, the ephemeris was not only in error, but this error was changing by about 120 μsec per day (5 μsec/hr). Deviations larger than $\pm$20 μsec are probably due to surface features.

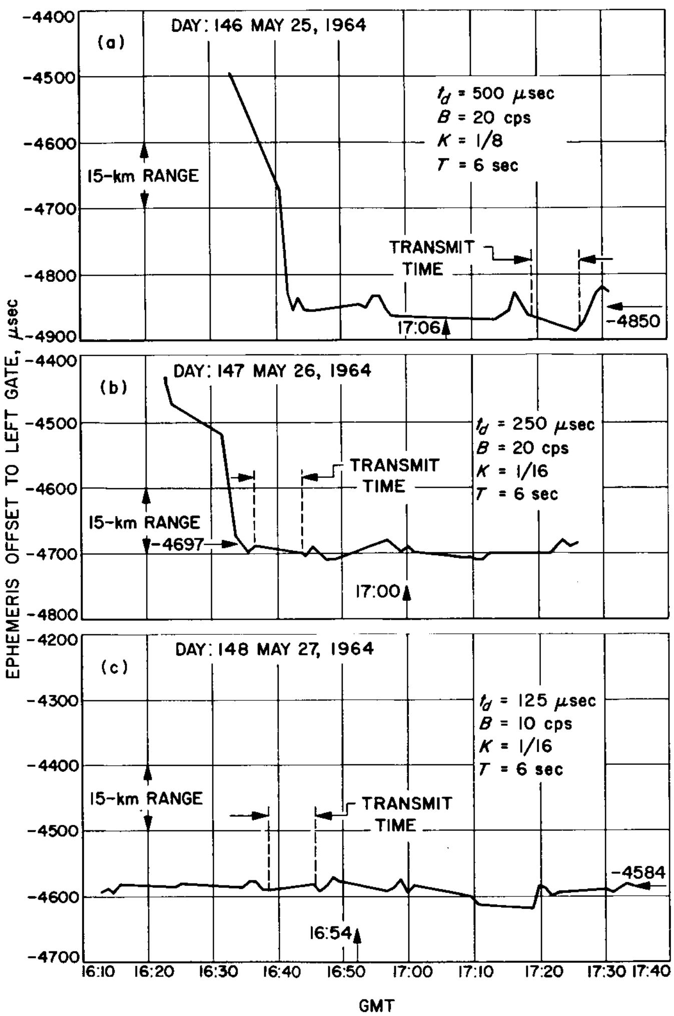

Fig. 5. Lock-in and tracking data, Venus (May 25, 26, 27, 1964)

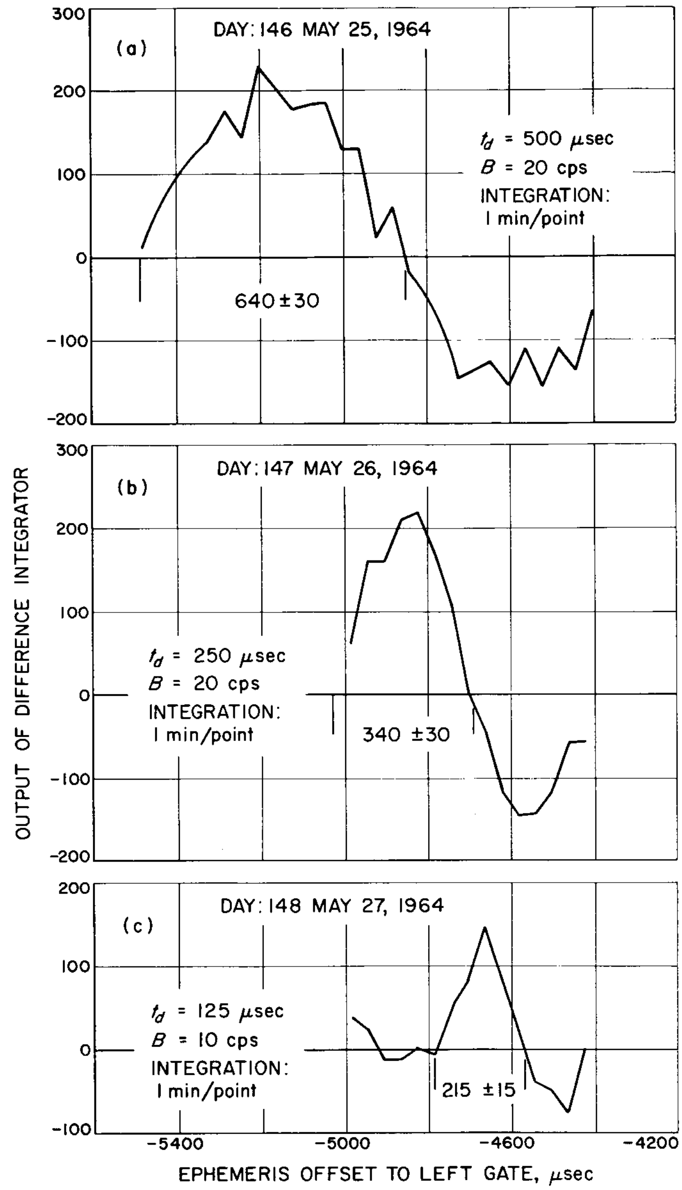

Fig. 6. Error curves for calibration, Venus (May 25, 26, 27, 1964)

5. *Components of X-Band Lunar/Planetary Radar System*

An 8448-Mc Dewar-mounted maser amplifier (Fig. 8) will be used in a low-noise radiometer/radar-astronomy receiver for advanced communications systems and components experiments on the 30-ft antenna at the Goldstone Venus site.

The maser assembly will be mounted in the electronics cage of the 30-ft antenna below the antenna surface. The input of the maser can be switched to either the antenna, the liquid-nitrogen termination, or the liquid-helium termination, allowing accurate noise temperature measurements to be made. The output of the maser can be fed to the X-band radar receiver or the monitor receiver. The monitor receiver, mounted in the electronics cage, will have high-gain stability and will be used for maser evaluation and radio-astronomy measurements. The maser gain will be measured by setting the signal generator attenuator for equal output when the continuous wave signal from the signal generator in the control room is switched between the maser input and output.

The waveguide and calibration system to be used for the 30-ft antenna X-band system is similar to that used for the 85-ft S-band radar system. The major differences in the X- and S-band waveguide systems are due to the greater flexibility available in waveguide design of the

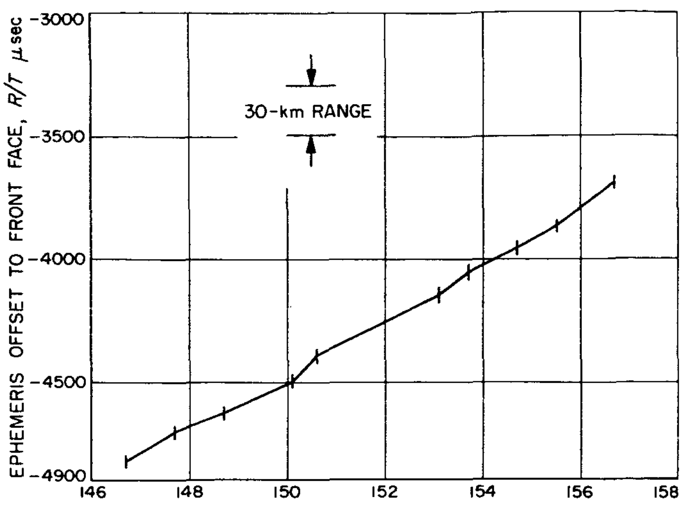

Fig. 7. Day-to-day tracking data, Venus (May 25, 26, 27, 1964)

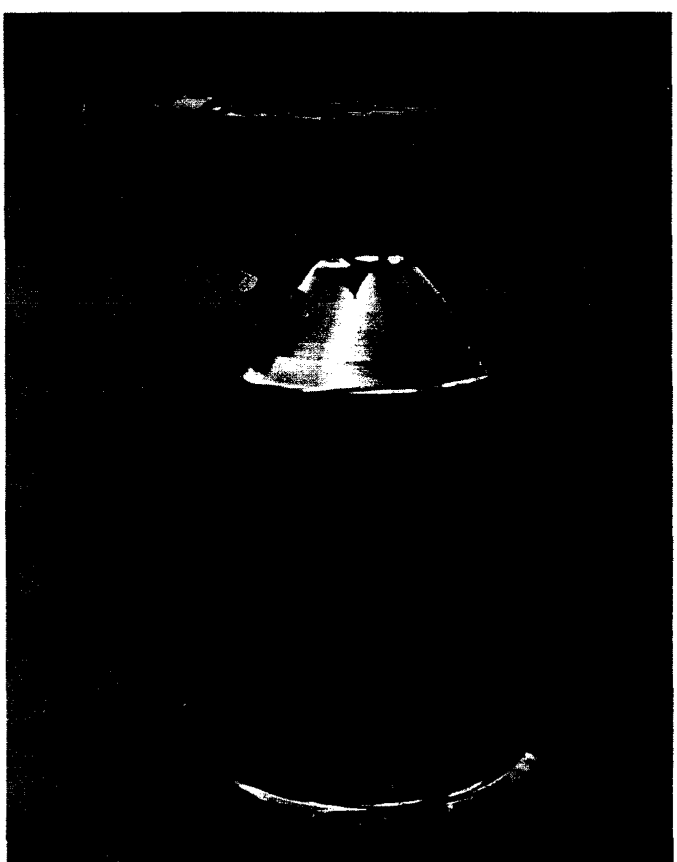

Fig. 8. 8448-Mc, 9-cavity maser amplifier mounted in a 6-liter Dewar

smaller dimensional X-band guide. The smaller dimensions of the 30-ft dish, however, make it impossible for the Cassegrain cone to contain as much instrumentation as at S-band.

The feed for the 8448-Mc X-band radar will provide switchable circular and orthogonal linear polarization through the use of a turnstile junction polarizer. Components used in previous X-band projects are being modified for high-power use.

Three complete frequency multiplier chains are required for conversion of the existing S-band equipment to X-band for the Lunar Radar Project. One each of these chains is used for the transmitter exciter, signal generator, and receiver local oscillator; all are capable of digital phase modulation and keying.

C. Advanced Antenna System Hydrostatic Thrust Bearing

The hydrostatic thrust bearing supports the rotating parts of the Advanced Antenna System on three bearing pads, one at each corner of the alidade base triangle. Other components of the bearing are the hydraulic power supply system and the runner and oil reservoir. The general configuration is shown in Fig. 9.

The bearing pads are carbon steel forgings $60 \times 40 \times 20$ in. thick. Each pad has six recesses in the pressure side through which oil is supplied for bearing operation. A spherical seat is provided in the connection to the alidade to minimize the moment reaction on the pads.

The bearing runner is made in ten segments of low carbon steel 5 in. thick and 44 in. wide. A special joint has been designed to provide maximum stiffness against the bending under the pads and to provide an adequate seal against the oil film pressure. The runner rests on a steel sole plate on nonshrinking grout. It is free to move radially to permit thermal expansion, but is restrained tangentially by stops embedded in the pedestal concrete.

The oil reservoir is formed by walls fastened and sealed to the edges of the runner. The oil level in the reservoir will be approximately 9 in. deep to permit suction recovery of oil by the hydraulic power supply system.

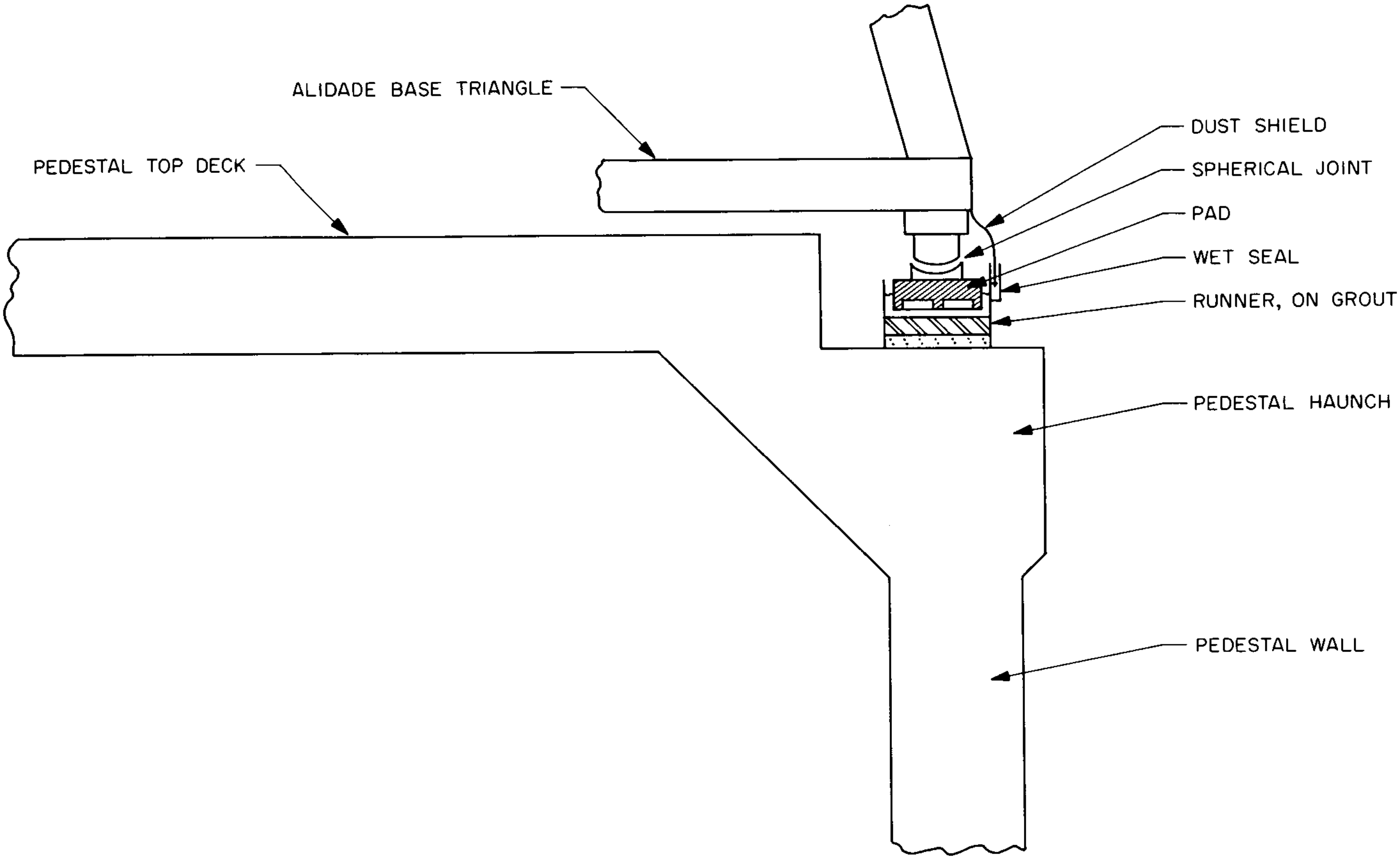

Fig. 9. Azimuth hydrostatic thrust bearing, general arrangement

The entire bearing system is enclosed by a shield mounted on the alidade. This shield joins the outer reservoir wall in a wet-type seal, providing complete isolation from the outside atmosphere.

The hydraulic power supply system consists of a precharge subsystem, which draws oil from the reservoir and supplies it to the high pressure units, and a high pressure subsystem, which supplies the high pressure oil to the pad recesses. The precharge subsystem consists of two 165-gal/min gear pumps, either of which can supply the entire flow requirements, two 10-μ filters, and a heat exchanger and heater to maintain the oil temperature at approximately 100°F. There are three high pressure units, one for each pad. Each unit includes three electric motors driving six pumps. The pumps are arranged so that one motor drives pumps serving opposite recesses on the pad. In this manner, a balanced pressure pattern is maintained under the pad in the event of failure of one motor. Included with each unit is a separate accumulator system which can maintain bearing operation for a period of several seconds after a power failure. This will assure that the azimuth drive has brought the antenna to a stop before the bearing touches down.

The bearing pad was designed to match the runner deflection with a 0.001-in. maximum film height variation under the pad. The nominal film height under dead load (1.5×10^6 lb per pad) and full hydraulic system operation is 0.010 in. The bearing will remain fully operational after loss of flow to any two recesses and marginally operational with loss of flow to any three recesses.

Reference

1. "A Range-Gated Lunar Radar Experiment, *SPS 37-25*, Vol. III, pp. 38–47, Jet Propulsion Laboratory, Pasadena, California, January 31, 1964.

SPACE SCIENCES

VI. Space Instruments Development

A. *Mariner* TV Subsystem Science and Engineering Calibration

Introduction. As is the case with all scientific instruments, the *Mariner* TV subsystem must receive detail calibration prior to flight. Two goals of such a calibration are:

(1) To assure that each particular system is operated in an optimum manner.

(2) To provide information for interpretation and/or enhancement of the mission picture data.

Since no inflight calibration is possible because of power, weight, and command restrictions, a control model will receive the same prelaunch calibration as the flight models and will, as closely as possible, duplicate the flight conditions during the transfer time from Earth to Mars. Every effort has been made to incorporate into the design the stability necessary to accurately interpret the final picture data at encounter. Each flight system will receive complete calibration prior to final spacecraft system testing. It is planned to perform a simplified recalibration at the Air Force Eastern Test Range (formerly Atlantic Missile Range) prior to the final commitment of a particular system to flight. The following four general categories of information are obtained during calibration: (1) radiometric response, (2) resolution, (3) geometrical characteristics, and (4) vidicon photosurface characteristics.

Radiometric response. The data obtained as radiometric response include vidicon-spectral response, system-spectral response, static light transfer function, and dynamic range.

The relative spectral response of the vidicon is obtained utilizing the equipment and personnel of the JPL Imaging Systems Test Facility. Basically, the vidicon tube output signal response to monochromatic light is plotted against a thermopile response to the same monochromator. Fig. 1 shows typical spectral response for vidicons currently being used in the *Mariner* program. A Bausch and Lomb Model 33-86-25-01 monochrometer is being used with a 0.50-mm slit width, giving a spectral dispersion of 32 Å. Data points are taken every 10 mμ from 400 to 640 mμ. The procedure is as follows:

(1) The maximum response point of the tube is obtained to ensure that the output current will not saturate.

(2) The monochrometer output energy is then varied as a function of wavelength to maintain a constant output current from the vidicon.

(3) The monochrometer lamp current and voltage are measured for each data point in order to maintain a constant output from the vidicon.

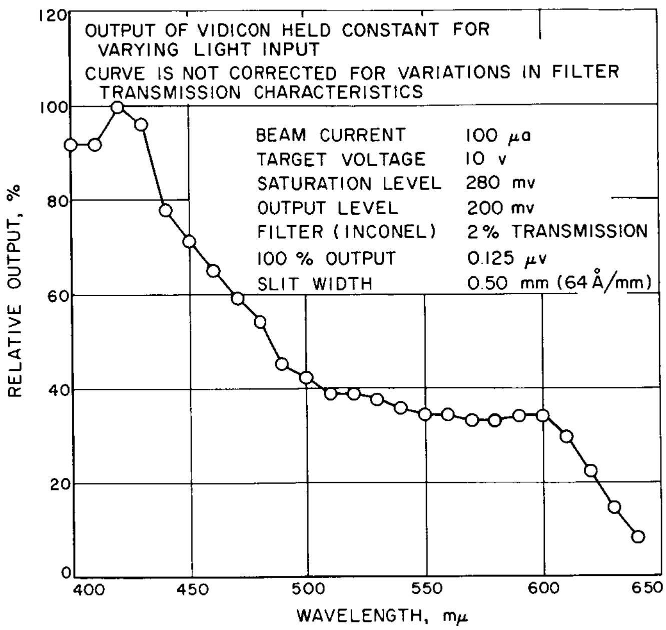

Fig. 1. Vidicon relative spectral response

(4) An Inconel neutral-density filter is used in series with the vidicon so that enough energy will be used from the monochrometer to adequately stimulate a somewhat insensitive thermopile.

(5) The response of a thermopile is then measured as a function of wavelength, with the current and voltage to the lamp adjusted in accordance with the reading obtained in Step (3).

Table 1 gives the raw data plotted in Fig. 1. The reciprocal of the thermopile response is normalized, yielding relative output, which is then plotted as a function of wavelength, thus giving the vidicon's relative spectral response curve.

System spectral response will be obtained by using narrow-band interference filters and plotting the video amplifier output signal as a function of wavelength.

The static light transfer function will be obtained using a 9-in. optical collimator whose spectral output has been adjusted with filters to closely approximate a 3000°K color temperature. Flat-field illumination is used, the intensity of which is varied by placing various Inconel neutral-density filters in series with the collimator light output. Inconel filters were chosen because of their favorable spectral response characteristics. A typical Inconel filter response curve is shown in Fig. 2. The TV subsystem incorporates an automatic gain control which

Table 1. Raw spectral response data

Wavelength, mμ	Thermopile response, μv	Reciprocal of thermopile response	Relative output, %
400	0.135	7.40	92.5
410	0.135	7.40	92.5
420	0.125	8.00	100
430	0.130	7.70	96.3
440	0.160	6.25	78.2
450	0.175	5.72	71.6
460	0.190	5.26	65.8
470	0.210	4.76	59.5
480	0.230	4.35	54.4
490	0.275	3.64	45.5
500	0.295	3.39	42.4
510	0.320	3.12	39.0
520	0.320	3.12	39.0
530	0.330	3.03	37.9
540	0.345	2.90	36.3
550	0.360	2.78	34.8
560	0.360	2.78	34.8
570	0.370	2.70	33.8
580	0.375	2.67	33.4
590	0.360	2.78	34.8
600	0.360	2.78	34.8
610	0.420	2.38	29.8
620	0.550	1.82	22.7
630	0.880	1.14	14.3
640	1.45	0.69	8.6

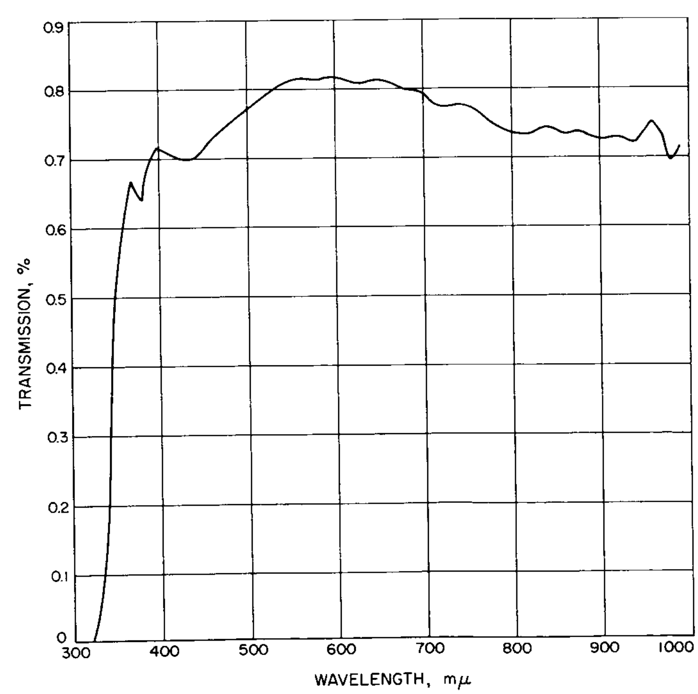

Fig. 2. Inconel neutral-density filter response

yields four possible amplifier gain figures; therefore, a light transfer characteristic curve is plotted for each gain position. Fig. 3 shows a typical set of static characteristics that will be obtained for each camera system. The collimator luminance must be accurately measured for the transfer function data. A discussion of collimator calibration is presented in *Calibration equipment*, below.

System dynamic range capability is obtained in part from the static transfer function. In addition, however, a gray-scale test slide having 10 shades of linear density is used to measure dynamic range at various average illumination levels. This slide is used in conjunction with

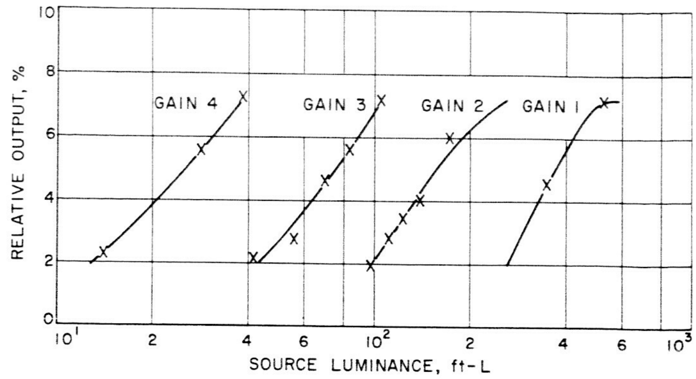

Fig. 3. Static light transfer characteristics

(a) TYPICAL SINE-WAVE RESPONSE CHARACTERISTIC

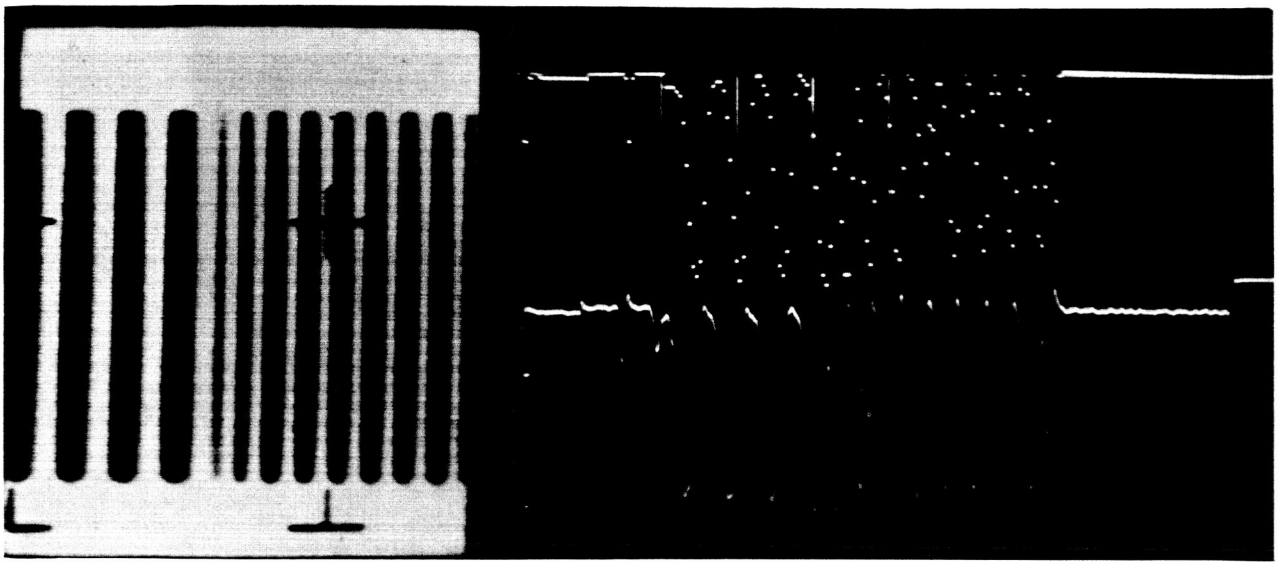

(b) BLOWUP OF "A" TRACE OF PART (a)

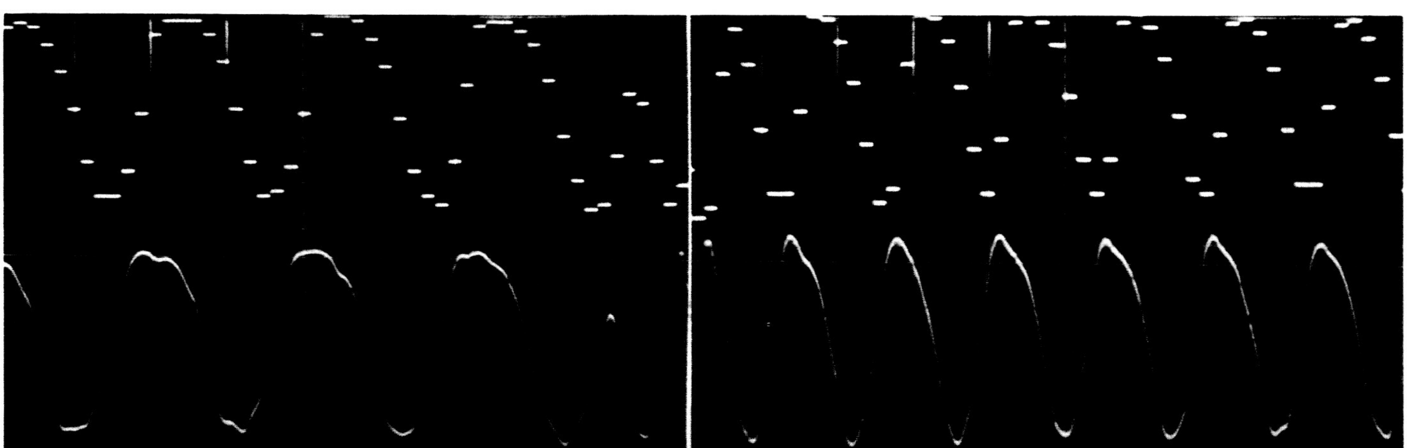

Fig. 4. Sine-wave response characteristic

a 40-in. optical collimator, the luminance level of which is accurately known.

Resolution. System resolution will be defined in terms of the modulation transfer function obtained with sine-wave optical stimulus as a system input and percentage response measured at the output of the video chain as the system output. Sine-wave transparencies of varying spatial frequencies will be used in conjunction with the 40-in. collimator. The test slides have a contrast ratio of approximately 10:1 and are accurately measured using a microdensitometer. A typical sine-wave measurement is shown in Fig. 4 giving field and "A"trace displays. An Air Force resolution target (Fig. 5) is used during thermal testing to observe optical and electrical focus as a function of temperature.

Geometrical characteristics. Geometrical charäcteristics are obtained using a ball chart in conjunction with the vidicon fiducial marks (Fig. 6). The fiducial marks are accurately vacuum-deposited on the inside face of the vidicon face plate (Fig. 7). These marks serve as a precise reference for measuring geometrical distortion over the entire raster. The black mask which provides an optical black illumination reference and dark current clamp voltage can also be seen in Fig. 7. Geometrical distortion within the raster can be determined from the shape of the balls on the ball chart display.

Vidicon photosurface characteristics. Obtaining slow-scan vidicon photoconductive surfaces is still an art and, therefore, a perfect photoconductor is impossible to obtain. For this reason, its characteristics must be carefully measured to aid in data interpretation and enhancement. These characteristics include shading or vignetting,

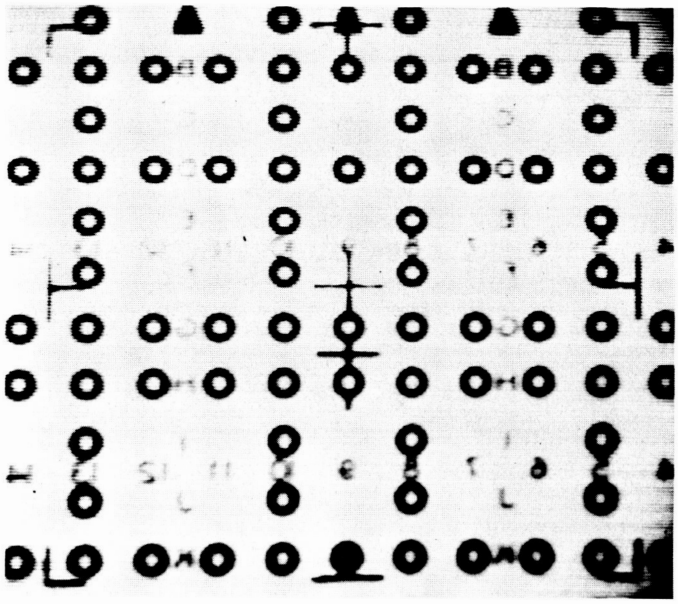

Fig. 6. Ball chart

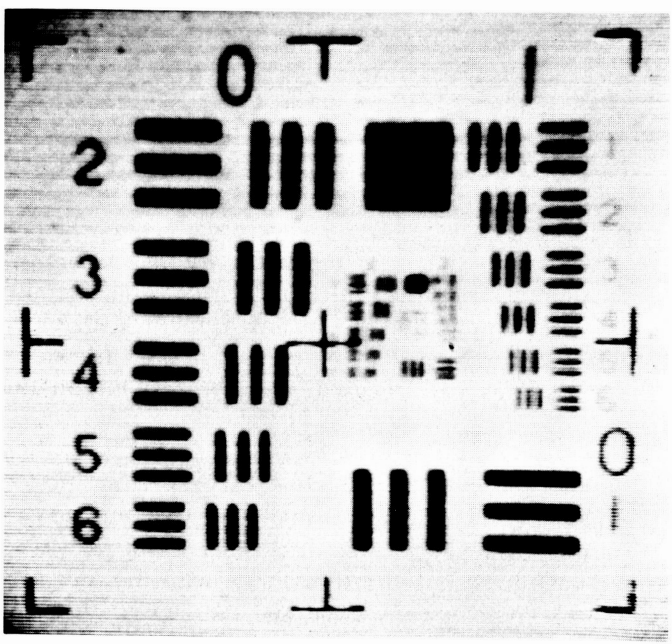

Fig. 5. Air Force resolution target

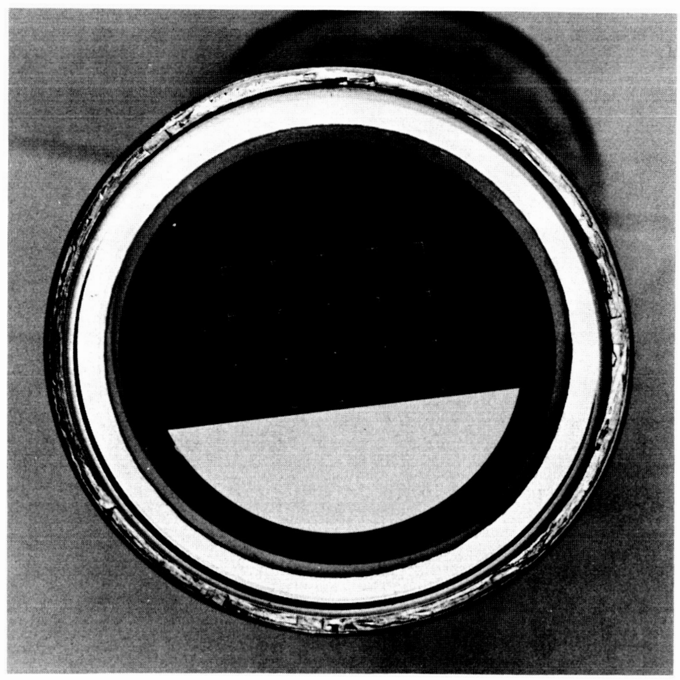

Fig. 7. Vidicon face plate

coherent target noise, target blemishes, and erasure properties. Shading is measured using flat-field illumination from the 9-in. collimator. The shading characteristics are measured at three different illumination levels, yielding high-, low-, and average-illumination characteristics. The data are displayed in the form of a 200×200 decimal matrix, with each picture element level being represented by a decimal number. (This scheme is described in more detail under *Calibration equipment.*) Target noise and blemishes are charted in the same manner.

The erasure characteristic is measured for a target having a high contrast ratio ($>$30:1), the high light being adjusted to the highest anticipated during the mission. The telescope on the TV camera is uncapped for one picture and then recapped. The peak-to-peak signal ratio is then measured on the "A" trace between the uncapped and the capped pictures after one complete erase cycle. This signal voltage ratio must be $\geqq$20 db.

Calibration equipment. The equipment to be used for the calibration procedures includes:

Mariner C TV development support equipment. This equipment will be used to provide electrical activation of the TV subsystem plus qualitative field and "A" trace displays (Ref. 1). Controlled access to engineering test points and TV engineering telemetry outputs is also provided.

Imaging tube test set. The tube test set and associated equipment are used to obtain initial performance data on vidicon tubes as received from the manufacturer, as well as the relative spectral response measurements described above.

Collimators. Two collimators will be used: a Farrand Optical Company 9-in. collimator to perform radiometric measurements, and a JPL 40-in. collimator for obtaining resolution and geometrical characteristics.

Spectral radiometer. The spectral radiometer consists of a 3000°K standard lamp, a regulated lamp power supply, a monochrometer, and photomultiplier tubes with current readout. The radiometer is used to select filters for the 9-in. collimators by comparing the spectral distribution of the source with the standard lamp. Actual spectral distribution will be obtained for the 9-in. collimators used for calibration purposes.

Photometer. The photometer (spot brightness meter) will be used to determine the luminance of the field looking into the collimator. The observed luminance values will be used, together with photometer calibration data and the collimator spectral distribution, to determine the absolute brightness distribution of the sources used in calibration. A working brightness standard will be employed to maintain calibration of the photometer during use.

Photometer calibration equipment. Photometer calibration equipment will consist of a standard lamp and a reflectance standard to obtain an absolute luminance calibration of the photometer, plus a bright gas lamp and an optical bench to determine a scale correction curve.

Microdensitometer. A Gerald Ash Model 23-050 microdensitometer is used to obtain transmission and waveform data from the sine-wave and gray-scale test slides.

Spectrophotometer. A spectrophotometer is used to obtain spectral transmission data on the various filters to be used.

Filters and test slides. This equipment will include neutral-density Inconel filters, narrow-band interference filters, sine-wave and gray-scale test slides, a ball chart, and an Air Force resolution chart.

Data-handling and data-display equipment. Ideally, the data-display equipment should not affect the calibration data at all. Cathode-ray-tube field displays are typically not usable for quantitative information display without tedious and somewhat time-consuming calibrations of their own. Since the *Mariner C* TV subsystem is a digital system, quantitative data display will be in the form of a printed page having a matrix of 200×200 decimal numbers corresponding to the digitized signal level of each picture element. The basic 83.3-kilobit/sec TV subsystem picture data will be recorded using the *Mariner C* science data-handling PDP-4 (programmed data processor) computer. The recorded data will then be processed by the telemetry processing station, the JPL 7094 computer, and the Link film recorder. The computer will format outputs for the decimal printout and for the Link film recordings. The information obtained from the film recordings will be used as qualitative information only.

Future activity. During the next reporting period, five *Mariner C* TV subsystems will receive complete calibration as presented in this discussion. All of the procedures have been tested satisfactorily, with the exception of the photometer calibration and the PDP-4 checkout. The telemetry processing station, the 7094 computer, and the Link film recorder have been used many times during spacecraft systems tests to process the 10.7-kilobit/sec data-automation-system output picture data.

B. The *Mariner* Vidicon as a Ruggedized Space Component

Space sensor. Most of the components used in a space-science instrument have well-established and successful backgrounds in the space environment. Other components, even though specially designed, may be correlated to similar items that have performed successfully. Hence, with these components and with reasonable care in design and selection, a high degree of confidence can be established for an over-all assembly. The sensors for a space-science experiment are rarely in this position and frequently represent highly specialized state-of-the-art development. Assessment of performance and integration with other space-science experiments is generally complex, and any restrictions in power and weight often present a severe handicap. Also, uncertainty in the magnitude of the parameters to be measured in space requires an extended dynamic range with concomitant complexities in the associated circuitry. Fabrication is almost always highly specialized, costly, and time-consuming. To this must be added economic difficulties that inevitably arise with any science experiment that is not completely assured of a place in the mission at an early stage in development.

Mariner vidicon. A typical space-science sensor in this category is the *Mariner* vidicon, the photosensor for the Mars photographic experiment. The vidicon forms part of a telescopic-objective subassembly that is mounted on the *Mariner* scan platform. The physical environment includes extremes of temperature, mechanical vibration, and the long-term effects of an extended trip into outer space. The highly experimental status of the slow-scan vidicon has presented a number of special problems in the evaluation of the TV camera for the *Mariner* spacecraft. One problem in particular is related to the number of satisfactory vidicons that can be made available for the diverse phases of the program. To cover the various development and test requirements, the availability of 50 to 100 vidicons would not be unreasonable.

An early assessment of possible camera tubes for *Mariner* ruled out all sensors but two because of inadequate environmental histories. There remained a choice then between the magnetic and the electrostatic vidicons, both of which have been used in space programs. The magnetic tube has the simpler, and therefore more rugged, electrode assembly. However, power and weight considerations, plus possible magnetic-field interference with the magnetometer, caused the electrostatic tube to be the preferred unit. Environmental experience gained with an early *Ranger* program led to a preliminary choice of the 1351-B electrostatic vidicon manufactured by General Electrodynamics Corporation (GEC) of Garland, Texas. The development of this tube was a joint venture between RCA and GEC, where RCA developed the sensor faceplate and GEC built the ruggedized electrode assembly.

Vibration environment. The multiplicity of problems arising in camera-tube picture performance evaluation tend to force environmental considerations into the later phases of the program. Picture quality with a slow-scan vidicon is almost entirely dependent on the characteristics of the photoconductor. These characteristics, in turn, determine the philosophy of the electronic circuitry associated with the tube. A change in the photoconductor may require substantial changes in the electronics. This was experienced, for example, in the *Mariner* program when a move was made from the antimony surface to the selenium surface in the effort to maintain high-quality pictures. Delays in implementing the vibration environmental evaluations were increased due to uncertainties in the knowledge of the *Mariner* spacecraft structural reactions to a vibration input. Because of the location of the camera on the scan platform and the need for all subassemblies to be extremely lightweight, complete spacecraft structural testing was required to determine the magnitude of any spacecraft resonances that would significantly affect the vidicon.

As a result of the *Mariner* structural test model (STM) tests, the type-approval (TA) specifications for the camera called for an additional low-frequency sinusoidal three-axis shake of several seconds duration with levels up to 30 *g* rms. The normal *Mariner* TA specification for subunits under 10 lb (which includes the camera) calls for three orthogonal tests of 10-min duration, with Gaussian noise to 14 *g* rms added with sinusoidal vibration to 9 *g* rms. Preliminary tests indicated that the 1351 vidicon was quite marginal and could not be relied upon to meet the *Mariner* TA specifications. Therefore, a change was made to a still more ruggedized electrostatic version of the 1351 vidicon that was being fabricated by GEC for fast-scan TV rocketry applications.

Vidicon construction. The mechanical construction of the electrostatic vidicon is illustrated in Fig. 8. The original ruggedized 1351 vidicon, Type 1351-B, is shown in Fig. 8(a), and the structurally modified unit developed

Fig. 8. Environmentally improved construction of electrostatic vidicon

to meet the more stringent TA specifications, now known as Type 1343-010, is shown in Fig. 8(b). As will be noted, the tube electrodes are strap-welded to ceramic rods in order to provide a single integrated mechanical structure within the glass envelope. Connections to the various electrodes are made through hollow ceramic support members. Strap-welds to the 13-pin base anchor the structure in the axial direction. The 130 individual pieces in the assembly add up to an over-all tube weight of 80 g.

A major vibrational problem is the relationship of the electrode assembly to the glass walls. Some flexibility is required during the glass-sealing processes to prevent glass fracture. The necessary flexibility is obtained by close-knit wire-mesh spacers placed fore and aft of the electrode assembly. While the welded construction has assured axial stability of the electrodes, radial flexing with high radial accelerations tends to cause vidicon failure. When this occurs, the electrode assembly is crushed and distorted against the glass walls with a possible fracture of the interconnecting leads. The 1343 vidicon represents an effort by JPL quality control and the manufacturer to maximize structural strength within the basic limitations of the electrode-assembly structural design. Changes which were recommended included increased welding at the supports and an improved lead arrangement, particularly the G_2 lead which had consistently fractured.

Tube mounting. As originally designed, the vidicon was solidly clamped within the camera housing. Vibration tests have indicated that a hard-mounted 1343 vidicon in a unity-gain fixture will pass the *Mariner* camera TA specifications. However, there is less assurance when the same tube is hard-mounted in a resonant configuration, i.e., the camera head, where the acceleration may be amplified several times due to camera-head structural resonances. While the hard-mounted 1343-010 vidicon in the camera head survived the spacecraft environmental test, the same vidicon in the camera head was unable to survive the more severe TA-specified tests at the subassembly level.

Modified tube mounting. To provide a higher level of confidence in the TV camera operation by assuring performance at the TA subassembly level, the tube suspension in the camera head was changed from a hard mount to a radially flexing mount. This so-called soft-mount technique is illustrated in Fig. 9. Two cylindrical polyurethane-foam dampers support the tube radially. A spring-loaded centering device assists the foam in centering the tube optically. The tube is constrained axially by the flat spring-loaded tube socket, while Teflon bearing surfaces permit the tube to slide freely in the radial direction. The axial socket pressure and the mechanical centering device provide additional assurance of correct tube alignment should there be any deterioration of the foam in space. With the tube mounted in the camera head, tri-axial accelerometers have indicated that the gain is less than 2 over a 25- to 2000-cycle range. The gain was measured between the tube socket and the accelerometer input to the camera-head mounting flange. No problems have been experienced in passing full TA specifications for the camera subassembly with this arrangement. Optical centering is well within the specified tolerances after vibration, i.e., less than 6 min of arc relative movement before and after vibration.

Tube life. Tube life over a non-operating flight time of 275 days to Mars is related to the emission stability of the cathode. The cathode emission is controlled by the G_1 grid potential and is an important factor in optimizing the discharge of the photoconductor charge image. While an automatic beam-control regulator can be useful for control of emission, implementation in a slow-scan system becomes quite complex. This is emphasized as the G_1 potentials approach the maximum breakdown potentials of available transistors. Fortunately, long-term experience with GEC tubes both at GEC and at JPL has indicated excellent aging characteristics. There is no known case of a GEC slow-scan vidicon having failed to operate after either storage or intermittent operation for periods of 2 to 3 yr.

The mechanical spacing of the G_1 grid cylinder to the cathode is critical and is secured as shown in Fig. 10. The cathode sleeve, which is held in the ceramic wafer, is positioned in the G_1 electrode with welded rings. Even

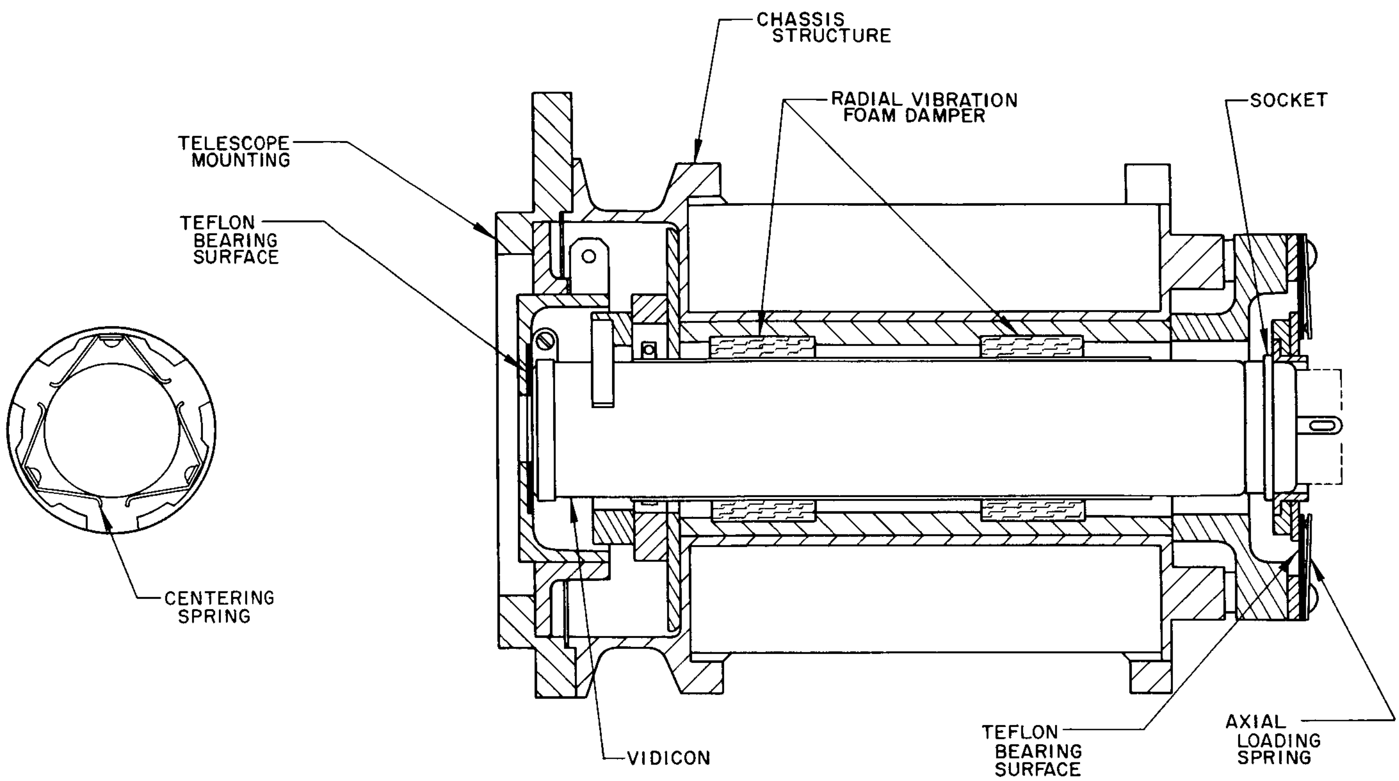

Fig. 9. Flexible mounting of vidicon in camera head

after extensive damage by vibration, there has been no observed change in the G_1 potential requirement. Several tubes were stored in order to more accurately determine the stability of the G_1 potential and the emission following extensive periods of storage. Environmental demands for test tubes forced down the number available for emission life tests to two tubes. With these two tubes, after 4 mo of storage, there was no discernible change in emission or G_1 control characteristics. Since the tube can withstand substantial filament overload (10% or more) without change in emission or detriment to life, it was decided, for this mission, to arrange for a marginal increase of filament potential (3%) to take place at some selected time during the flight-camera test period. Circuital arrangements are included to change filament potential at this time from 6.3 to 6.6 v and, thus, further ensure normal emission. Run-in tests to stabilize emission characteristics for flight vidicons were discarded due to ion bombardment and possible damage to the photosensor. The G_1 potential will be constantly monitored during the flight-camera evaluation time to determine stability of characteristics prior to liftoff. To ensure the requisite accuracy with the pulsed G_1 signal, measurements will be digitally monitored with a Tektronix, Inc., digital oscilloscope.

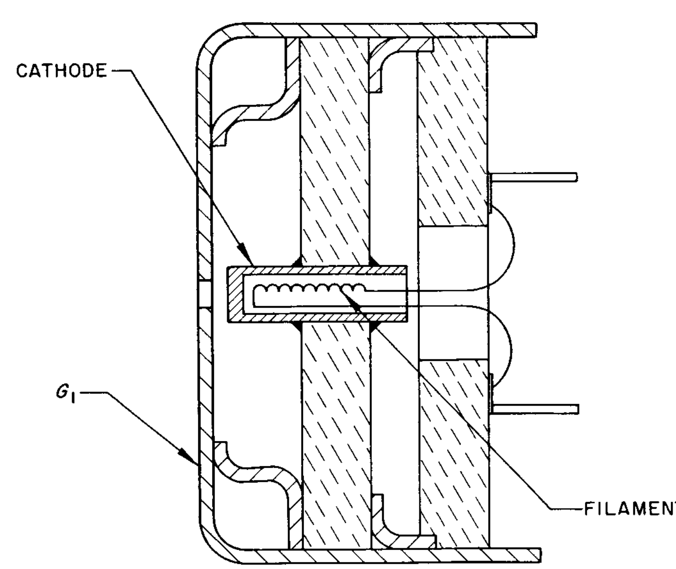

Fig. 10. Cathode and G_1 support in vidicon

Temperature. Mariner TA temperature requirements range from −10 to 75°C. Spacecraft thermal tests indicate that the TV camera head will settle toward the lower end of this range. But, since earlier estimates had predicted temperatures of $-20°C$ or lower at the scan platform, the camera head uses thermally compensated circuitry that provides a satisfactory level of picture quality over a range of -40 to 55°C. Vidicons have been immersed for several hours at temperatures ranging from -50 to 70°C without any noticeable change in performance. A "catastrophic" failure of the photosensor has been noted at a temperature below $-60°C$, and experience at GEC and JPL appears to indicate that similar problems will arise at temperatures above 100°C. Because there is much less likelihood of upper extremes of temperature in the *Mariner* spacecraft, vidicon evaluation has not been made in this area for the *Mariner* program.

The thermal isolation of the tube with the modified flexible mounting produces bulb temperatures up to 40°C for a 20°C ambient temperature. The tube has a 1-w heater. As the platform is not expected to exceed a 20°C ambient temperature the additional thermal heating does not present a problem.

Extensive thermal- and vacuum-chamber tests, with 16-day operation in the temperature range of -20 to 55°C, show no appreciable degradation in image quality.

Conclusions. Space-science sensors typified by the *Mariner* vidicon are highly specialized components that present special problems in the implementation of a space program. Because of the small-quantity production of tubes, environmental capabilities are particularly difficult to assess. The *Mariner* program has not only made a significant advance in slow-scan sensor development, but has produced a more satisfactory tube environmentally. The manufacture of high-quality vidicons that will meet all the diverse requirements of a deep-space program is still unpredictable and appears to require a continued long-term effort to stabilize the significant characteristics.

Reference

1. "*Mariner C* TV Development Support Equipment," *SPS 37-25*, Vol. VI, pp. 43–46, Jet Propulsion Laboratory, Pasadena, California, January 31, 1964.

VII. Applied Science

A. Utilization of *Surveyor* TV Imagery for Photogrammetry and Construction of Photomosaics

Photogrammetry. The concept of stereoscopic viewing of photographs for mapping or interpretation purposes is dependent upon the ability of man, or machine, to perceive parallax displacements in the selected imagery. The precision to which the various distances may be determined is dependent upon the precision of the specific parallax measurements themselves. The ability to physically measure parallax is a characteristic inherent in the instrument design utilized in the measurement and will not be elaborated upon here.

In this discussion, the major effort will be directed towards an analysis of those factors which directly affect the amount of parallax which is recorded in a stereoscopic imaging system. These parameters are: (1) base length, which is the distance between the two camera stations from which the stereoscopic imagery is obtained; (2) focal length of the camera; and (3) the distance to which it is desired to have stereoscopic measurement capability.

The most critical factors in the collection of photogrammetric measurements from stereo photographs are the effective base-to-distance ratio[1] and the over-all quality of the viewed imagery. The accuracies of conventional, off-the-shelf, parallax measuring devices are as high as 0.003 mm and are considered to be significantly better than the accuracy required for currently anticipated lunar mapping or reconnaissance systems. Therefore, the topographic or photogrammetric mapping potential of *Surveyor*-type systems is primarily restricted by image quality and the base-to-distance ratio. The primary emphasis here will be on the base-to-distance ratio and a general evaluation of parallaxes as related to the pertinent *Surveyor* mapping and photo-interpretation tasks.

In conventional photogrammetric distance determinations, an accuracy of one part in a thousand (0.1%) is considered to be readily achievable using a high-precision instrument. "Conventional" photogrammetric procedures utilize a relatively high image quality and large base-to-height ratios to obtain the precision required to meet

[1]This ratio is normally defined as a base-to-height ratio, but here we are primarily evaluating terrestrial photogrammetry where camera axes are essentially horizontal and not vertical; therefore, the ratio will be described here as a base-to-distance ratio. It is the same as the base-to-height ratio of normal aerial photogrammetry.

mapping standards. Parallax determinations accurate to 0.01 mm are common in photogrammetric mapping practice. Base-to-height ratios generally vary between 0.30 and 0.60; however, in special cases they may be as high as 2.0.

In the following paragraphs, data are presented to assist in the estimation of the maximum distance at which significant stereoscopic parallaxes will exist in order to provide a reasonable topographic mapping capability under the constraints of optimum *Surveyor*-type imaging systems.

The factors which govern the amount of parallax recorded by a camera system are the focal length of the camera, the distance to the object, and the separation or base length between cameras or camera stations. A relationship which may be established among these elements is derived from the following illustration:

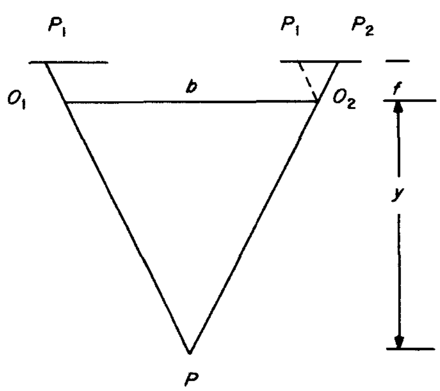

where f is the focal length; b, the effective base length with the camera axes parallel; and y, the distance to object point P. The camera stations from which the images of point P are recorded are designated O_1 and O_2. The corresponding image points are represented by P_1 and P_2, respectively. The distance P_1P_2 on the right image plane is the parallax of point P as recorded in the system. From similar triangles, the following relationship is established:

$$\frac{b}{y} = \frac{P_1P_2}{f}$$

We now designate the parallax P_1P_2 as p and obtain:

$$p = \frac{bf}{y} \tag{1}$$

This simple relationship is established for conditions where the camera axes are parallel to each other and normal to the base b and lie in the same plane.

Eq. (1) was used to determine the theoretical curves shown in Fig. 1. These curves relate the image parallax (in mm) for distances normal to the base line and at selected base lengths. The base lengths selected were 0.5, 1.2, and 2.0 m. For all curves, the camera axes are assumed to be parallel to each other and perpendicular to the base line. This assumption was made in order to provide an estimate of the maximum distance from a given camera station to which reliable stereoscopic observations may be made. Convergent camera axes decrease the parallax for relatively close points and, consequently, do not increase the maximum range to which stereo information can be recorded. The theoretical determination of the maximum parallax observable, regardless of the base length, is based upon the assumption that, with a 100% overlap of photographs, this parallax would be equal to the width of the field-of-view of the image plane (taken here to be 10 mm), corresponding to the approximate image area of the vidicon tube.

By differentiation of Eq. (1), we obtain the following:

$$dy = \frac{y^2}{bf}dp + y\frac{df}{f} + y\frac{db}{b} \tag{2}$$

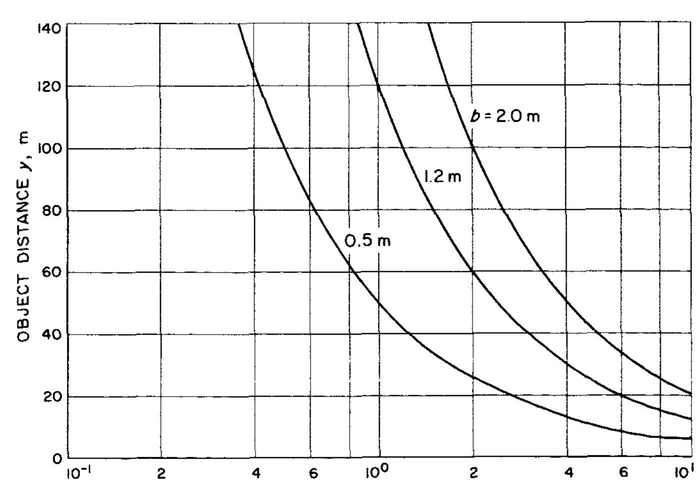

Fig. 1. Relationship between parallax and object distance for three base lengths with a 100-mm focal-length lens and parallel camera axes

where dy represents the error in the stereoscopic determination of the distance y to an object, dp is the stereoscopic measuring accuracy, df is the error in the determination of the focal length f, and db is the error in the determination of the base length b. For application in this example, we assume that the relative errors df/f and db/b are very small in comparison to dy and dp and, therefore, may be neglected in the following analysis. By dividing Eq. (2) by y, we obtain:

$$\frac{dy}{y} = \frac{ydp}{bf} \tag{3}$$

In Fig. 2, Eq. (3) has been used to show the relative distance measurement error dy/y in relation to parallax mensuration accuracies. For this example, a focal length of 100 mm and base lengths of 2.0, 1.2, and 0.5 m were selected. The relationship between the parallax measuring accuracy and the image quality, as expressed in lines/mm, has been taken to be ⅕ of a resolution element.

From Fig. 2, we see that, if we assume a parallax measuring accuracy of 0.1 mm, the distance error we can expect with a base length of 1.2 m is approximately 0.8%. The parallax measuring accuracy in this case is dependent upon image quality. Because of the problems related to the prediction of image quality, it becomes important to establish the maximum error which can be tolerated in distance measurements for mapping purposes. After such a value is established, it is then possible to determine from Fig. 2 the approximate accuracy to which parallaxes should be recorded by the system. It should be remembered that the data given in the figures presented here represent information under perfect or optimum conditions only; i.e., no allowance is made for effective spacecraft tilts, lens degradations, or other distortions in the imaging system. In the case of a *Surveyor*-type system, it can be anticipated that the total realistic photogrammetric errors may be as much as five times the errors estimated here.

The basic relationship between object distance, focal length, base length, and parallax was established by Eq. (1). The amount of parallax recorded by any system was shown to depend upon the base length, object distance, and the focal length of the camera. Fig. 3 illustrates the amount of parallax available to selected systems as a function of the base-to-distance ratio and the focal length. Three possible ratios were selected: 0.05, 0.10 and 0.30. These ratios were considered as a representative range of values for providing a reasonable mapping capability for the type of systems under consideration. If it is assumed that a base-to-distance ratio of 0.05 is the least value which will satisfy any proposed mapping accuracy requirements, then from Fig. 3 we find that the maximum parallax recorded by a 100-mm focal-length system is 5 mm. To obtain greater parallaxes with a 100-mm focal length, it would be necessary to increase the base-to-distance ratio. Similar analysis of Fig. 3 reveals that a

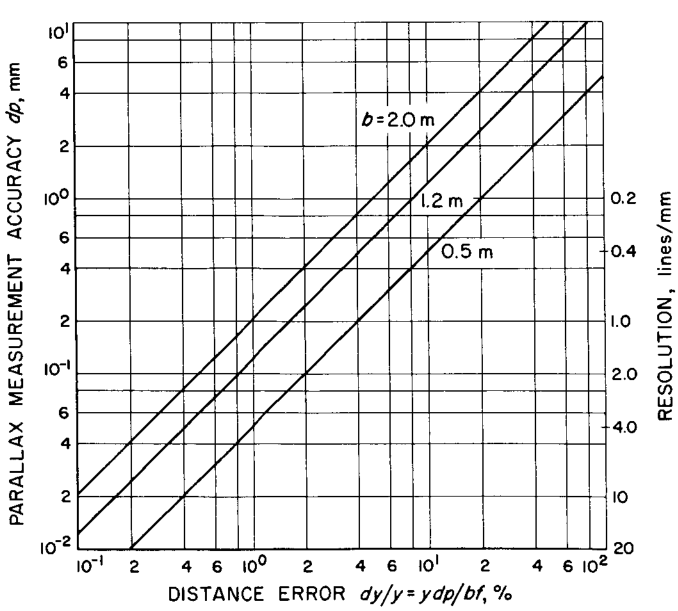

Fig. 2. Relative distance measurement error vs parallax measurement accuracy and resolution

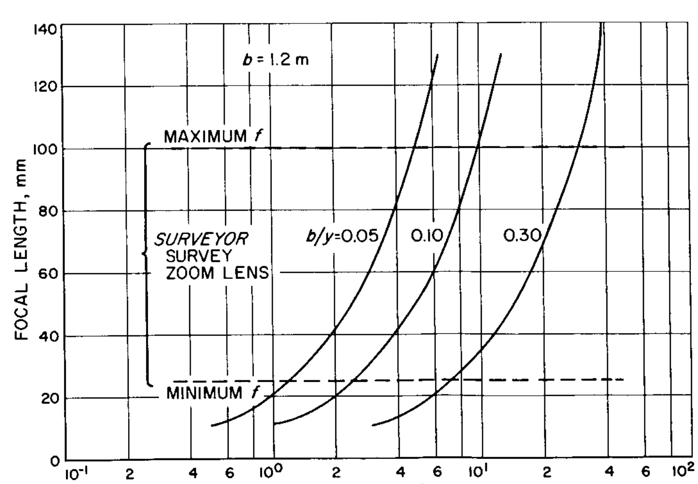

Fig. 3. Relationship between focal length, base-to-distance ratio (b/y), and system parallax

25-mm focal-length system would result in maximum parallaxes on the order of 1.25 mm, if the same base-to-distance ratio is maintained as the minimum acceptable to meet the system requirements. Utilizing the assumption that the maximum parallax recorded by the system is 10 mm, as limited by the image format, in Fig. 4 it can be seen that the maximum base-to-distance ratios which the system can handle are 0.10 and 0.40 for 100-mm and 25-mm focal lengths, respectively. These values for optimum conditions may be taken as upper limits for the system operation.

In this discussion, some preliminary ranges for an optimum *Surveyor*-type mapping capability were described. In all probability, requirements for the actual operational *Surveyor* system will be in the form of a "best possible" criterion. Under such conditions, it becomes of prime importance to define as many as possible of the variable parameters affecting the system output. The geometric constraints of the *Surveyor* TV camera system have been investigated in detail, and verification of some of their theoretical parameters will be accomplished through an elaborate testing program supported by actual field-test operations.

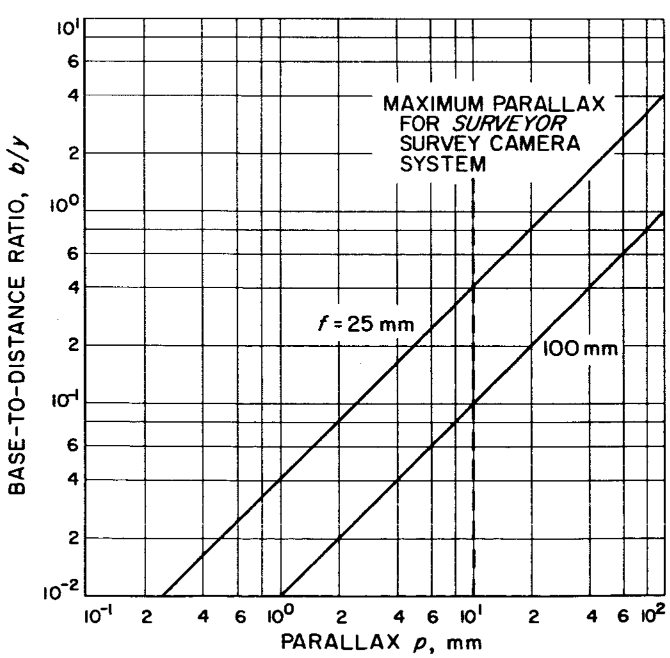

Fig. 4. Relationship between parallax and base-to-distance ratio for 25- and 100-mm focal-length lenses

Photomosaics. The scientific information to be gained from the *Surveyor* TV experiment will be based primarily upon the analysis of composite pictures formed by making mosaics of numerous individual frames of TV imagery recorded on a conventional silver halide film. These mosaics differ greatly from conventional aerial photographic mosaics, which basically contain imagery of a generally uniform scale. The *Surveyor* mosaics represent a panoramic view of the area in the vicinity of the camera station, and scale variations increase greatly from the foreground to the more distant object. In addition, the field-of-view from the cameras is very small, being only approximately 25 deg for the 25-mm focal-length mode and 6 deg for the 100-mm focal-length mode. Therefore, a large number of individual frames is necessary to cover the area visible from any one camera location.

The basic presentations for the mosaics will be two entirely different formats. The first, known as a preliminary mosaic, is constructed as promptly as possible after the data are received at the ground data-handling system. It is constructed on a flat surface upon which is a guide grid to facilitate the placement of the individual pictures. Because of the large number of pictures in a survey at the narrow-angle (100-mm focal-length) camera mode, these mosaics will be constructed in separate sections. Fig. 5 represents two adjacent sections of a narrow-angle mosaic on a flat format. These pictures, which were obtained at a field-test site, consist of a total of 72 deg of the complete 360-deg coverage. For comparison of information content between the narrow-angle and wide-angle (25-mm focal-length) mosaics, reference should be made to Fig. 6, which shows the wide-angle coverage of the same area as in Fig. 5. One of the camera positions with its viewing optics can be seen at the left in Fig. 6.

The second basic format utilized in the presentation of the TV data for scientific purposes is the spherical format. This type of mosaic is considered to be primarily an improved mosaic constructed for maximum information and accuracy and not under the rigid time constraints of the preliminary mosaics. It utilizes the best possible pictures after all image enhancement and rectification procedures and techniques have been applied to improve the image quality and minimize geometrical distortions. These mosaics are then assembled on the inside of a hemisphere so that the composite picture will represent

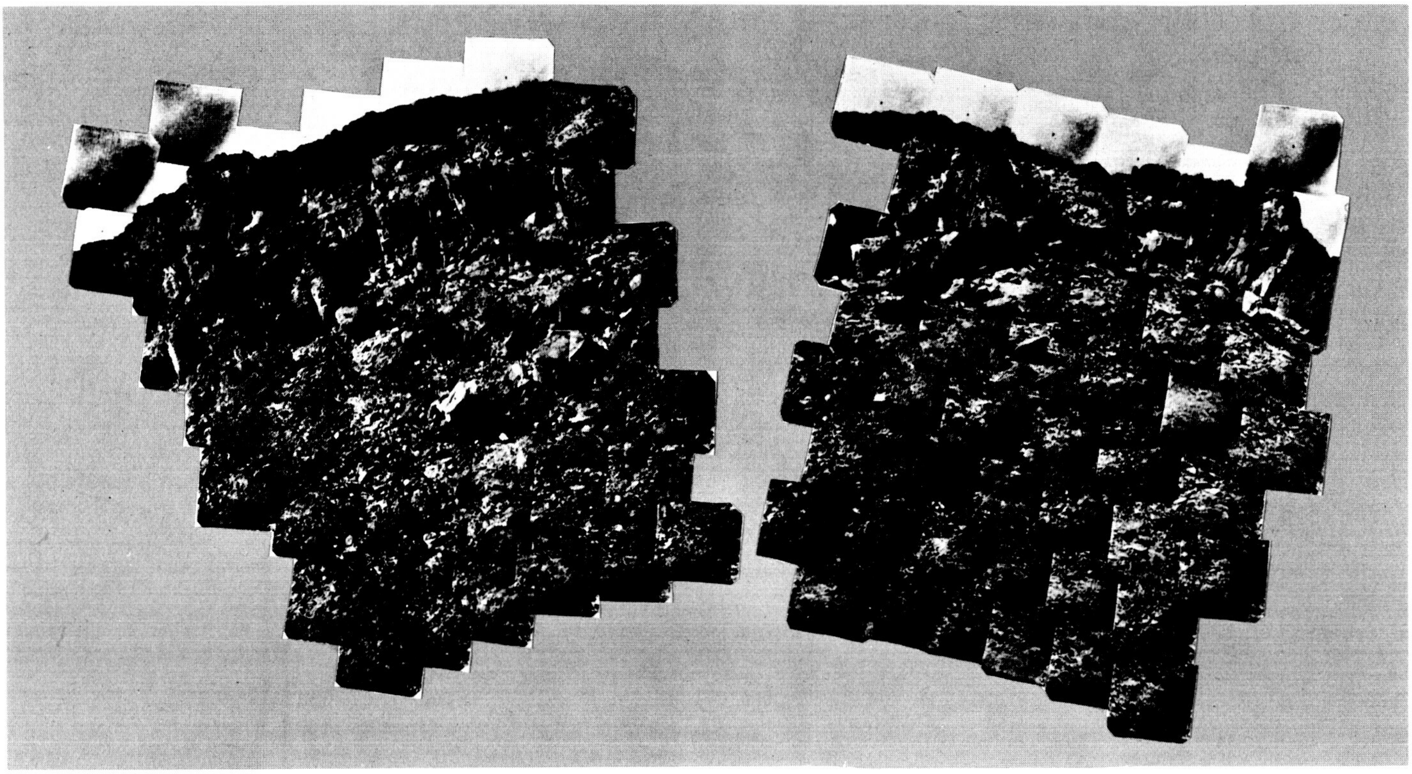

Fig. 5. Narrow-angle mosaic

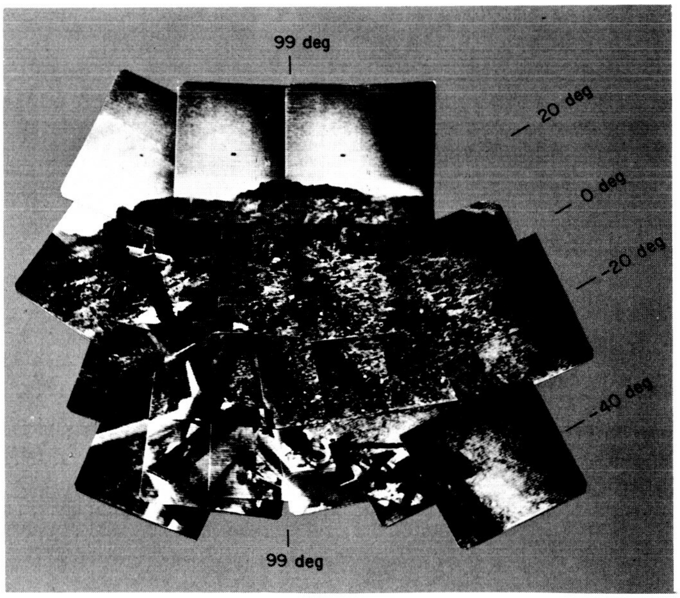

Fig. 6. Wide-angle mosaic

the most realistic view of the lunar surface. The actual construction of the spherical mosaic is assisted by a control grid scribed on the sphere, which permits the locating of an individual frame by the azimuth and elevation settings of the camera optics at the time of exposure. The construction of mosaics will also be aided by the use of a network of reseau marks placed on the face of the camera vidicon tube. These marks will be visible in the pictures and will serve as a guide for the placement of individual frames, as well as for measuring distortions within individual TV frames.

Stereoscopic study of *Surveyor* imagery will be done with individual frames from the two survey camera stations and also with mosaic sections. Scientific investigation of this type will provide detailed information about the lunar surface and, thus, necessary support data for manned lunar exploration.